0952

PB 209 290

3SR-844

VOLUME I

NOVEMBER 1971

SYSTEMS, SCIENCE AND SOFTWARE

P.O. BOX 1620, LA JOLLA, CALIFORNIA 92037. TELEPHONE (714) 453-[illegible]

A PARTICLE-IN-CELL METHOD FOR NUMERICAL SOLUTION OF THE ATMOSPHERIC DIFFUSION EQUATION, AND APPLICATIONS TO AIR POLLUTION PROBLEMS

BY

R. C. SKLAREW, A. J. FABRICK AND J. E. PRAGER

FINAL REPORT
FOR THE
DIVISION OF METEOROLOGY
NATIONAL ENVIRONMENTAL RESEARCH CENTER
RESEARCH TRIANGLE PARK, NORTH CAROLINA 27711

Reproduced by
NATIONAL TECHNICAL
INFORMATION SERVICE
Springfield, Va. 22151

UNDER
EPA CONTRACT NO. 68-02-0006

173

BIBLIOGRAPHIC DATA SHEET

1. Report No. APTD-0952

2.

3. Recipient's Accession No.

4. Title and Subtitle
A Particle-in-Cell Method for Numerical Solution of the Atmospheric Diffusion Equation, and Applications to Air Pollution Problems - Volume I

5. Report Date
November 1971

6.

7. Author(s)
R.C. Sklarew, A. J. Fabrick and J. E. Prager

8. Performing Organization Rept. No. 3SR-844

9. Performing Organization Name and Address
Systems, Science and Software
P. O. Box 1620
La Jolla, California 92037

10. Project/Task/Work Unit No.

11. Contract/~~Grant~~ No.
68-02-0006

12. Sponsoring Organization Name and Address
National Environmental Research Center
Division of Meteorology
Research Triangle Park, North Carolina 27711

13. Type of Report & Period Covered
Final

14.

15. Supplementary Notes

16. Abstracts

The document reports the development and initial applications of a new method for the solution of the turbulent atmospheric diffusion equation. The method, called PICK, is based on the use of Langrangian mass points and is one of a family of Particle-in-Cell techniques for the solution of partial differential equations. The purpose of this study was the development of the PICK method and the demonstration of the method in the solution of evaluation test cases and actual air pollution problems. Test cases for the evaluation of feasibility and accuracy and for comparison to finite difference solutions were conducted with a two-dimensional computer code PICFIC, as described in Section 2. For actual air pollution studies, the PICK method was used in the three dimensional code NEXUS. The description of NEXUS and its application to the simulation of CO in Los Angeles is given in Section 3. The NEXUS/P code was developed to solve equations with photochemical terms. Section 4 reports its description and its application to photochemical fog in Los Angeles.

17. Key Words and Document Analysis. 17a. Descriptors

Air pollution
Equations
La Grange equations of motion
Turbulence
Diffusion
Coding
Computer programs
Simulation
Carbon monoxide
Smog
Photochemical reactions

17b. Identifiers/Open-Ended Terms

PICK method
NEXUS code
NEXUS/P code
PICFIC code

17c. COSATI Field/Group 13B, 12A, 9B

18. Availability Statement
Unlimited

19. Security Class (This Report)
UNCLASSIFIED

20. Security Class (This Page)
UNCLASSIFIED

21. No. of Pages
174

22. Price

3SR-844
VOLUME I
NOVEMBER 1971

SYSTEMS, SCIENCE AND SOFTWARE

P.O. BOX 1620, LA JOLLA, CALIFORNIA 92037. TELEPHONE (714) 453-0060

A PARTICLE-IN-CELL METHOD FOR NUMERICAL SOLUTION OF THE ATMOSPHERIC DIFFUSION EQUATION, AND APPLICATIONS TO AIR POLLUTION PROBLEMS

BY
R. C. SKLAREW, A. J. FABRICK AND J. E. PRAGER

FINAL REPORT
FOR THE
DIVISION OF METEOROLOGY
NATIONAL ENVIRONMENTAL RESEARCH CENTER
RESEARCH TRIANGLE PARK, NORTH CAROLINA 27711

UNDER
EPA CONTRACT NO. 68-02-0006

ACKNOWLEDGMENTS

The authors gratefully acknowledge the technical assistance of S^3 scientists Burton Freeman, Manuel Rotenberg and Albert Petschek; the comments and advice of the project technical monitor, Mr. Kenneth Calder, Division of Meteorology, Environmental Protection Agency, and the many technical discussions and required input data supplied by Mr. Alan Eschenroeder, General Research Corporation, Mr. Raymond Dickson, Air Resources Laboratory, National Oceanographic and Atmospheric Administration, Mr. Robert Lamb, University of California at Los Angeles, Mr. Philip Roth, Systems Applications, Inc., and Mr. Gene Start, Air Resources Laboratory, National Oceanographic and Atmospheric Administration. This study would not have been possible without the support and encouragement of the S^3 management.

TABLE OF CONTENTS

Page

VOLUME I

INTRODUCTION 1

1. DESCRIPTION OF THE PICK METHOD 3

1.1 The Diffusion Equation 3
1.2 The PICK Method 9
1.3 Simulation of Emissions and Chemical Reactions 15
1.4 One-Dimensional Example of the PICK Method . 16
1.5 Accuracy of the PICK Method 23
1.6 Summary of the PICK Method 25

2. TESTING THE PICK METHOD 27

2.1 Description of the PICFIC Code 27
2.2 Comparison of Methods for Pure Advection . . 32
2.3 Evaluation of Diffusion Simulation 47
2.4 PICFIC Simulation 55
2.5 Summary 63

3. NEXUS SIMULATION OF CARBON MONOXIDE IN LOS ANGELES 67

3.1 Description of the NEXUS Model 70
3.2 Input Data 78
3.3 Results of NEXUS Simulation 89
3.4 Testing of NEXUS 104
3.5 Summary and Conclusions 116

4. NEXUS/P SIMULATION OF PHOTOCHEMICAL SMOG 119

4.1 Description of NEXUS/P 120
4.2 Photochemical Simulation 123
4.3 NEXUS/P Testing 130
4.4 Input Data 134

TABLE OF CONTENTS, contd.

Page

4.5 Results of the NEXUS/P Simulation 138
4.6 Summary and Conclusions 149

5. SUMMARY AND CONCLUSIONS 157

REFERENCES 161

VOLUME II – PICFIC and NEXUS Computer Code Listings

VOLUME III – NEXUS/P Operations Manual

LIST OF ILLUSTRATIONS

Number	Title	Page
1	Calculation of cellular concentration from particle masses	11
2	Area-Weighting interpolation for total velocity	13
3	Gaussian distribution with the approximate cell concentrations	17
4	Macro flow chart of the PICFIC code	28
5	PICFIC advection simulation test with $\sigma = 2.5$ Km, contours at 0.1, 10, 20, 40 and 60	34
6	First-order finite difference advection test with $\sigma = 2.5$ Km	36
7	Fromm fourth-order method advection test with $\sigma = 2.5$ Km	41
8	PICFIC advection test with $\sigma = 1$ Km	43
9	Fromm fourth-order method advection test with $\sigma = 1$ Km	44
10	Crowley fourth-order method advection test with $\sigma = 1$ Km	45
11	Curve fitting with a polynomial. Pictured is a Gaussian curve and an approximating cubic polynomial. This picture corresponds to the polynomial fitting used in calculating the fourth-order flux scheme for the $\sigma = 1$ initial distribution. The shaded areas correspond to the errors in the fit.	46
12	Histogram of initial cell concentrations compared to normalized Gaussian distribution . . .	53
13	Renormalized 41st cycle of PICFIC calculation (both advection and diffusion) compared to normalized Gaussian distribution	54
14a	Pollutant cloud advection in constant wind field with no diffusion. Three time instants are displayed together for comparison.	56

LIST OF ILLUSTRATIONS, contd.

Number	Title	Page
14b	Same as Figure 14a. The contours are for integer powers of 2 in pollutant concentration	56
15a	Pollutant cloud advection in constant wind field with spherically symmetric diffusion . .	57
15b	Same as Figure 15a. Contours at integer powers of two.	57
16a	Pollutant cloud advection in constant wind field with aspherical constant diffusion . . .	58
16b	Same as Figure 16a. Contours at integer powers of two.	58
17a	Pollutant cloud advection in constant wind field with aspherical, position-dependent diffusion. Model of an inversion at the source height.	60
17b	Same as Figure 17a. Contours at integer powers of two.	60
18a	Pollutant cloud advection in shear wind field with spherically symmetric diffusion, three separate times are depicted as the cloud moves to the right.	61
18b	Same as Figure 18a. Contours at integer powers of two.	61
19	Calculational grid for NEXUS CO simulation . .	69
20	Macro flow chart of NEXUS main program	71
20a	Macro flow charts of NEXUS subroutines INPUT and RESTRT	72
20b	Macro flow charts of NEXUS subroutines SETUP and OUTPUT	73
20c	Macro flow charts of NEXUS subroutines DIFFUS and PARCEL	74

U.S. DEPARTMENT OF COMMERCE
National Technical Information Service
5285 Port Royal Road
Springfield, Virginia 22151

April 10, 1972

Environmental Protection Agency
Air Pollution Technical Information Center
Attention: Input Section
Research Triangle Park, NC 27711

Re your report: 3SR-844-II A Particle-in-Cell Method for Numerical Solution of the Atmospheric Diffusion Equation...

Gentlemen:

We are not able to process your report for the following reasons. Please make the corrections necessary and return the document and this letter to us. You will find the publication entitled Guidelines to Format Standards for Scientific and Technical Reports Prepared By or For the Federal Government helpful when preparing documents in the future. It is available from NTIS as ORDER NO. PB-180 600 in paper copy at $3 or 95¢ for microfiche.

☐ 1. Pages are missing.

☐ 2. All pages are not numbered and some could therefore be missing. We suggest author or editor number the pages consecutively throughout the document, or within chapters if prefixed by the chapter designation.

☒ 3. Some pages are not reproducible. Pages 39,70,114,135,137 and 143

☐ 4. A Bibliographic Data Sheet (BDS) must accompany each report. Blank BDS forms are enclosed.

☐ 5. This document has copyright or other restrictions. Please furnish written authorization for NTIS to reproduce and sell to the public.

☐ 6. An Accession Notice Card must accompany each report. Blank forms are enclosed.

☐ 7. We will announce your report as available in paper copy from the source shown in the report if you send us a completed Bibliographic Data Sheet (BDS). NTIS will sell microfiche only. Blank BDS forms are enclosed.

☐ 8. The document is more than 2 years old. Unless you can assure us that current demand exceeds 10 requests a year we suggest you fill requests through an established library reproduction service. We reserve the right not to announce. To serve the public better please send future reports when new.

☒ 9. Other: Pages 77,78,94,99,121 and 122 are scalped. Vol 1 returned to keep from breaking the set.

Sincerely,

Bo W. Thott

BO W. THOTT
Chief, Input Section
Phone: 703-321-8517

TL
Form NTIS-63 (Rev. 12-71)

LIST OF ILLUSTRATIONS, contd.

Number	Title	Page
20d	Macro flow charts of NEXUS subroutines BORDER and SOURCE	75
21	Supplied wind data (Ref. 16). The streamlines are shown by solid lines. Isotacks in miles per hour are dashed contours.	79
22	Winds in NEXUS grid. The arrowhead points in the direction of motion and the arrow lengths is proportional to the wind speed.	80
23	Initial (3:00 A.M.) CO surface concentration (ppm) (Ref. 16).	82
24	Los Angeles County traffic distribution (unnormalized relative car miles per cell)	83
25	Temporal distribution for Los Angeles Basin traffic	84
26	Macro flow chart for SETUP	85
27	Isopleths for CO at 10:00 A.M.	90
28	Plot of particle positions at 10:00 A.M. . . .	91
29	Isopleths for CO (in ppm) at 10:00 A.M. as simulated by Lamb's model (Ref. 16)	95
30	Surface winds at 10:00 A.M. showing convergences near Downtown and Long Beach	96
31	Simulated hour-averaged CO concentrations compared to measured concentrations at Downtown, Los Angeles, Lennox, Long Beach and Hollywood .	98
32	Surface CO concentrations used for 3:00 A.M. initial concentrations	99
33	At 3:00 A.M. the winds were calm and generally toward the coast	100
34	High winds throughout most of the basin with convergence near Burbank	102

LIST OF ILLUSTRATIONS, contd.

Number	Title	Page
35	The morning high concentrations have been blown into the San Gabriel Mountains and Puente Hills but a new build-up is forming in the Northwest	103
36	Evening traffic has produced a local build-up of CO over Long Beach and a large region of high concentrations corresponding to the surface wind convergence in the Burbank-Pasadena-Hollywood area	105
37	Temporal distribution of traffic for freeways and surface streets (Ref. 23)	109
38	Spatial distribution of freeway traffic (thousand vehicle miles per day) (Ref. 23)	110
39	Spatial distribution of non-freeway traffic (thousand vehicle miles per day) (Ref. 23) . .	111
40	Hour-averaged CO (in ppm) calculated with an inversion rising height is compared to the standard results with a fixed inversion height and to the measured concentrations	113
41	Macro flow diagram for computing photochemical pollution	122
42a	Initial distribution of primary pollutant A . .	131
42b	Distribution of primary pollutant A after advection	132
42c	Distribution of secondary pollutant, B, calculated from cell concentrations given in Figure 42b	133
42d	Distribution of secondary pollutant, B, calculated from Lagrangian concentration	133
43	Inversion height (feet above sea level) at 12 noon on September 30, 1969 (Ref. 17)	137
44	NO concentration in pphm at 6:00 A.M.	144

LIST OF ILLUSTRATIONS, contd.

Number	Title	Page
45	NO_2 concentration in pphm at 6:00 A.M.	145
46	NO_2 concentration in pphm at 10:00 A.M.	146
47	O_3 concentration in pphm at 10:00 A.M.	147
48	HC concentration in ppm at 10:00 A.M.	148
49	NO_2 concentration in pphm at 3:00 P.M.	150
50	O_3 concentration in pphm at 3:00 P.M.	151
51	HC concentration in ppm at 3:00 P.M.	152
52	NO_2 concentration in pphm at 6:00 P.M.	153
53	HC concentration in ppm at 6:00 P.M.	154
54	O_3 concentration in pphm at 6:00 P.M.	155

LIST OF TABLES

Table Title Page

I Calculated central values after 45 cycles for different methods (correct result: 69) 40

II PICFIC diffusion evaluation varying the number of particles per cell using the area-weighting procedure 49

III PICFIC diffusion evaluation varying the cell size using 1000 mass point particles 51

IV Results of calculation compared to analytic solution of Neuringer 62

V 3:00 A.M. to 8:00 P.M. average carbon monoxide concentrations (CO in ppm) 92

VI Results of series of tests with NEXUS 117

VII Rate coefficients for Eschenroeder's model of the hydrocarbon/nitric oxide mechanism 124

VIII Gaussian puff $(\sigma_x = 2\Delta x, \sigma_y = 2\Delta y, \sigma_z = 2\Delta z)$ central cell concentrations 135

IX Regional average of stations reporting 139

X Los Angeles APCD stations reporting most complete data -- Station 1, Downtown Los Angeles . 140
Station 60, Azusa 141
Station 79, Pasadena 142

INTRODUCTION

This paper reports the development and initial applications of a new method for the solution of the turbulent atmospheric diffusion equation. The method, called PICK, is based on the use of Lagrangian mass points and is one of a family of Particle-In-Cell techniques for the solution of partial differential equations. The turbulent atmospheric diffusion equation is the standard description of the behavior of pollutants in the atmosphere and solutions of the equation have been used extensively for air pollution simulation and prediction.

Other methods employed for the solution of the equation include analytic solutions and finite difference methods. An analytic solution of the equation can only be obtained with simplifying assumptions on the winds and diffusivities which limit the generality of the solution. Finite difference methods have difficulties in treating large gradients in the solution and also may introduce a truncation dispersion of the solution that masks the atmospheric turbulent diffusion. The PICK method is the most accurate general technique for solution of the equations. With the PICK method a solution can be obtained for any specified condition, and the method does not suffer from the difficulties encountered with finite difference methods.

The purpose of this study was the development of the PICK method (Section 1) and the demonstration of the method in the solution of evaluation test cases and actual air pollution problems. Test cases for the evaluation of feasibility and accuracy and for comparison to finite difference solutions were conducted with a two-dimensional computer code PICFIC, as described in Section 2. For actual air pollution studies, the PICK method was used in the three-dimensional code NEXUS. The description of NEXUS and its application to the simulation of CO in Los Angeles is given in Section 3. The computer codes PICFIC and NEXUS were developed completely by Systems, Science and Software (S^3) as proprietary S^3 computer software.

The description of photochemical smog requires terms for the chemical reactions to be added to the turbulent atmospheric diffusion equations. These additional terms are non-linear and couple the equation for each pollutant species. The NEXUS/P code was developed to solve the equations with the photochemical terms. In Section 4 the code NEXUS/P is described and its application to photochemical smog in Los Angeles is reported.

1. DESCRIPTION OF THE PICK METHOD

1.1 THE DIFFUSION EQUATION

This report describes a method for the numerical solution of the equation of turbulent atmospheric diffusion using Lagrangian mass points (called particles). The method is called "PICK" to emphasize the Particle-In-Cell nature of the technique as well as the K-theory approximations used in developing the atmospheric diffusion equation. The atmospheric diffusion equation is the standard mathematical description of the motion of pollutants in the atmosphere. This PICK method has been applied to the simulation of air pollution in two and three dimensions. The applications will be described in the following sections.

Particle-In-Cell methods have been developed and used in the PIC computer code for simulating compressible hydrodynamics[1] and in the MAC (Marker And Cell) computer code for incompressible fluid dynamics.[2] These applications have been reviewed by Harlow.[3] In the PIC code, mass is associated with each particle and as it crosses a cell boundary it transports cell averaged momentum and energy. Cell quantities for density, pressure, velocity and temperature are calculated from the particles and an equation of state for the fluid. The particle positions are changed satisfying mass, momentum and energy conservation during each time increment. In the MAC code, the particles are Lagrangian markers that are used to delineate fluid boundaries or free surfaces, or to tag the fluid. The MAC particles are Lagrangian positions and do not enter directly into any calculation, whereas the PIC particles are used to represent the fluid.

Diffusion is not simulated in either the PIC or the MAC code. These codes were developed using particles, in part, to eliminate the dispersive errors inherent in other methods. The PICK method introduced in this report also has been developed to eliminate dispersive errors, those found in finite difference solutions of the atmospheric diffusion equation. The particles in PICK represent pollutant mass. Changes in particle position are calculated to simulate pollutant mass transport due to both advection and diffusion as specified by the turbulent atmospheric diffusion equation.

The equation describing turbulent atmospheric diffusion,

$$\frac{\partial c}{\partial t} = -\overline{u}\frac{\partial c}{\partial x} - \overline{v}\frac{\partial c}{\partial y} - \overline{w}\frac{\partial c}{\partial z} + \frac{\partial}{\partial x}\left\{K_x \frac{\partial c}{\partial x}\right\} + \frac{\partial}{\partial y}\left\{K_y \frac{\partial c}{\partial y}\right\} + \frac{\partial}{\partial z}\left\{K_z \frac{\partial c}{\partial z}\right\} , \qquad (1.1)$$

equates the time rate of change of concentration c , $\frac{\partial c}{\partial t}$, to advective rate of change of c , $-\overline{u}\frac{\partial c}{\partial x} - \overline{v}\frac{\partial c}{\partial y} - \overline{w}\frac{\partial c}{\partial z}$, due to the mean velocity field $(\overline{u},\overline{v},\overline{w})$ plus the divergence of the turbulent flux with the position dependent eddy diffusivity (K_x,K_y,K_z) ,

$$\frac{\partial}{\partial x}\left\{K_x \frac{\partial c}{\partial x}\right\} + \frac{\partial}{\partial y}\left\{K_y \frac{\partial c}{\partial y}\right\} + \frac{\partial}{\partial z}\left\{K_z \frac{\partial c}{\partial z}\right\} .$$

Since we will be considering general wind fields, there is no assumption that the x-direction diffusion term is negligible. The PICK method could actually be developed for a tensor eddy diffusivity as discussed by Calder,[4] but for simplicity and clarity the coordinate axis have been assumed to be the principle axes for the diffusivity tensor. Discussions of the derivation of this equation are given in several sources, e.g., Sutton,[5] Section 4 and of the applications to atmospheric diffusion in Sutton, Section 8 and Pasquill,[6] Section 3.

The diffusion equation can be re-written in a form suitable for the PICK method by use of the following definitions. The turbulent flux, for example, in the x-direction is $-K_x \frac{\partial c}{\partial x}$, so an equivalent velocity, the "turbulent flux velocity," can be defined such that

$$u_f c = -K_x \frac{\partial c}{\partial x} \qquad (1,2a)$$

or

$$u_f = -\frac{K_x}{c} \frac{\partial c}{\partial x} \quad . \qquad (1,2b)$$

In a similar manner, in the other directions, the turbulent flux velocity will be

$$v_f = -\frac{K_y}{c} \frac{\partial c}{\partial y} \qquad (1.2c)$$

and

$$w_f = -\frac{K_z}{c} \frac{\partial c}{\partial z} \quad . \qquad (1.2d)$$

If a tensor eddy diffusivity were used, the turbulent flux velocity could be written as

$$u_{fi} = -\sum_j \frac{K_{ij}}{c} \frac{\partial c}{\partial x_j} \quad , \qquad (1.2e)$$

where the subscripts are used for the three directions. This is the novel feature at the heart of the PICK method — the diffusion terms are incorporated into a velocity. With these definitions, Eq. (1.1) becomes

$$\frac{\partial c}{\partial t} + \overline{u}\frac{\partial c}{\partial x} + \overline{v}\frac{\partial c}{\partial y} + \overline{w}\frac{\partial c}{\partial z} = - \frac{\partial}{\partial x}(u_f c) - \frac{\partial}{\partial y}(v_f c) - \frac{\partial}{\partial z}(w_f c) \qquad (1.3a)$$

or by substituting the divergence of the mean wind fluxes, ($\overline{u}c$, $\overline{v}c$ and $\overline{w}c$):

$$\frac{\partial c}{\partial t} + \frac{\partial(\overline{u}c)}{\partial x} + \frac{\partial(\overline{v}c)}{\partial y} + \frac{\partial(\overline{w}c)}{\partial z} - c\left(\frac{\partial \overline{u}}{\partial x} + \frac{\partial \overline{v}}{\partial y} + \frac{\partial \overline{w}}{\partial z}\right) = - \frac{\partial(u_f c)}{\partial x}$$

$$- \frac{\partial(v_f c)}{\partial y} - \frac{\partial(w_f c)}{\partial z} \quad . \qquad (1.3b)$$

Now and in all further discussions we will restrict our considerations to a divergence-free mean velocity (an incompressible mean flow) field which can be expressed as

$$\frac{\partial \overline{u}}{\partial x} + \frac{\partial \overline{v}}{\partial y} + \frac{\partial \overline{w}}{\partial z} = 0 \quad . \qquad (1.4)$$

That is, the mean velocity field $(\overline{u},\overline{v},\overline{w})$ is solenoidal. Thus, the term multiplying the concentration in Eq. (1.3b) is zero and the remaining terms can be regrouped to give

$$\frac{\partial c}{\partial t} = - \frac{\partial(u+u_f)c}{\partial x} - \frac{\partial(v+v_f)c}{\partial y} - \frac{\partial(w+w_f)c}{\partial z} \quad . \qquad (1.5)$$

It is apparent in this form of the diffusion equation that the concentration is being transported by the sum of the mean and turbulent flux velocities. This sum, called the "total equivalent transport velocity," is

$$\begin{aligned} u &= \bar{u} + u_f \\ v &= \bar{v} + v_f \qquad (1.6) \\ w &= \bar{w} + w_f \ . \end{aligned}$$

The diffusion equation then reduces to the form

$$\frac{\partial c}{\partial t} + \frac{\partial uc}{\partial x} + \frac{\partial vc}{\partial y} + \frac{\partial wc}{\partial z} = 0 \ . \qquad (1.7)$$

This equation is identical in form with the equation of continuity for a general compressible fluid, namely,

$$\frac{\partial \rho}{\partial t} + \frac{\partial u\rho}{\partial x} + \frac{\partial v\rho}{\partial y} + \frac{\partial w\rho}{\partial z} = 0 \qquad (1.8)$$

where ρ denotes the fluid density. It is this special fact that is the basis for the PICK method as applied to the diffusion problem. By the device of introducing the "turbulent flux velocity" through Eq. (1.2) and the artifact of the "total equivalent transport velocity," the original problem of turbulent atmospheric diffusion is transformed into one describing the advective changes of fluid density in a compressible fluid moving in the fictitious velocity field (u,v,w) of total equivalent transport velocities. Since the continuous field variable ρ representing the fluid density can be visualized in a discrete manner as the total mass of elementary fluid particles in a unit volume of space, while the changes of density may be considered in terms of changes in the number of elementary mass particles occupying the unit volume, the fundamental basis for the particle-in-cell treatment becomes evident. The mass particles follow the fluid motion in the fictitious velocity field (u,v,w). That is to say, they are Lagrangian particles in the non-solenoidal field of total equivalent transport velocity. Their number in any cell will determine the concentration of pollutant for the original diffusion problem.

Eq. (1.7) will be the working equation for the PICK method and will be referred to as the diffusion equation later in this paper.

To complete the discussion, the boundary conditions for the original problem must be transformed into conditions within the field of fictitious total velocities. For the original problem governed by Eq. (1.1), the boundary conditions will involve specification of the domain boundaries of the vector of total material flux, i.e., the vector $\vec{F}$ having components:

$$
\begin{aligned}
F_x &= \bar{u}c - K_x \frac{\partial c}{\partial x} \\
F_y &= \bar{v}c - K_y \frac{\partial c}{\partial y} \qquad (1.9) \\
F_z &= \bar{w}c - K_z \frac{\partial c}{\partial z} \ .
\end{aligned}
$$

Evidently,

$$
\begin{aligned}
F_x &= uc \\
F_y &= vc \qquad (1.10) \\
F_z &= wc
\end{aligned}
$$

so that the vector $\vec{F}$ is directly proportional to the fictitious total velocity vector. For typical boundary conditions the flux normal to a boundary is required to be zero (simulating an impervious surface), or to equal a specified value (simulating a transmittive boundary with flow into the region) or to be proportional to the local concentration (simulating reactions or absorption at a surface). The next section describes how the diffusion equation is solved and how these boundary conditions are handled in the PICK method.

1.2 THE PICK METHOD

The diffusion equation as written in Eq. (1.7) expresses the conservation of matter for pollutant when considered as a compressible fluid being advected by the field of fictitious total velocity. It expresses the fact that for any small fixed volume of space the rate of increase of pollutant concentration must equal the net pollutant flux that is produced by the fictitious total velocity through the boundary surface.

In the PICK method the spatial distribution of pollutant is represented by means of a large number of Lagrangian mass particles, i.e., ones of constant mass of pollutant that are simply advected in the fictitious field of total velocity. Physical space is divided into cells of a fixed Eulerian grid and the particles carry pollution from cell to cell as they are moved by the fictitious velocity field. Since this field is a non-solenoidal one, it will cause particles to move apart or together, and thus uneven distributions may result. In order to simulate satisfactorily the spatial distribution of pollution, a sufficiently large number of particles must be used in each grid cell. This requirement is examined and quantified in a later section.

Concentrations in the PIC method are computed as cell averages. Two prescriptions for calculating cell concentrations from the particle masses have been tried. In the simplest prescription the cell concentration is the sum of the masses of all particles in the cell divided by the cell volume. Thus, when a particle crosses a cell boundary, the particle mass is added to the cell entered and subtracted from the cell it has left. The second prescription is equivalent to an area (or volume) apportionment of a particle's mass between cells based upon overlap considerations. For this purpose the particle mass is regarded as uniformly spread over an area (or volume) the size of a cell and centered on the particle position. The overlap with adjacent cells then determines the mass apportionment between them. These alternatives are illustrated for two dimensions in Figure 1. The first alternative, being simpler, is faster to compute while the area-averaging procedure has the effect of smoothing out the artificial gradients caused by quantizing the pollutant mass into particles. The results of calculations comparing these alternatives will be discussed in Section 2. In both cases the values of the cell concentration is associated with the cell center. Initially, the particles are placed at random within each cell. The number of particles in a cell is determined by the initial concentration in the cell.

The fictitious total velocity field that is used to transport the particles in the PICK method is defined by its values at the centers of the cells. For each such center, the mean velocity vector $(\bar{u},\bar{v},\bar{w})$ for the original real velocity field must be specified and the turbulent flux velocity calculated utilizing Eq. (1.2) with the derivatives approximated by a finite difference algorithm. For example, in the x-direction the simplest finite differencing corresponds to

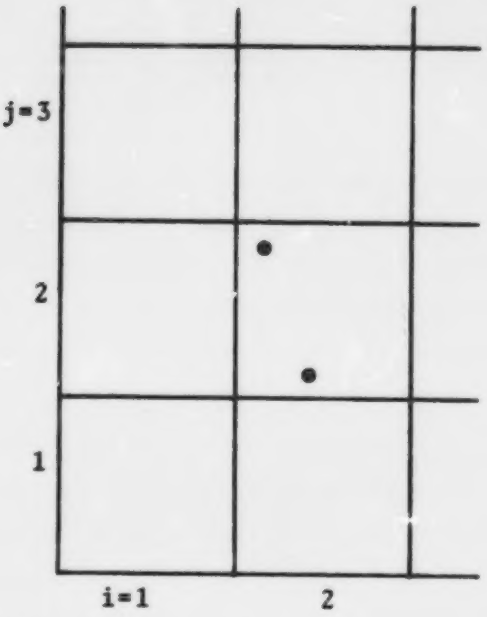

Cellular concentration in

Cell (2,2) = 2.0

(a) — Particles having infinitesimal extent.

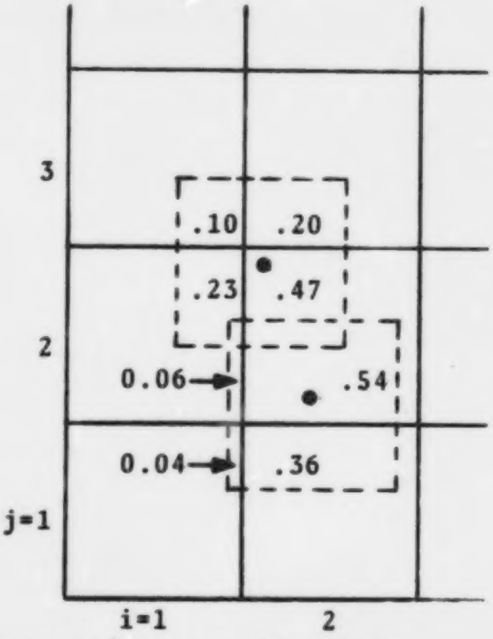
3
2
j=1
i=1
2
.10
.20
.23
.47
0.06
.54
0.04
.36

Cellular concentration in

Cell (1,1) = 0.04
(1,2) = 0.36
(2,1) = 0.29
(2,2) = 1.01
(1,3) = 0.10
(2,3) = 0.20

(b) — Particles averaged over cell volume.

Figure 1 — Calculation of Cellular Concentration from Particle Masses.

$$\left(\frac{1}{c}\frac{\partial c}{\partial x}\right)_{x_i} \approx \frac{C_{i+1} - C_{i-1}}{2\Delta x\, C_i} \tag{1.11}$$

where the concentration at the cell center $x = x_i$ is C_i and $(x_{i+1} - x_{i-1}) = 2\Delta x$. Alternative differencing algorithms are possible (such as directly approximating the logarithmic derivative), but in view of the accuracy achieved by this simple algorithm (as will be discussed in Section 2) no others have been used.

The fictitious total velocity at each cell center is then given by the sum of the original mean velocity and the turbulent flux velocity. Once this has been calculated for any elementary time-interval $(t, t+\Delta t)$ the particles in the cells are then moved for this interval with a velocity obtained by linear interpolation according to the position of the particle between the centers of adjacent cells, using the velocity at each center. This is illustrated for two dimensions in Figure 2. Using $\vec{v}$ to denote the total velocity vector (u,v)

$$\vec{v}(x,y) = \left\{(y - y_j)\left[\frac{\vec{v}_{i+1,j+1}(x - x_i) + \vec{v}_{i,j+1}(x'_{i+1} - x)}{\Delta x}\right]\right.$$
$$\left. + (y_{j+1} - y)\left[\frac{\vec{v}_{i+1,j}(x - x_i) + \vec{v}_{ij}(x_{i+1} - x)}{\Delta x}\right]\right\} \Big/ \Delta y \tag{1.12}$$

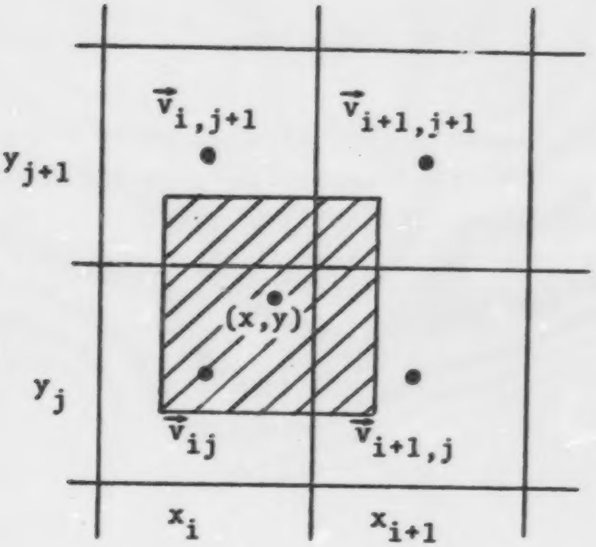

Figure 2 — Area Weighting Interpolation for Total Velocity.

The shaded rectangular area is cell-sized and centered at the particle position. Rearranging the terms in Eq. (1.12) gives

$$\begin{aligned}\vec{v}(x,y) = \frac{1}{\Delta x \Delta y}\Big[&(x - x_i)(y - y_j)\vec{v}_{i+1,j+1} \\ &+ (x_{i+1} - x)(y - y_j)\vec{v}_{i,j+1} \\ &+ (x - x_i)(y_{j+1} - y)\vec{v}_{i+1,j} \\ &+ (x_{i+1} - x)(y_{j+1} - y)\vec{v}_{ij}\Big] \;. \qquad (1.13)\end{aligned}$$

The product $(x - x_i)(y - y_j)$ multiplying $\vec{v}_{i+1,j+1}$ is the shaded area overlapping cell (i+1,j+1) in Figure 2. Similarly, the other products give the areas of the overlap with the other cells. In three dimensions the analogous volume overlap is used.

In the PICK method the calculation to advance the particle configuration in time proceeds in steps or cycles, each of which calculates the desired quantities for time $t + \Delta t$ in terms of those at time t (an "explicit" time advancement procedure)

$$\begin{aligned} x(t + \Delta t) &= x(t) + u\Delta t \\ y(t + \Delta t) &= y(t) + v\Delta t \quad . \end{aligned} \tag{1.14}$$

The velocities are the fictitious total velocities determined for the beginning of the time interval and interpolated to initial particle positions. These are held constant throughout any elementary time interval. It is evident that the magnitude of the time interval Δt must be restricted, as otherwise a particle could pass through many cells in a cycle and well out of the region for which its velocity was interpolated. This could result in large inaccuracies and even instabilities in the solution. Limiting the time step so that no particle moves more than four-tenths of a cell within any one cycle has been used as an empirical rule to avoid this problem.

Every particle is advanced each cycle to a new position using Eq. (1.14). Thus, the particle traces out in time a trajectory for the pollutant mass. Movies of these trajectories can be made showing the flow of pollutants.

Boundary conditions are introduced by modifications of the fictitious total velocities. Thus, impervious barriers are simulated by not allowing particles to be transported across these boundaries. Transmittive boundaries are permeable to particles which continue to pass through them with the total velocity.

This completes the cycle by which the particle method solves the diffusion equation for a time step. In each cycle the cellular concentrations are calculated from particle masses, the fictitious total velocity for each cell is calculated as the sum of mean wind velocity and the turbulent flux velocity (which is calculated by finite differencing the cellular concentrations), and the particle positions are updated using an interpolated total velocity. Time is stepped along cycle by cycle and the position of each particle traces a trajectory of the pollutant mass.

1.3 SIMULATION OF EMISSIONS AND CHEMICAL REACTIONS

As pollutants are emitted into the atmosphere, additional pollutant mass must be added to the simulation. The additional pollutant mass may be added to the mass associated with a pre-existing particle at the source location, or a new particle may be generated. The new particle would enter the simulation at the source location with pollutant mass equal to that physically generated during the time interval. Pollutant generation is treated separately for each cell of the grid. Point, line, area and volume sources can easily be simulated.

The simulation of the chemical reactions begins with a chemical mechanism — a set of chemical reactions and their reaction rate constants — assumed to be an adequate description of the relevant pollutant reactions. The chemical mechanisms can be translated into a set of chemical kinetics rate equations — coupled first-order differential equations describing the time rate of change of each reactant and product pollutant species. This will be discussed in detail in Section 4.2.

The solutions of the chemical kinetics equations determine the cell concentrations but the changes in concentrations have to be related back to particle masses. Within each cell the particle masses are re-weighted by the fractional change in concentration due to chemical reactions,

$$m(t + \Delta t) = m(t) \frac{c(t + \Delta t)}{c(t)} \quad . \qquad (1.15)$$

For each chemical species and each cell the fraction is calculated. If a pollutant species were first generated in a cell by chemical reactions, there would be no pre-existing particle to re-weight and a new particle would be introduced into the cell.

1.4 ONE-DIMENSIONAL EXAMPLE OF THE PICK METHOD

In this section a solution of a diffusion equation by the PICK method will be developed and its accuracy analyzed by comparison with a known exact analytic solution. For this purpose the diffusion equation to be solved has been simplified to describe one-dimensional constant advection, i.e., with constant and uniform velocity u and Fickian diffusion (K_x = constant K), without sources or boundaries, but including a removal rate proportional to the local concentration, as given by:

$$\frac{\partial c}{\partial t} + \bar{u}\frac{\partial c}{\partial x} = \frac{\partial}{\partial x}\left(K \frac{\partial c}{\partial x}\right) - \lambda c \quad . \qquad (1.16)$$

This removal rate can be thought of as simulating a chemical reaction of the pollutant with a major atmosphere species whose concentration is essentially unchanged by the reaction. The exact analytic solution, for constant $\bar{u}$ and K, and for an initial concentration distribution that is Gaussian centered at x = 0, of mean square deviation σ_0^2 and total mass Q, is given by

$$c(x,t) = \frac{Q}{\sqrt{\pi(2\sigma_0^2 + 4Kt)}} \exp\left[-\left\{\frac{(x - \bar{u}t)}{2\sigma_0^2 + 4Kt} + \lambda t\right\}\right]. \qquad (1.17)$$

In the PICK method, the initial concentration distribution is represented by a distribution of particles. For simplicity we will use particles of equal mass. Each of the N particles has an initial pollutant mass $m(0) = Q/N$ where N must be a large number for an accurate simulation.

The one-dimensional space is divided into cells of size Δx, with the cells numbered as in Figure 3.

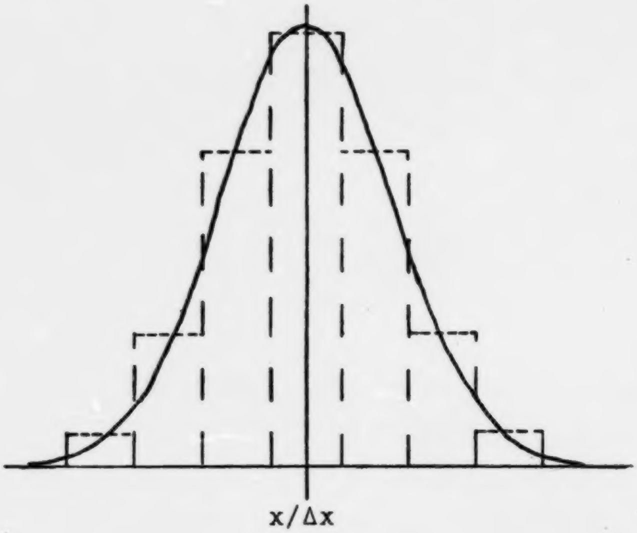

Figure 3 — Gaussian Distribution with the Approximate Cell Concentrations.

Thus, initially at $t = 0$, the number of particles in cell i centered about $x_i = i\Delta x$ is

$$n_i(0) = \frac{N}{\sqrt{2\pi\sigma_0^2}} \int_{x_i-\Delta x/2}^{x_i+\Delta x/2} \exp\left[-\frac{x^2}{2\sigma_0^2}\right] dx \tag{1.18}$$

which is a histogram of the Gaussian distribution. Note that n_i is an integer approximation to the integral the accuracy of which increases with N. If Δx is sufficiently small this can obviously be approximated by

$$n_i(0) \simeq \frac{N\,\Delta x}{\sqrt{2\pi\sigma_0^2}} \exp\left[-\frac{x_i^2}{2\sigma_0^2}\right] \tag{1.19}$$

which, of course, is also a Gaussian distribution. The steps taken in the PIC method to simulate advection, diffusion and chemical reaction will be described below using this initial distribution of particles in cells.

First the mean turbulent flux velocity is calculated for each cell. Following Eq. (1.12) this is given initially by

$$u_{fi} = -\frac{K}{2\Delta x}\left(\frac{n_{i+1} - n_{i-1}}{n_i}\right) \tag{1.20}$$

where the particle mass m_o has cancelled in the ratio of the concentrations. The number of particles per cell n_i can be substituted from Eq. (1.19) to give

$$u_{fi} = -\frac{K}{2\Delta x}\left\{ e^{(x_i^2 - x_{i+1}^2)/2\sigma_0^2} - e^{(x_i^2 - x_{i-1}^2)/2\sigma_0^2} \right\} , \quad (1.21)$$

Hence, by power series expansion of the two exponentials, assuming $(x_{i+1}^2 - x_i^2)$ and $(x_i^2 - x_{i-1}^2)$ are both small compared to σ_0^2 ,

$$u_{fi} \simeq -\frac{K}{2\Delta x}\left\{ \frac{(x_i^2 - x_{i+1}^2) - (x_i^2 - x_{i-1}^2)}{2\sigma_0^2} \right\}$$

$$\simeq \frac{K}{2\Delta x}\left\{ \frac{(x_{i+1} - x_{i-1})(x_{i+1} + x_{i-1})}{2\sigma_0^2} \right\}$$

$$\simeq \frac{Kx_i}{\sigma_0^2} \quad . \qquad (1.22)$$

The cell-centered fictitious total velocity is

$$u_i = \bar{u} + \frac{Kx_i}{\sigma_0^2} \quad . \qquad (1.23)$$

This is the fictitious total velocity that appears in Eq. (1.6) and is non-solenoidal. A particle at an initial position, say x , between x_i and x_{i+1} will have a weighted velocity given by the one-dimensional form of Eq. (1.13), namely

$$u(x) = u_i\left(\frac{x_{i+1} - x}{\Delta x}\right) + u_{i+1}\left(\frac{x - x_i}{\Delta x}\right)$$

$$= \left(\bar{u} + \frac{Kx_i}{\sigma_0^2}\right)\left(\frac{x_{i+1} - x}{\Delta x}\right) + \left(\bar{u} + \frac{Kx_{i+1}}{\sigma_0^2}\right)\left(\frac{x - x_i}{\Delta x}\right)$$

(1.24)

or by simplifying

$$u(x) = \overline{u} + \frac{Kx}{\sigma_0^2} \; . \qquad (1.24b)$$

We note in the above that although the real fluid velocity $\overline{u}$ is here postulated to be constant and uniform (and, hence, solenoidal so that $\partial\overline{u}/\partial x = 0$), both the turbulent flux velocity and fictitious total velocity are time- and space-dependent. For $t = 0$, both increase linearly with distance from the origin. In a time interval Δt the position of the particle that is initially at x will be changed by $u(x)\Delta t$ and the new position x' will be given by

$$x' = x + \left(\overline{u} + \frac{Kx}{\sigma_0^2}\right)\Delta t \qquad (1.25)$$

so that

$$x = \frac{x' - \overline{u}\Delta t}{1 + \frac{K\Delta t}{\sigma_0^2}} \; . \qquad (1.26)$$

It follows that the $n_i(\Delta t)$ particles lying in the i-th cell at the end of the time interval Δt, i.e., whose positions lie between $x' = x_i - \frac{\Delta x}{2}$ and $x' = x_i + \frac{\Delta x}{2}$ at time Δt, were initially located between the positions

$$\frac{\left(x_i - \frac{\Delta x}{2}\right) - \overline{u}\Delta t}{1 + \frac{K\Delta t}{\sigma_0^2}} \quad \text{and} \quad \frac{\left(x_i + \frac{\Delta x}{2}\right) - \overline{u}\Delta t}{1 + \frac{K\Delta t}{\sigma_0^2}}$$

respectively, that is for a total distance, say $\Delta\ell$, centered about the position $(x_i - \overline{u}\Delta t)/(1 + K\Delta t/\sigma_0^2)$ and given by

$$\Delta \ell = \frac{\Delta x}{1 + \frac{K\Delta t}{\sigma_0^2}} < \Delta x \quad . \tag{1.27}$$

But, initially, the number of particles centered in the line segment of length Δx centered on position x_i is given by Eq. (1.19), from which it follows that initially the number of particles contained in a segment of length $\Delta \ell$ centered on the position $(x_i - \bar{u}\Delta t)/(1 + K\Delta t/\sigma_0^2)$ is given by

$$\frac{N\Delta \ell}{\sqrt{2\pi\sigma_0^2}} \, e^{-\frac{(x_i - \bar{u}\Delta t)^2}{2\sigma_0^2 \, (1 + K\Delta t/\sigma_0^2)^2}} \simeq \frac{N\Delta \ell}{\sqrt{2\pi\sigma_0^2}} \, e^{-\frac{(x_i - \bar{u}\Delta t)^2}{2\sigma_0^2 + 4\, K\Delta t}} \, . \tag{1.28}$$

It follows from conservation of particles that

$$n_i(\Delta t) = \frac{N\Delta \ell}{\sqrt{2\pi\sigma_0^2}} \, e^{-\frac{(x_i - \bar{u}\Delta t)^2}{(2\sigma_0^2 + 4\, K\Delta t)}}$$

or by using Eq. (1.27) that

$$n_i(\Delta t) = \frac{1}{1 + \frac{K\Delta t}{\sigma_0^2}} \, \frac{N\Delta x}{\sqrt{2\pi\sigma_0^2}} \, e^{-\frac{(x_i - \bar{u}\Delta t)^2}{(2\sigma_0^2 + 4\, K\Delta t)}}$$

$$\approx \frac{N\Delta x}{\sqrt{\pi(2\sigma_0^2 + 4\, K\Delta t)}} \, e^{-\frac{(x_i - \bar{u}\Delta t)^2}{2\sigma_0^2 + 4\, K\Delta t}} \tag{1.29}$$

provided $K\Delta t/\sigma_0^2$ is small.

So far the effects of advection and diffusion in Eq. (1.16) have been considered. To include also the effect of the removal rate term simulating a chemical reaction, we note that this by itself produces an exponential decay of concentration so that

$$c(t + \Delta t) = c(t)\, e^{-\lambda \Delta t} \quad . \tag{1.30}$$

However, the changes in cell concentration have to be related to particle masses. Within each cell the particle masses are reweighted by the fractional change in concentration due to the chemical reaction, as specified in general by Eq. (1.15) and in particular by

$$m(\Delta t) = m(0)\, \frac{c(\Delta t)}{c(0)} = m(0)\, e^{-\lambda \Delta t} \; . \tag{1.31}$$

Finally, the cell concentration is given as the product of the number of particles in the cell and particle mass divided by the cell volume, so that

$$c(x_i, \Delta t) = n_i(\Delta t)\, m(\Delta t)/\Delta x$$

and hence for the above example

$$c(x_i, \Delta t) = \frac{Q}{\sqrt{\pi (2\sigma_0^2 + 4\, K\Delta t)}} \exp\left\{- \frac{(x_i - \overline{u}\Delta t)^2}{2\sigma_0^2 + 4\, K\Delta t} - \lambda \Delta t\right\} \tag{1.32}$$

where $Q = Nm_o$ has been used. This is in agreement with the analytic solution as given by Eq. (1.17).

1.5 ACCURACY OF THE PICK METHOD

The PICK method is a hybrid of Eulerian and Lagrangian techniques and has some of the advantages and disadvantages of each. The Eulerian nature requires an assumption of homogeneity within each fixed grid cell. The Lagrangian nature is introduced by quantization of the pollutant mass (a continuous variable) into particles (a discrete variable). The errors introduced by the quantization into particles has been evaluated operationally and is discussed in Section 2. The more particles that are used, the less mass (on the average) is represented by each particle, and the greater the variation and resolution of concentration that can be simulated. A minimum number of particles exists below which resolution and accuracy are severely degraded while the maximum number of particles is usually determined by computer capacity.

The Eulerian grid size determines the maximum spatial resolution of the solution of the atmospheric diffusion equation. Though distributions smaller than grid size are visible in the particle positions, only cell averaged concentrations are solutions of the equation. Smaller than grid size phenomena (for example, point emissions) can be represented by particles, and the accuracy of such simulations has been demonstrated by tests reported in Section 2.

The accuracy of advection simulation is limited by the Eulerian grid size and the velocity interpolation prescription. Mean wind patterns having a sub-grid scale, such as smaller atmospheric eddies, can only be included in an averaged sense as turbulent diffusion or by increasing the resolution. If the wind field for advection at time t were known sufficiently, the particle position could be expanded in a Taylor series; for example in one dimension:

$$x(t + \Delta t) = x(t) + u(x(t))\Delta t + \tfrac{1}{2}u\frac{\partial u}{\partial x}\,\Delta t^2 + \dots , \quad (1.33)$$

where $u = \partial x/\partial t$ and $\partial u/\partial t = u(\partial u/\partial x)$ have been used. The first two terms on the right correspond to Eq. (1.14) (in which $u = u(x(t))$) and the error to lowest order is given by the last term, $\tfrac{1}{2}u(\partial u/\partial x)\Delta t^2$. Thus, in order to limit errors, a limitation on the time interval is required. The time limit employed has been chosen arbitrarily and empirically, and restricts the maximum change in parcel position to four-tenths of the cell dimension. Thus, the maximum relative error in particle transport is

$$\frac{u\,\frac{\partial u}{\partial x}\,\frac{\Delta t^2}{2}}{u\Delta t} = \frac{(0.4\Delta x)^2\,\frac{1}{2u}\,\frac{\partial u}{\partial x}}{0.4\Delta x} = 0.2\,\frac{\Delta x}{u}\,\frac{\partial u}{\partial x} \quad . \quad (1.34)$$

As an upper limit $\partial u/\partial x \leq 2u/\Delta x$, then this relative error is bounded by 0.4. In actual practice, this error is less than 10 percent.

Additional inaccuracies are introduced in the simulation of diffusion – from the finite differencing used in replacing the diffusion term by the turbulent flux velocity, Eq. (1.2) and Eq. (1.12). The approximation to the logrithmic derivative in Eq. (1.12) can be expanded in a Taylor series to show the inaccuracies incurred in the prescription in Eq. (1.12) as follows:

$$\frac{c_{i+1} - c_{i-1}}{2\Delta x\ c_i} = \frac{1}{2\Delta x\ c_i}\Big\{(c_i + c_i'\Delta x + \frac{1}{2}c_i''\Delta x^2 + \frac{1}{6}c_i'''\Delta x^3 \ldots)$$

$$- (c_i - c_i'\Delta x + \frac{1}{2}c_i''\Delta x - \frac{1}{6}c_i'''\Delta x^3 \ldots)\Big\}$$

$$= \frac{c_i'}{c_i} + \frac{c_i'''\ \Delta x^2}{6c_i} + O(\Delta x^4) \quad .$$

That is, the lowest order error term in this approximation is $\frac{1}{6}\,\frac{1}{c}\,\frac{\partial^3 c}{\partial x^3}\,\Delta x^2$. This has been acceptable in all applications attempted to date since it is a small error in the diffusion term, which itself is small.

Errors introduced by the simulation of reactions will be discussed in Section 4.

1.6 SUMMARY OF THE PICK METHOD

In summary, the PICK method uses Lagrangian mass points to simulate transport by advection and diffusion as described by the differential equation for turbulent atmospheric diffusion. An Eulerian grid is used for winds, emissions and values of the concentration. The velocities used for the transport are fictitious, non-solenoidal velocities which, when multiplied by the local concentration, have a divergence equal to the turbulent diffusion and advection in the original equation. Boundary conditions of the differential equation become conditions on the particle motion and are introduced through modifications of the fictitious velocity field.

By use of the PICK method, three-dimensional solutions of the atmospheric diffusion with temporally and spatially dependent winds and diffusivities are practical. The Lagrangian particles eliminate the problems of artificially introduced dispersion that are associated with finite difference solutions of the differential equation. In applications, air pollution can even be simulated for zero wind conditions. The PICK method also lends itself to a new output form (movies of pollution as represented by particle positions) in addition to the conventional forms.

2. TESTING THE PICK METHOD

2.1 DESCRIPTION OF THE PICFIC CODE

In order to test the concepts discussed in Section 1, the PICFIC (Particle-In-Cell with FICkian diffusion) code was developed (actually PICFIC treats non-constant diffusivities and so is not restricted to Fickian diffusion). The equation being solved is the two-dimensional analogue of Eq. (1.1) (for convenience the z-direction was dropped). Boundary conditions for the edges of the grid were also ignored and all simulations were ended before any pollutants reached the grid edge. These simplifications were used because PICFIC was developed to test the advection and diffusion techniques proposed for the PICK method. The results of these tests will be discussed in Sections 2.2 and 2.3. Some additional simulations using PICFIC will be presented in Section 2.4.

A simplified flow chart of PICFIC is given in Figure 4. A detailed computer-generated flow chart is given in Volume II, Section 1, along with a listing of the coding.

PICFIC consists of three routines — the main program, CALCP and CELL. The main program sets up the problem. CALCP is the subroutine in which new particle positions are calculated using the total velocity field. CELL is an output subroutine for printing the cell concentrations.

In the main program, the 2-D velocity components U_{ij} and V_{ij}, and diffusivities K_{xij} and K_{yij} are specified

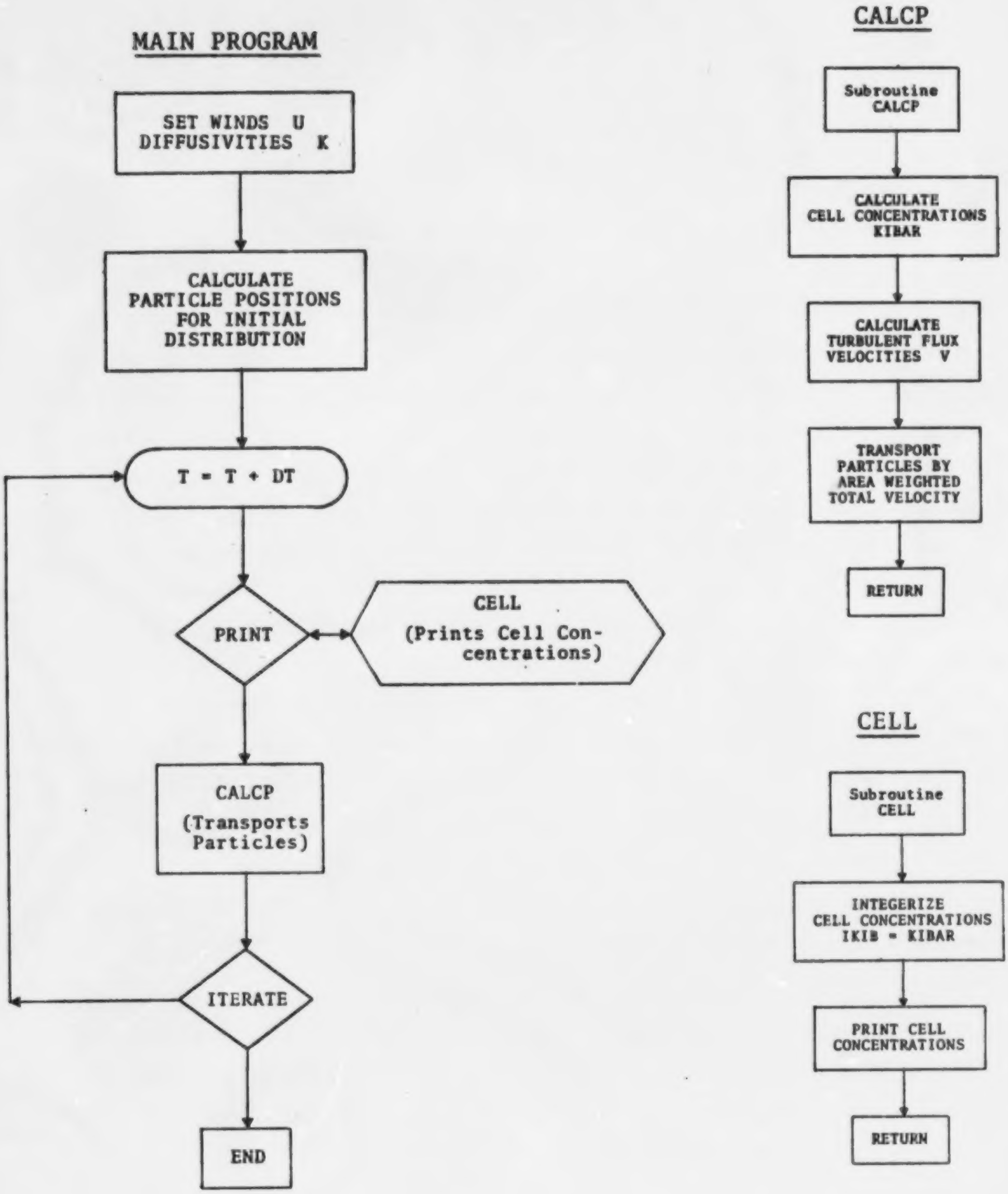
MAIN PROGRAM
SET WINDS U
DIFFUSIVITIES K
CALCULATE
PARTICLE POSITIONS
FOR INITIAL
DISTRIBUTION
T = T + DT
PRINT
CELL
(Prints Cell Concentrations)
CALCP
(Transports Particles)
ITERATE
END
CALCP
Subroutine
CALCP
CALCULATE
CELL CONCENTRATIONS
KIBAR
CALCULATE
TURBULENT FLUX
VELOCITIES V
TRANSPORT
PARTICLES BY
AREA WEIGHTED
TOTAL VELOCITY
RETURN
CELL
Subroutine
CELL
INTEGERIZE
CELL CONCENTRATIONS
IKIB = KIBAR
PRINT CELL
CONCENTRATIONS
RETURN

Figure 4 – Macro Flow Chart of the PICFIC Code.

(computer representations used are: u_{ij} = U(I,J,1) , v_{ij} = U(I,J,2) , K_{xij} = D(I,J,1) and K_{yij} = D(I,J,2) . For the problems used in testing PICFIC these values were initialized and not changed during the simulation. The test problems used a Gaussian distribution for the initial distribution of the numbers of particles per cell. The UNIVAC 1108 operating system available at S^3 has a generator for normally distributed random numbers. This was used to position particles so that the cell concentration distribution was Gaussian.

The heart of PICFIC is CALCP which transports the particles according to the PICK method. The PICK method requires the calculation of the turbulent flux velocities, from Eq. (1.2), which in turn use cell concentrations. As mentioned in Section 1, two prescriptions have been used, the first of which treats particles as mass points, the second uses an area-weighting procedure. In the first method, the cell concentration is calculated by summing the mass associated with particles in the cell. With the area-weighting procedure, each particle mass is divided among the four closest cells, in the following steps:

(1) The particle at position (X,Y) is determined to be in cell (N,M) by

$$\begin{aligned} N &= \text{TRUNCATED INTEGER}(X/DX) \\ M &= \text{TRUNCATED INTEGER}(Y/DY) \quad . \end{aligned} \tag{2.1}$$

(2) The fractional distance of the particle from the center of cell (N,M) is calculated from

$$\begin{aligned} FX &= X/DX - (N+\tfrac{1}{2}) \\ FY &= Y/DY - (M+\tfrac{1}{2}) \quad . \end{aligned} \tag{2.2}$$

(3) If these fractions are positive the particle is in the forward portion of the cell and the other closest cells have $NN = N+1$ or $MM = M+1$ indices; if negative the indices are $NN = N-1$ or $MM = M-1$.

(4) The particle mass is divided among the four cells by the fractional overlap such that

$$\begin{aligned} KIBAR(N,M) &= KIBAR(N,M) + (1-FX)\cdot(1-FY)\cdot KI \\ KIBAR(NN,M) &= KIBAR(NN,M) + FX\cdot(1-FY)\cdot KI \\ KIBAR(N,MM) &= KIBAR(N,MM) + (1-FX)\cdot FY\cdot KI \\ KIBAR(NN,MM) &= KIBAR(NN,MM) + FX\cdot FY\cdot KI \quad , \end{aligned} \tag{2.3}$$

where KIBAR is the storage location of the cell concentration and KI contains the particle mass.

Once the cell concentrations have been calculated, the difference algorithm, Eq. (1.12), is used to compute the cell centered turbulent flux velocity for each cell. The last step in CALCP is the moving of each particle. The particle's fractional overlap with the four closest cells is determined as in the above area-weighting, Steps 1 - 3. These are the fractions needed in the area-weighting for interpolation of cell velocities to the particle position,

$$\begin{aligned} VX = {} & (1-FX)\cdot(1-FY)\cdot U(N,M,1) + (1-FX)\cdot(FY\cdot U(N,MM,1) \\ & + FX\cdot(1-FY)\cdot U(NN,M,1) + FX\cdot FY\cdot U(NN,MM,1) \end{aligned} \tag{2.4a}$$

$$\begin{aligned} VY = {} & (1-FX)\cdot(1-FY)\cdot U(N,M,2) + (1-FX)\cdot(FY\cdot U(N,MM,1) \\ & + FX\cdot(1-FX)\cdot U(NN,M,1) + FX\cdot FY\cdot U(NN,MM,2) \ . \end{aligned} \tag{2.4b}$$

The interpolated X and Y components of velocity are multiplied by the time step, DT , and added to the particle coordinates:

$$\begin{aligned} X &= X + VX\cdot DT \\ Y &= Y + VY\cdot DT \ . \end{aligned} \tag{2.5}$$

This completes the particle transport cycle as coded in CALCP.

The PICFIC code requires the following computer storage:

(1) For each cell of the grid -- 7 variables;

(2) For each particle -- 3 variables .

In addition, 3,000 variables are used for storing the normally distributed random numbers and a few hundred for miscellaneous storage. For example, as compiled on the S^3 UNIVAC 1108, the PICFIC program size was 20,000 words, of which 3,000 were particle variables, 9,500 cell variables and 3,000 random numbers.

A fully commented listing of PICFIC, a computer-generated flow chart and a sample problem output are given in Volume II, Section 1. The tests made with PICFIC used the code as described and compared the calculational results with theoretical or analytic solutions.

2.2 COMPARISON OF METHODS FOR PURE ADVECTION

The accuracy of the PICK method for advection was analyzed using an off-axis wind field. The wind field was chosen off-axis because neither PICFIC nor the finite difference methods used for comparison to PICFIC are rotationally invariant. This corresponds to solving the 2-D advection equation:

$$\frac{\partial c}{\partial t} + \bar{u}\frac{\partial c}{\partial x} + \bar{v}\frac{\partial c}{\partial y} = 0 \qquad (2.6)$$

where c is the pollutant concentration, $\bar{u}$ is the x-component of velocity ($\bar{u}$ = 10 meters/second), and $\bar{v}$ is the y-component of velocity ($\bar{v}$ = 5 meters/second). The initial tribution of pollutant concentrations is given by the Gaussian:

$$c(x,y,0) = 711 \exp\left\{-\left[(x-9)^2 + (y-9)^2\right]/12.5\right\} \quad , \qquad (2.7)$$

in which $\sigma_x = \sigma_y = 2.5$ Km. The cell averaged concentration of the center cell, cell (9,9) is 69. The exact solution at time t is

$$c(x,y,t) = 711 \exp\left\{-\left[(x-9-\bar{u}t)^2 + (y-9-\bar{v}t)^2\right]/12.5\right\} \ . \qquad (2.8)$$

The calculation using the PICFIC code had a 30 × 50 grid with each cell one kilometer on a side. The size of the grid was selected to be large enough so that the deviations from the exact solution would be seen and small enough that computer costs would be kept to a minimum.

The initial distribution was constrained within the grid boundaries by setting to zero cell concentrations over eight cells from the center of the distribution. Each of the 256 cells with a non-zero concentration had a single particle. The results of this calculation are shown as a contour plot of cell concentrations in Figure 5. The initial distribution is shown in the first diagram for $T = 0$. The contour values correspond to 0.1, 10, 20, 40, and 60. The squaring-off of the outermost contour, the 0.1 value, is due to the truncation of the initial distribution, i.e., cells over eight cells away from the center of the distribution were set to zero concentration.

The results in Figure 5 show that the PICK technique can simulate advection to the accuracy of the interpolated wind field or, in this example with a constant wind field, to the accuracy of the computer. The accuracy of the PICK technique for advection is inherent in the Lagrangian nature of the particles.

Similar advection tests were made using a first-order, Fromm's fourth-order[7] and Crowley's fourth-order[8] schemes. Each of these schemes uses a splitting technique to combine integrations in each direction.[9] The first-order scheme uses the algorithm

$$c_{ij}^{n+\frac{1}{2}} = c_{ij}^{n} + \frac{\overline{u}\Delta t}{\Delta x}\left(c_{i-1,j}^{n} - c_{ij}^{n}\right)$$

$$c_{ij}^{n+1} = c_{ij}^{n+\frac{1}{2}} + \frac{\overline{v}\Delta t}{\Delta y}\left(c_{i,j-1}^{n+\frac{1}{2}} - c_{ij}^{n+\frac{1}{2}}\right) \qquad (2.9)$$

for velocities $\overline{u}$, $\overline{v} \geq 0$, and with superscripts referring to time $(t = n\Delta t)$ and subscripts for position $(x = i\Delta x$, $y = j\Delta y)$. This "upstream" differencing originated with Lelevier.[10] Mahoney and Egan[11] refer to this technique as a forward time and backward space differencing scheme and report

Time = 0 seconds

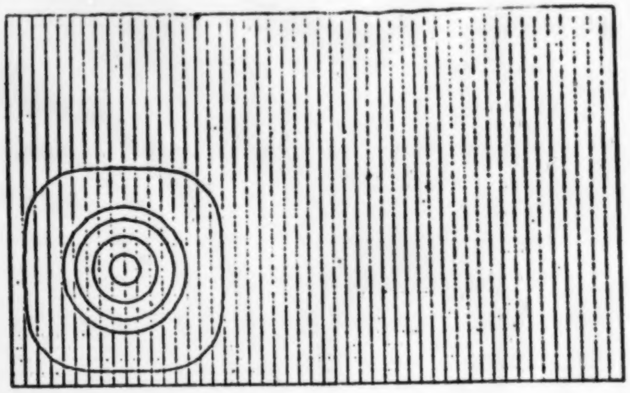

Time = 1200 seconds

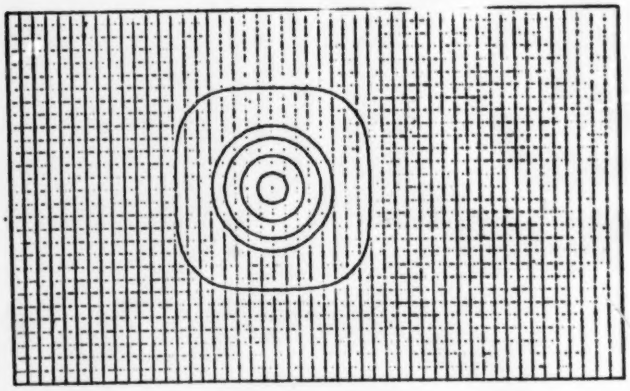

Time = 1800 seconds

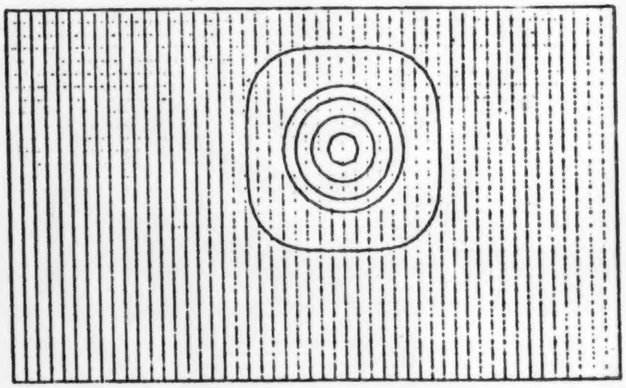

Figure 5 — PICFIC Advection Simulation Test with $\sigma_x = \sigma_y = 2.5$ Km, Contours at 0.1, 10, 20, 40 and 60.

on an artificial diffusion from the differencing truncation error having a diffusion coefficient

$$K = \frac{\bar{u}\Delta x}{2}\left[1 - \frac{\bar{u}\Delta t}{\Delta x}\right] \tag{2.10}$$

for one dimension.

A criteria for time step limitation can be based on Eq. (2.10). If the diffusivity were to be negative, spatial gradients would be amplified each time cycle and the solution would soon become meaningless. To prevent this instability, Δt is chosen such that $\left|\frac{\bar{u}\Delta t}{\Delta x}\right| \leq 1$. In two dimensions the same criteria must be met for each direction separately $\left|\frac{\bar{u}\Delta t}{\Delta x}\right| \leq 1$ and $\left|\frac{\bar{v}\Delta t}{\Delta y}\right| \leq 1$. If splitting were not used in an explicit scheme (for example, as reported by Pandolfo[12]), then the restriction is

$$\left|\frac{\bar{u}\Delta t}{\Delta x}\right| + \left|\frac{\bar{v}\Delta t}{\Delta y}\right| \leq 1 \quad .$$

With splitting the truncation diffusion is independent in each direction and the same expression holds for two and three dimensions, i.e.:

$$\begin{aligned} K_x &= \frac{\bar{u}\Delta x}{2}\left[1 - \frac{\bar{u}\Delta t}{\Delta x}\right] \\ K_y &= \frac{\bar{v}\Delta y}{2}\left[1 - \frac{\bar{v}\Delta t}{\Delta y}\right] \end{aligned} \tag{2.11}$$

for two dimensions. The effects of the truncation diffusivity in the first order scheme can be seen by the spreading of the contours in Figure 6. The flattening of the outermost contour

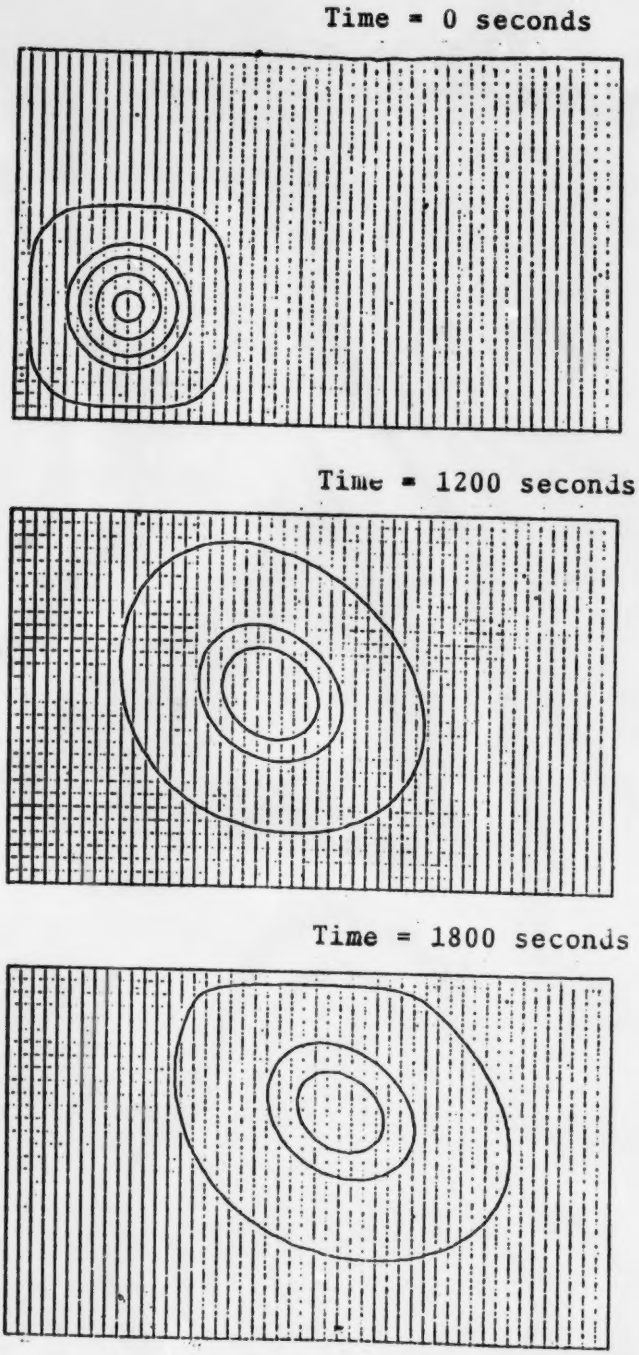

Time = 0 seconds

Time = 1200 seconds

Time = 1800 seconds

Figure 6 — First-Order Finite Difference Advection Test with $\sigma_x = \sigma_y = 2.5$ Km.

near the top of the grid is due to the distribution running off the edge of the grid.

The diffusivity calculated from the results pictured in Figure 6 was

$$K_x = 2900 \text{ m}^2/\text{sec} \qquad K_y = 1900 \text{ m}^2/\text{sec} \quad , \qquad (2.12)$$

whereas the expression for the truncation diffusivity, Eq. (2.11), gives

$$K_x = 3000 \text{ m}^2/\text{sec} \qquad K_y = 2000 \text{ m}^2/\text{sec} \qquad (2.13)$$

with $\bar{u} = 10$ m/sec , $\bar{v} = 5$ m/sec and $\Delta x = \Delta y = 1000$ m , $\Delta t = 40$ seconds. These can be contrasted with atmospheric diffusivities that have been measured in the range of 0.01 to 1000 m^2/sec. Thus, this first-order donor cell scheme would not be useful for simulating pollutant transport with these winds and cell size because the truncation diffusion would be greater than the atmospheric diffusion and would mask the real atmospheric diffusion.

The truncation diffusion originates from errors made in the truncation of the finite difference approximation of the derivatives. With the first order method, the advection equation (in one dimension) is differenced

$$\frac{c_i^{n+1} - c_i^n}{\Delta t} = -u\frac{c_i^n - c_{i-1}^n}{\Delta x} \quad . \qquad (2.14)$$

This can be expanded by a Taylor series about time n and position i , for example

$$c^n_{i-1} = c^n_i - \frac{\partial c}{\partial x}\Big)^n_i \Delta x + \frac{\partial^2 c}{\partial x^2}\Big)^n_i \frac{\Delta x^2}{2} - \dots \quad , \qquad (2.15)$$

to give the expression

$$\left\{\frac{\partial c}{\partial t}\Big)^n_i \Delta t + \frac{\partial^2 c}{\partial t^2}\Big)^n_i \frac{\Delta t^2}{2} + \dots\right\}/\Delta t = -u\left\{\frac{\partial c}{\partial x}\Big)^n_i \Delta x - \frac{\partial^2 c}{\partial x^2}\Big)^n_i \frac{\Delta x^2}{2} \dots\right\}/\Delta x \qquad (2.16)$$

The second derivatives can be related by differentiating the advection equation

$$\frac{\partial^2 c}{\partial t^2} = -u\frac{\partial}{\partial x}\left(\frac{\partial c}{\partial t}\right) = +u^2\frac{\partial^2 c}{\partial x^2} \quad . \qquad (2.17)$$

When this is substituted back into the expansion, the advection equation is recovered to first order and the coefficient of the second order term is the truncation diffusivity; dropping subscripts,

$$\frac{\partial c}{\partial t} = -u\frac{\partial c}{\partial x} + \left[\frac{u\Delta x}{2}\left(1 - \frac{u\Delta t}{\Delta x}\right)\right]\frac{\partial^2 c}{\partial x^2} + \dots \quad . \qquad (2.18)$$

One way of reducing the truncation error is to use a higher order difference scheme. In any finite difference scheme, the terms dropped can cause a dispersion of an initial distribution during each calculational time step. Higher order schemes in general increase the accuracy of the calculation and reduce the calculational dispersion. On the other hand, higher order schemes give overshoot errors in the presence of large spatial gradients and require more computations each time step. The same difficulty with large gradients is encountered in polynomial curve fitting where a high order polynomial may introduce large fluctuations in approximating a rapidly changing function.

Two fourth-order methods were compared to the PICFIC calculation (the term "fourth-order" comes from the fact that all terms up to fourth order are kept in the finite difference expansion of the time and space derivatives). Fromm's fourth-order method[7] is a space-centered flux conserving formulation; it can be expressed as follows:

$$\begin{aligned} c_{ij}^{n+1} &= c_{ij}^{n+\frac{1}{2}} + \left[F_{i-\frac{1}{2},j}^{n+\frac{1}{2}} - F_{i+\frac{1}{2},j}^{n+\frac{1}{2}}\right] \\ c_{ij}^{n+\frac{1}{2}} &= c_{ij}^{n} + \left[F_{i,j-\frac{1}{2}}^{n} - F_{i,j+\frac{1}{2}}^{n}\right] \end{aligned} \qquad (2,19)$$

where

$$\begin{aligned} F_{i,j-\frac{1}{2}}^{n} = {} & \left[7(c_{i,j-1}^{n} + c_{ij}^{n}) - (c_{i,j-2}^{n} + c_{i,j+1}^{n})\right]\alpha/12 \\ & + \left[15(c_{i,j-1}^{n} - c_{ij}^{n}) - (c_{i,j-2}^{n} - c_{i,j+1}^{n})\right]\alpha^2/24 \\ & + \left[-(c_{i,j-1}^{n} + c_{ij}^{n}) + (c_{i,j-2}^{n} + c_{i,j+1}^{n})\right]\alpha^3/12 \\ & + \left[-3(c_{i,j-1}^{n} - c_{ij}^{n}) + (c_{i,j-2}^{n} - c_{i,j+1}^{n})\right]\alpha^4/24 \quad , \end{aligned} \qquad (2,20)$$

and

$$\alpha = v\Delta t/\Delta y \quad .$$

$F_{i-\frac{1}{2},j}^{n+\frac{1}{2}}$ is obtained at time $n+\frac{1}{2}$ using similar displacements in the i subscript, with $\alpha = u\Delta t/\Delta x$. This method was used to calculate the results shown in Figure 7. The slight distortion of the outer contour is of minor importance since this is the 0.1 contour value. The major change between the first order scheme shown in Figure 6 and the Fromm fourth-order scheme is that the distribution remains peaked with the fourth order scheme but is dispersed in the first order scheme as shown by the maximum value at the center of the calculated distributions in Table I. An examination of the calculated distribution revealed that

(1) the σ^2 did not spread as a linear function, as would be the case for a diffusion error, and

(2) errors in σ^2 were less than 2×10^{-2} Km .

As mentioned previously, a higher order method would be expected to have increased accuracy over the first-order scheme and to eliminate the problem of truncation diffusion in the solution of the atmospheric diffusion equation.

TABLE I

CALCULATED CENTRAL VALUES AFTER 45 CYCLES
FOR DIFFERENT METHODS (Correct Result: 69)
$\Delta x = \Delta y = 1$

INITIAL DISTRIBUTION	METHOD	VALUE AT CENTER OF DISTRIBUTION
$\sigma = 2.5$	PICFIC	69
	First-Order	29
	Fromm Fourth-Order	68
$\sigma = 1.0$	PICFIC	69
	Fromm Fourth-Order	38
	Crowley Fourth-Order	37

Time = 0 seconds

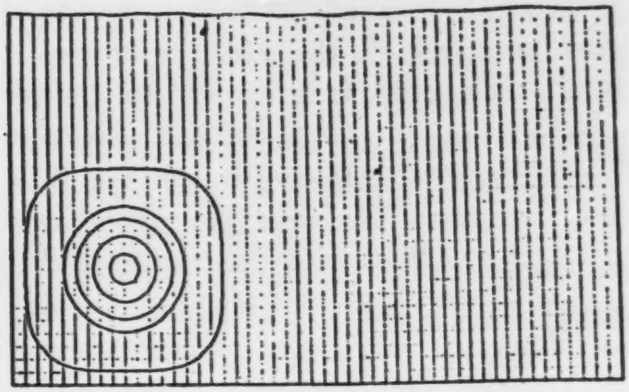

Time = 1200 seconds

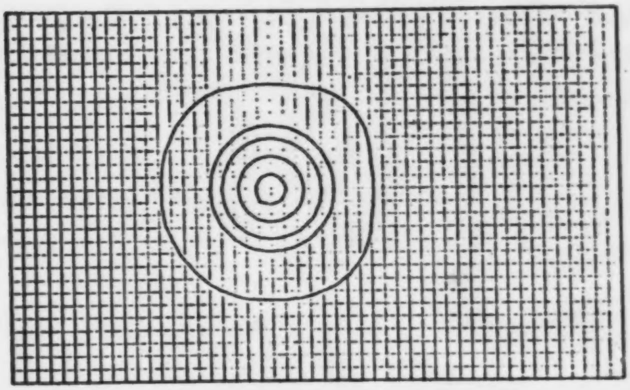

Time = 1800 seconds

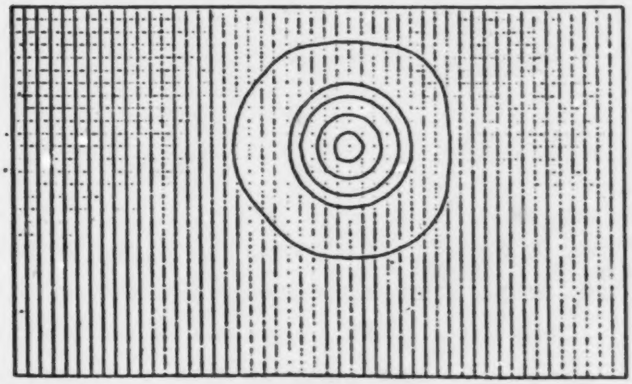

Figure 7 — Fromm Fourth-Order Method Advection Test with $\sigma_x = \sigma_y = 2.5$ Km.

A more sharply peaked distribution was also used to compare Fromm's method with the PICK technique. For an initial Gaussian distribution with $\sigma = 1$ Km (normalized to the center cell concentration = 69), PICFIC was used to calculate the diagrams of Figure 8. Again, using the PICK technique, there is no distortion. The same initial condition using Fromm's fourth-order method resulted in distortion of the distribution as shown in Figure 9. Again, the distortion of the outer contour (0.01) is not significant except to note that between these contours are negative values of concentration which are obviously unphysical. However, the major significance of this figure is the smearing of the peak values at center of the distribution. The center value is only 38 instead of the correct 69.

Crowley's fourth-order method[8] was also tested with the sharply peaked distribution. In Crowley's method, the fluxes used in Eq. (2.19) are:

$$\begin{aligned} F^n_{i,j-\frac{1}{2}} = {} & \left[9(c_{i,j-1} + c_{ij}) - (c_{i,j-2} + c_{i,j+1})\right]\alpha/16 \\ & + \left[27(c_{i,j-1} - c_{ij}) - (c_{i,j-2} - c_{i,j+1})\right]\alpha^2/48 \\ & + \left[-(c_{i,j-1} + c_{ij}) + (c_{i,j-2} + c_{i,j+1})\right]\alpha^3/12 \\ & + \left[-3(c_{i,j-1} - c_{ij}) + (c_{i,j-2} - c_{i,j+1})\right]\alpha^4/24 \end{aligned} \tag{2.22}$$

with notations and definitions as in Fromm's method. The results obtained with Crowley's fourth-order method are shown in Figure 10 for the $\sigma = 1$ Km initial distribution. These results are essentially the same as those from Fromm's method shown in Figure 9.

Time = 0 seconds

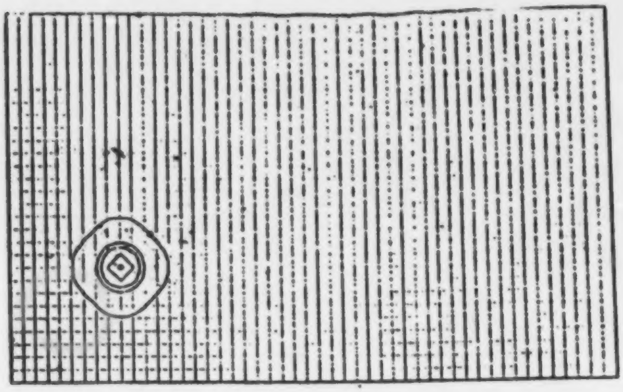

Time = 1200 seconds

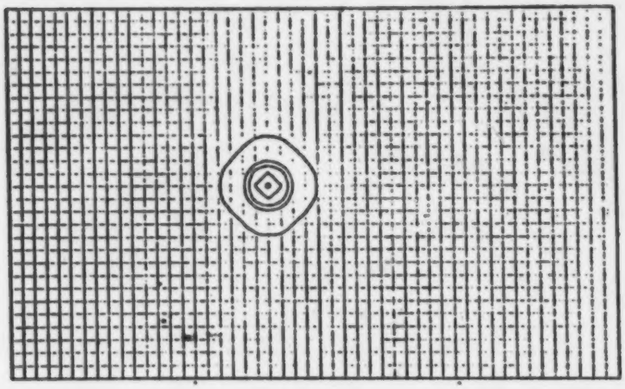

Time = 1800 seconds

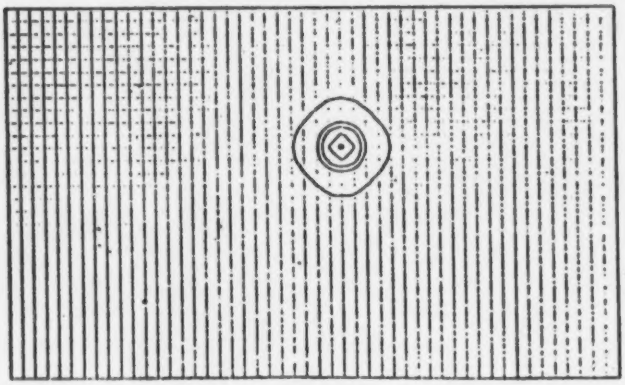

Figure 8 — PICFIC Advection Test with $\sigma_x = \sigma_y = 1$ Km.

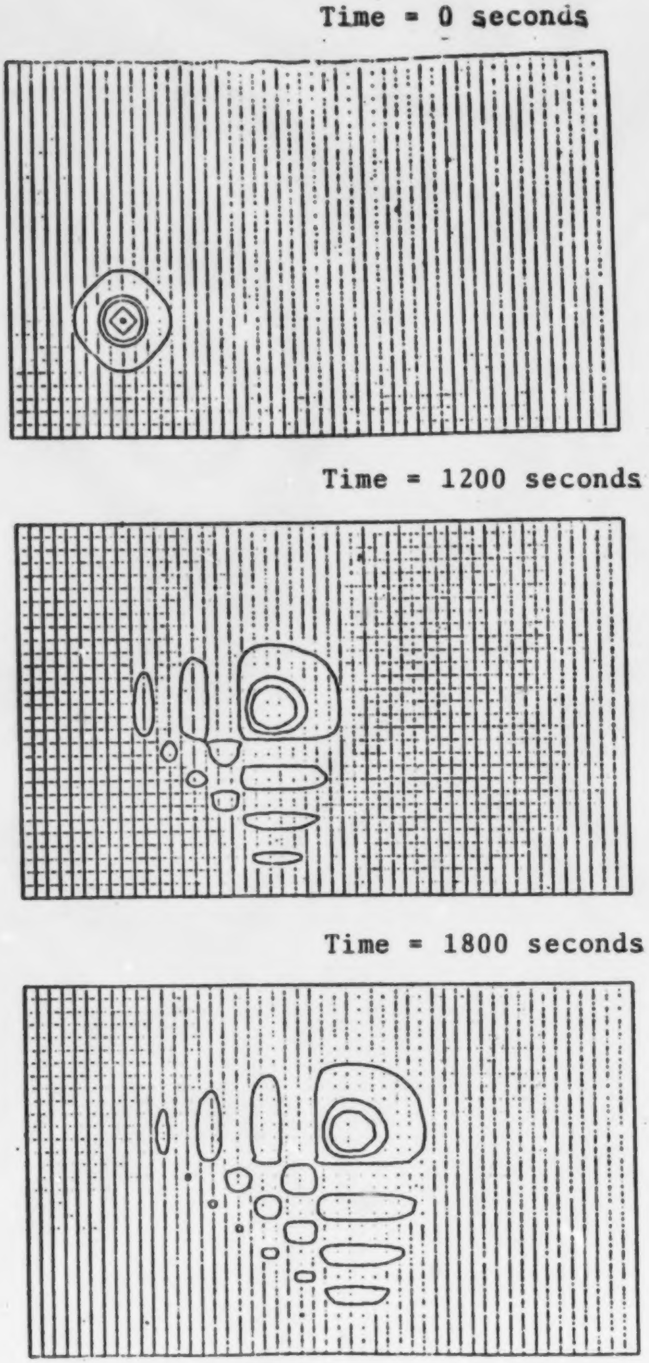

Time = 0 seconds

Time = 1200 seconds

Time = 1800 seconds

Figure 9 — Fromm Fourth-Order Method Advection Test with $\sigma_x = \sigma_y = 1$ Km.

Time = 0 seconds

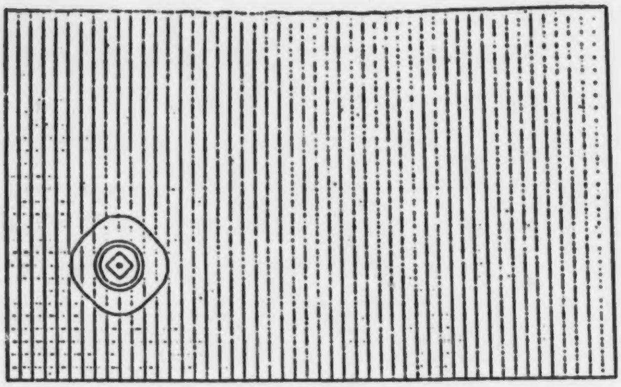

Time = 1200 seconds

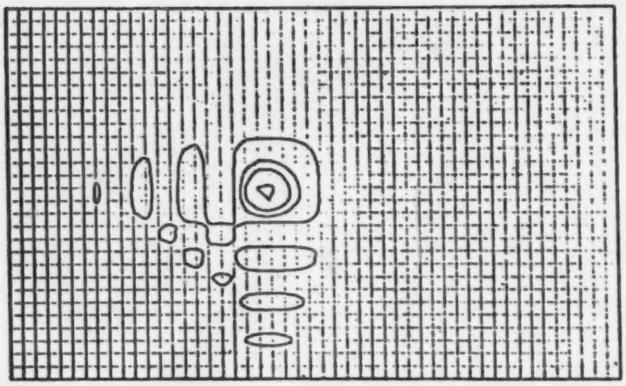

Time [illegible] 1800 seconds

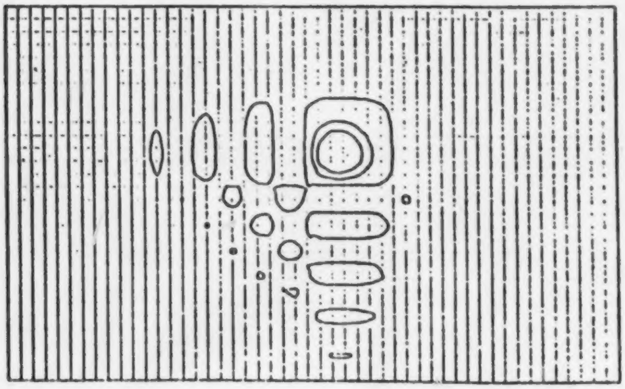

Figure 10 — Crowley Fourth-Order Method Advection Test with $\sigma_x = \sigma_y = 1$ Km.

Both fourth-order methods show an inability to treat a sharply peaked distribution. The cause of the error is depicted in Figure 11. In air pollution studies, such sharply peaked distributions could result from large single sources. Using a high order difference technique to eliminate the truncation diffusion in an air pollution model would then require special treatment of each large emission source. The PICK technique, on the other hand, permits simulation of advection irrespective of the nature of the distribution of concentration.

Computer time studies of each method were also made. The computer used for these calculations was a UNIVAC 1108 operating in a multi-processing mode with the EXEC 8 system. It was found for the illustrated calculations that the first-order method took 15 seconds, both fourth-order methods required 19 seconds, while the PICFIC calculation was completed in 12 seconds. The PICFIC calculation for which the results are plotted used 200 particles initially placed at cell centers within the initial distribution. Another calculation was performed with the PICFIC code in which 1,000 particles were placed at random within the initial distribution. The corresponding computational time increased to 18 seconds. The results of the PICFIC calculations for pure advection were independent of the number of particles used.

2.3 EVALUATION OF DIFFUSION SIMULATION

The second test of the PICK technique addressed the question of how many particles are needed for a given resolution. As mentioned above, the PICK technique accurately simulates advection with as few as one particle per cell for each cell having a non-zero concentration. On the other hand, with the simulation of diffusion the velocity field is non-solenoidal and requires that particles move apart or disperse,

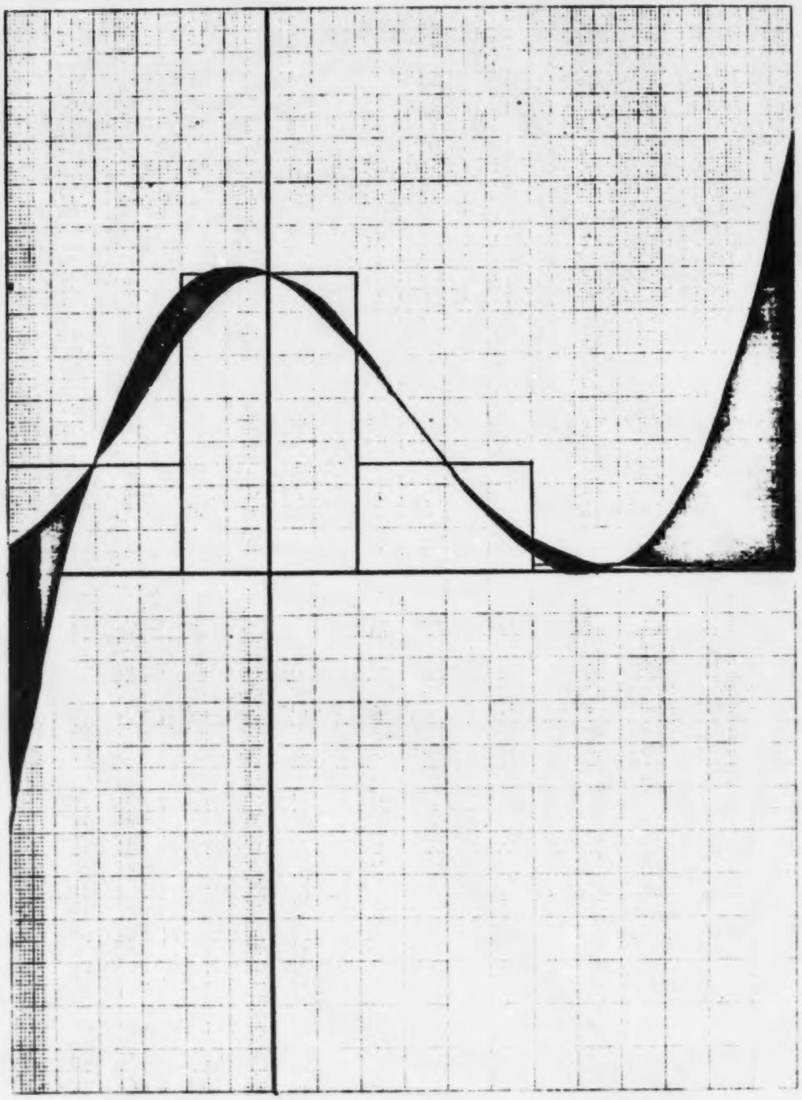

Figure 11 – Curve fitting with a polynomial. Pictured is a Gaussian curve and an approximating cubic polynomial. This picture corresponds to the polynomial fitting used in calculating the fourth-order flux scheme for the $\sigma = 1$ initial distribution. The shaded areas correspond to the errors in the fit.

even within a single cell. Diffusion can be calculated only in a collective sense, and a large number of particles are needed for accuracy.

A test problem was generated for evaluating the accuracy of the PICFIC code in simulating diffusion. The grid consisted of 50 by 27, 1 kilometer square cells. A wind parallel to the (x) axis having magnitude $\overline{u} = 10$ meters/second and a symmetric diffusivity constant $K_x = K_y = 10^3$ meters^2/second were used. The wind field parallel to the axis was chosen so that diffusion both parallel and perpendicular to advection could be studied, i.e., in the y-direction there is no wind so there is only pollutant transport by diffusion, and in the x-direction advection is much greater than diffusion so there is primarily advective transport. The initial pollutant distribution was Gaussian with $\sigma_x = \sigma_y =$ 1 Km. The solution was calculated to $t = 3200$ seconds and the mean position and standard deviation in both directions of the distribution were determined. Analytically, these are given by

$$
\begin{aligned}
\overline{x} &= x_o + \overline{u}t & \qquad \overline{y} &= y_o + \overline{v}t \\
\sigma_x^2 &= \sigma_o^2 + 2K_x t & \qquad \sigma_y^2 &= \sigma_o^2 + 2K_y t \quad .
\end{aligned}
\tag{2.23}
$$

The accuracy of the calculation was evaluated by comparing computed PICFIC results with the analytic formulas, Eq. (2.23). "Effective" velocities and "effective" diffusivities (corresponding to a linear least squares fit of the positions and standard deviations at each time cycle) were calculated and compared to the correct values ($\overline{u} = 10$ m/sec, $\overline{v} = 0$, $K_x = K_y = 10^3$ m^2/sec). Table II shows these values for four calculations corresponding to 1,000, 500, 100, and 10 particles, all using the area weighting procedure in the calculation of cell concentrations.

TABLE II

PICFIC DIFFUSION EVALUATION VARYING THE NUMBER OF PARTICLES PER CELL USING THE AREA-WEIGHTING PROCEDURE

	CORRECT	EFFECTIVE			
		Number of Particles Used			
		1000	500	100	10
$\overline{u}$	10.0 m/sec	10.0	10.0	10.0	10.0
$\overline{v}$	0.0 m/sec	-2.9×10^{-7}	3.0×10^{-7}	-1.4×10^{-7}	-3.6×10^{-5}
K_x	1.0×10^3 m^2/sec	0.93×10^3	0.92×10^3	0.81×10^3	0.42×10^3
K_y	1.0×10^3 m^2/sec	0.93×10^3	0.91×10^3	0.80×10^3	0.30×10^3
	Computational time (seconds)	37	23	11	8

These results once again confirm the ability of the PICK technique to simulate advection accurately. Even with as few as 10 particles the effective velocities are the same as the imposed wind velocity. The effective diffusivity does depend on the number of particles used in the calculation. The results show 93 percent agreement with 1,000 particles. With 100 particles, the agreement has dropped to 80 percent. There is only qualitative agreement in diffusivities with 10 particles. The correct final pollutant distribution has $\sigma^2 = 7.4 \text{ Km}^2$. Thus, 90 percent of the pollutant mass (corresponding to 2σ in each direction) is spread over a 90 Km^2 circle or the corresponding 100 cells. For 10 or even 100 particles, this distribution requires the particles to be spread thin, and, as a result, averaged processes may be poorly represented. Significantly, the effective diffusivity was less accurate towards the end of the calculation, when the distribution was the most diffuse. In the case of 100 particles, the effective diffusivity dropped to 60 percent of the correct value after the distribution was spread over 30 cells. This suggests that a lower limit of approximately three particles per cell is needed for accuracy. This agrees well with experience gained with PIC (the hydrodynamics code using the particle-in-cell method with no diffusion) where 10 particles per cell are recommended.[1]

Additional information was gained from these test calculations: an estimate of the speed of PICFIC and of the distribution of time between particle and cell related computations. Every time step requires $3\text{-}5 \times 10^{-5}$ seconds to process each cell in each dimension, and $1\text{-}3 \times 10^{-4}$ seconds for each particle computation. On the S^3 UNIVAC 1108, this corresponds to 10-15 operations per cell per cycle per dimension and 40-100 operations per particle per cycle per dimension. Computer storage requirements were described in Section 2.1.

The alternate method of calculating cell concentrations, using the mass point procedure, was also tested. It has advantages for the simulation of chemical reactions (as will be discussed in Section 4). The area-weighting procedure provided a smoothing in concentrations, but by not using area-weighting for concentrations, a computational time savings of 14 percent in the particle related computations was achieved for the PICFIC code. Area-weighting is still used to interpolate the velocity field in the calculation of particle velocities. This modification resulted in slightly poorer statistics for the diffusion simulation as shown in Table III for 1,000 particles and a 50 × 27 grid.

TABLE III

PICFIC DIFFUSION EVALUATION VARYING THE CELL SIZE USING 1000 MASS POINT PARTICLES

	CORRECT	EFFECTIVE		
		Grid Size		
		25 × 14	50 × 27	100 × 54
$\bar{u}$	10.0 m/sec	10.0	10.0	10.0
$\bar{v}$	0.0 m/sec	-6.8×10^{-6}	-6.5×10^{-6}	-5.4×10^{-6}
K_x	1.0×10^3 m²/sec	1.4×10^3	0.90×10^3	0.76×10^3
K_y	1.0×10^3 m²/sec	0.85×10^3	0.87×10^3	0.73×10^3
	Computational time (seconds)	14	32	107

A set of computations was made to determine the effects on diffusion simulation accuracy of doubling and halving the cell size. The PICFIC code without area-weighting (using the mass point procedure) was used for these test calculations. These results are shown in Table III. The accuracy of the advection simulation was unchanged by the grid size variation. In the case of double-sized cells (grid size 25 × 14), the accuracy of the simulated diffusion was degraded by lack of resolution. Physically, this case would correspond to a pollutant distribution localized to a variance of one-fourth of a cell size. When the resolution was increased by halving the cell size (grid size 100 × 54), the simulated diffusion was degraded. This degradation was due to an insufficient number of particles per cell to define the distribution accurately as it spreads. Towards the end of this calculation, the distribution is spread over 300 cells. This corresponds to about three particles per cell; with so few particles per cell, the diffusion calculation becomes inaccurate as was discussed previously. During the first 1,000 seconds of the calculation, the effective diffusivities averaged 0.84×10^3 meters/second in the x and y directions, respectively.

These tests have shown the accuracy of the PICK method by comparing the first (mean position) and second (mean square deviation) moments of the concentration distribution calculated by PICFIC with their correct values. Different distributions may have the same first and second moments. To demonstrate that the PICK method accurately simulates diffusion preserving the initial Gaussian shape of the distribution, normalized x and y distribution plots are shown in Figures 12 and 13. In Figure 12, the initial x and y cell concentration distributions used in the test are shown along with a normal curve. After 41 cycles of PICFIC (with both diffusion and advection)

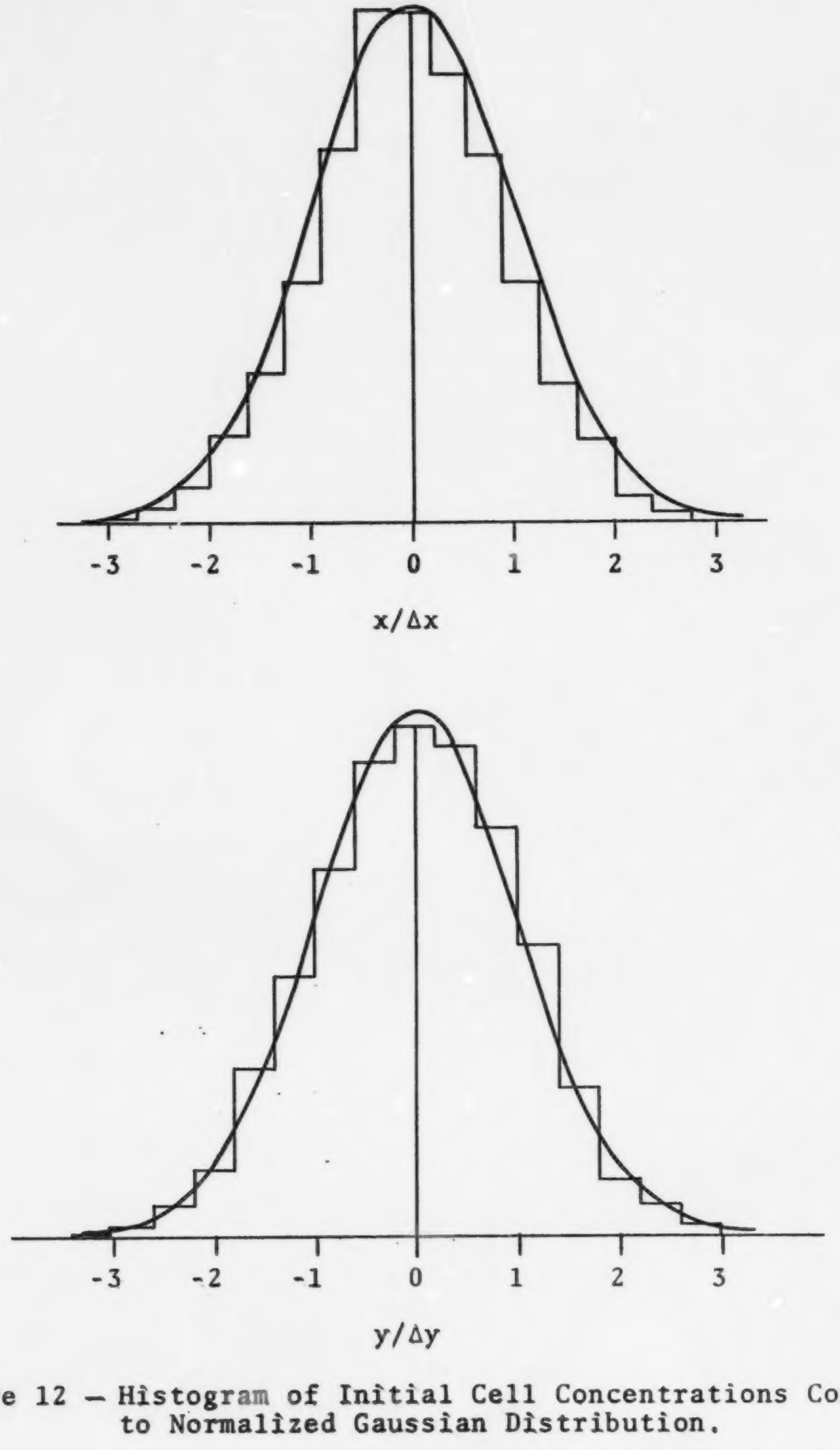

Figure 12 — Histogram of Initial Cell Concentrations Compared to Normalized Gaussian Distribution.

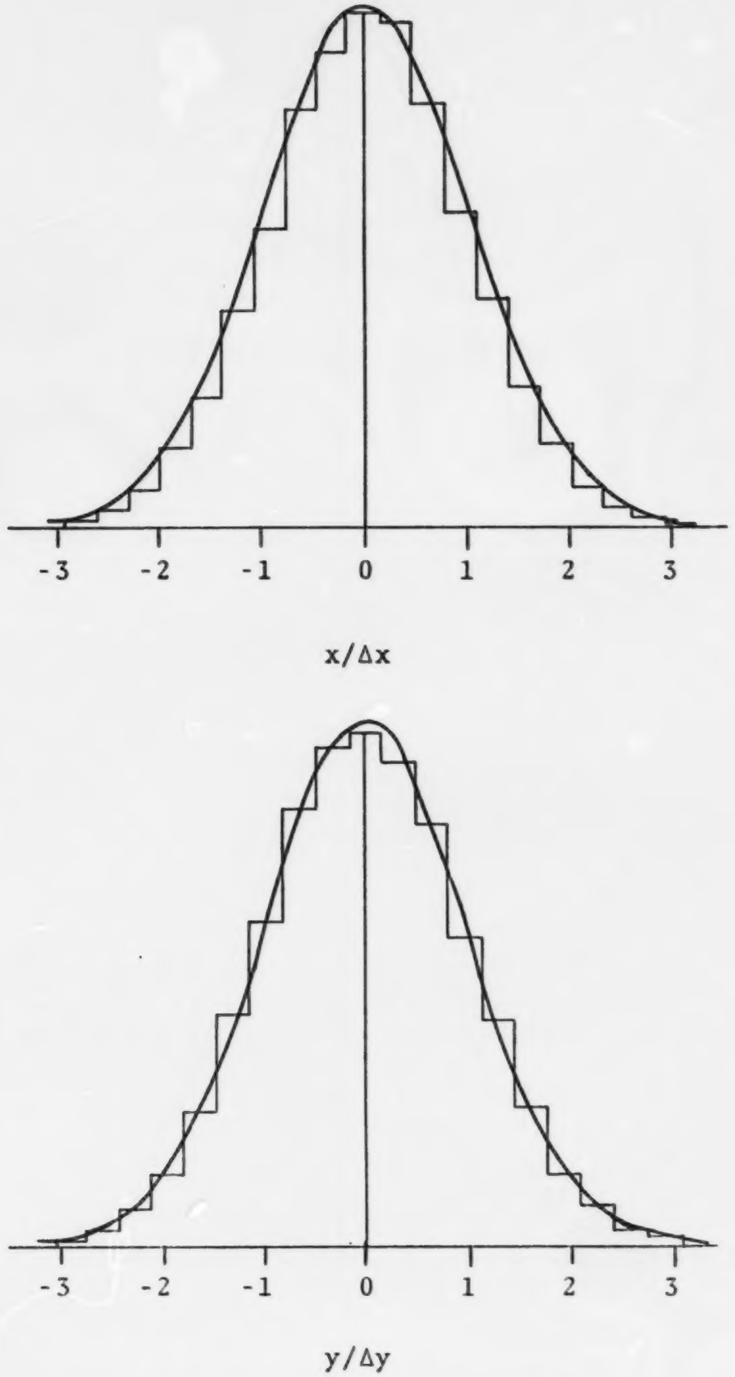

Figure 13 – Renormalized 41st Cycle of PICFIC Calculation (both Advection and Diffusion) Compared to Normalized Gaussian Distribution.

the calculated distributions are renormalized (to $c(0) = 1$ and $\sigma = 1$) and plotted with a normal curve in Figure 13. The shape of the distribution is properly maintained by the PICK method calculation. From these plots, it can be seen that the accuracy after 41 cycles is as good as the initial distribution.

2.4 PICFIC SIMULATIONS

In this section, a number of additional simulations using the PICFIC code will be presented. First, for completeness, the original PICFIC simulations are included even though they have been reported elsewhere.[13] These original simulations were made to show the capabilities of the PICK method to reproduce the effects found in the atmosphere — anisotropic diffusion, inversion layer and wind shear.

The PICFIC code permits two forms of graphically presenting calculated data: plots of particle positions and contour plots. Particle plots represent pollutant concentrations by density of particles and thus are useful for qualitative assessment of large amount of data. The contour plots are computer-generated and show the usual angularity due to computer contouring techniques. The calculational grid is not shown but consists of 1,250 cells (25 × 50).

Figure 14 illustrates a single puff of pollutant emitted on the left and carried downwind (to the right), and displayed at three instants of time. Both types of data plotting are shown for comparison. In this case no diffusion was permitted and Figure 14 shows that the PICK method introduces no artificial diffusion. When a constant diffusivity is assumed, the usual Gaussian puff results as shown in Figure 15. Figure 16 illustrates the effects of anisotropic diffusion. The effect of an inversion at the emission height

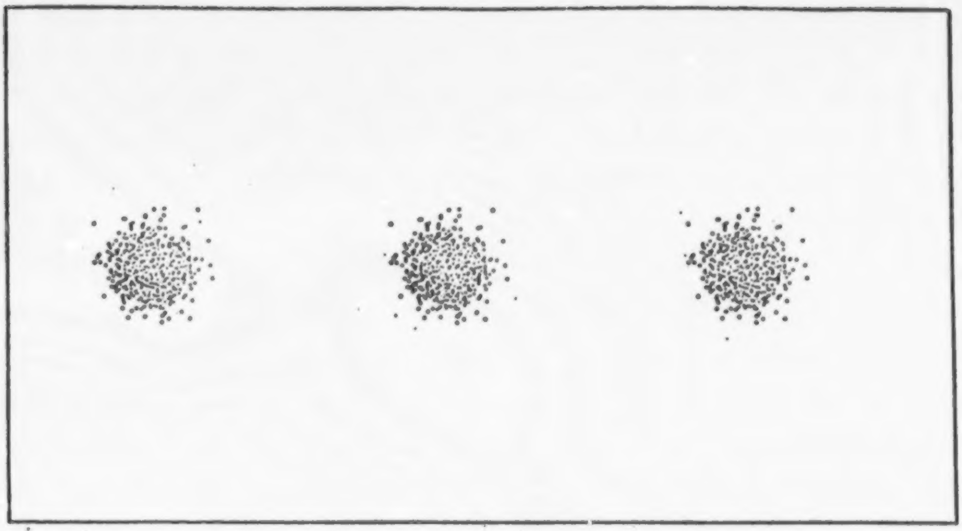

Figure 14a – Pollutant cloud advection in constant wind field with no diffusion. Three time instants are displayed together for comparison.

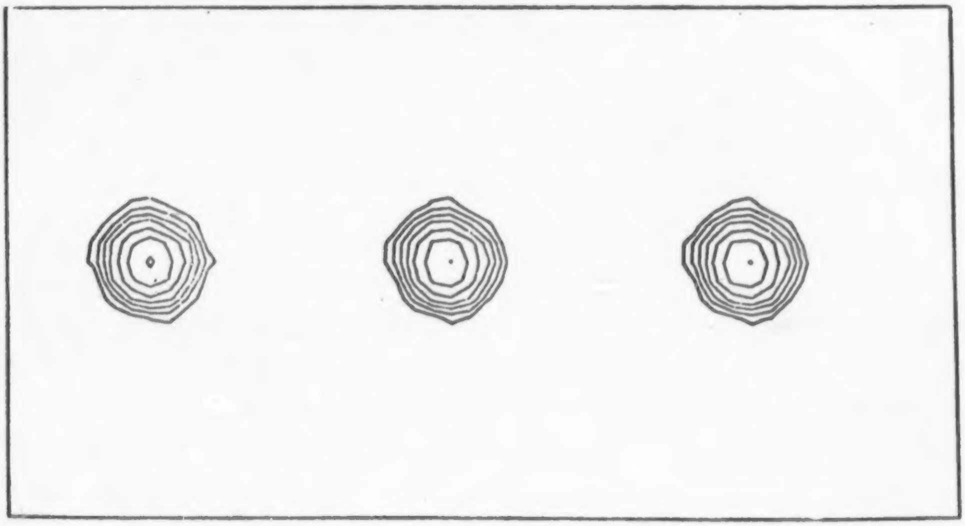

Figure 14b – Same as Figure 14a. The contours are for integer powers of 2 in pollutant concentration.

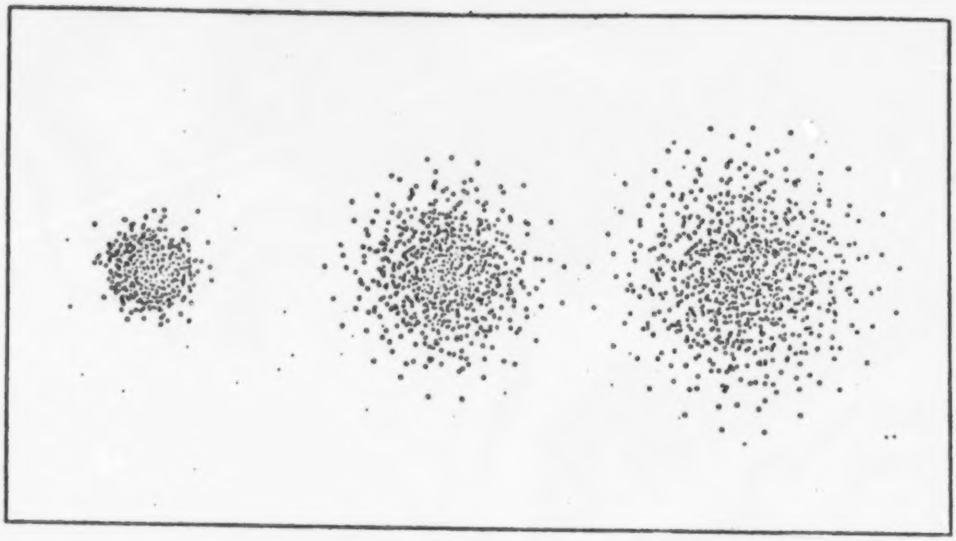

Figure 15a — Pollutant cloud advection in constant wind field with spherically symmetric diffusion.

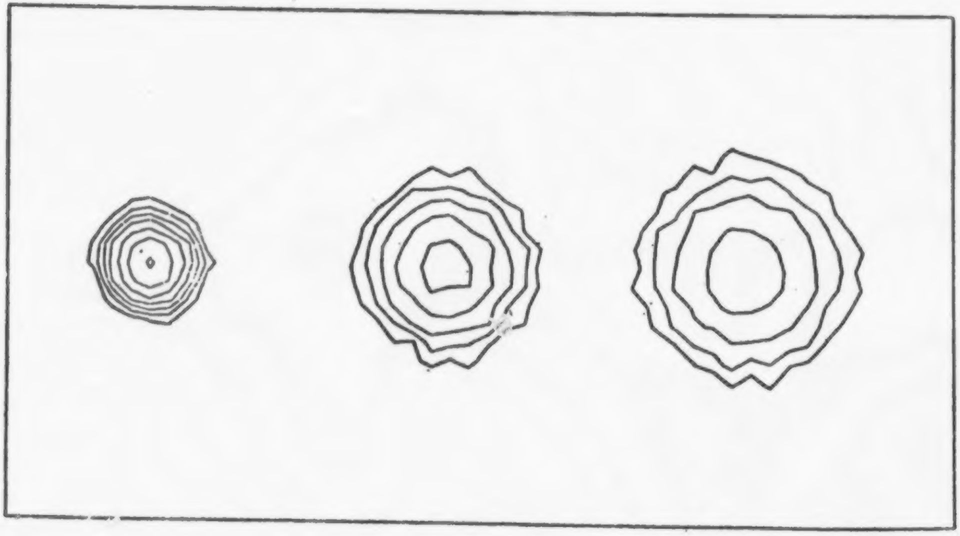

Figure 15b — Same as Figure 15a. Contours at integer powers of two.

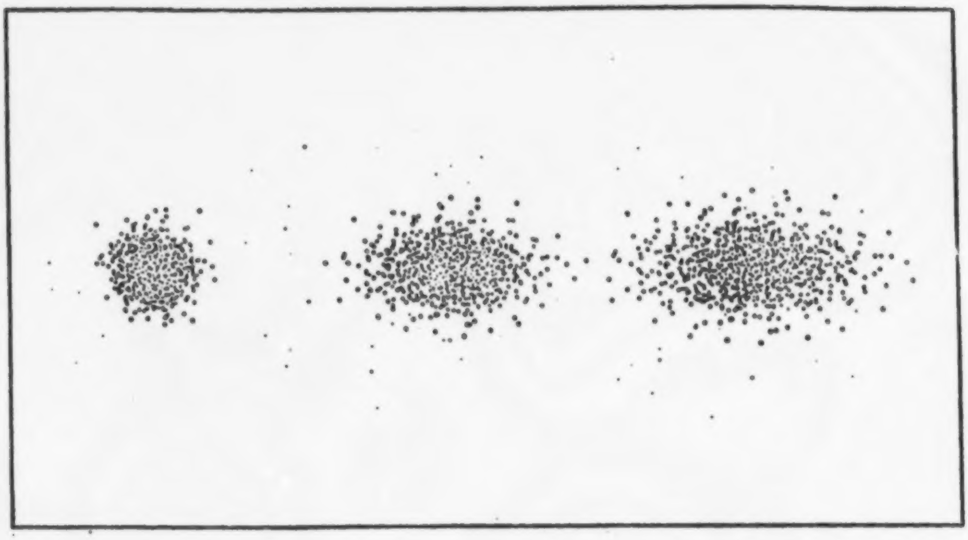

Figure 16a – Pollutant cloud advection in constant wind field with aspherical constant diffusion.

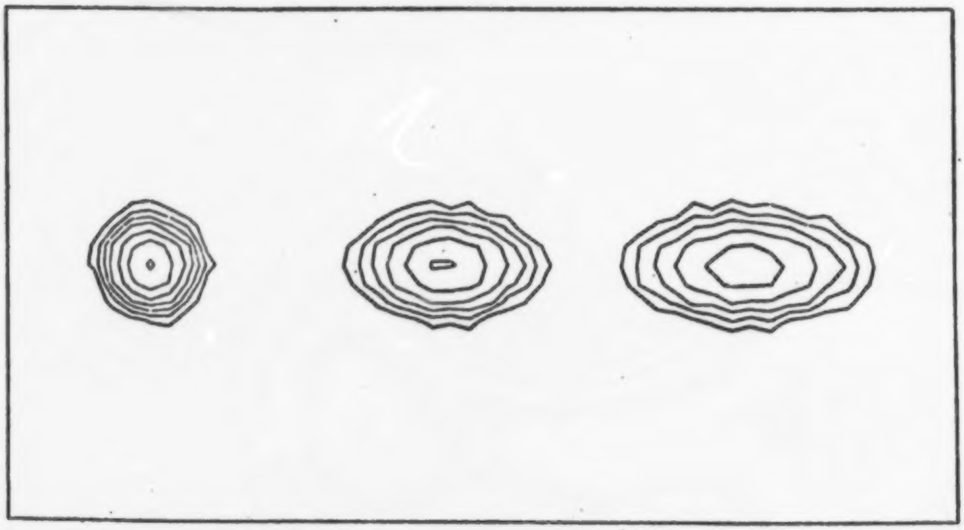

Figure 16b – Same as Figure 16a, Contours at integer powers of two,

is depicted in Figure 17. Lastly, the dispersion caused by wind shear and by constant diffusivity on a single puff is shown in Figure 18.

The most complex test case run to date was suggested by Taylor:[14] a particulate puff in a shear wind. The specifications of the test were: an initial two-dimensional point release at 10 meters above ground of particulate matter in a gravitational field in the negative y-direction, having a terminal velocity (v_t = 1 m/sec) in a linear shear wind ($\bar{u}$ = y m/sec) and isotropic turbulent diffusivity ($K_x = K_y$ = 1 m²/sec). The equation being solved is more general than the atmospheric diffusion equation, Eq. (1.1), due to a term for the terminal velocity of the particulate matter, $-v_t \frac{\partial c}{\partial t}$. The equation can be written as:

$$\frac{\partial c}{\partial t} + \bar{u}\frac{\partial c}{\partial x} - v_t\frac{\partial c}{\partial y} = \frac{\partial}{\partial x}\left\{K_x\frac{\partial c}{\partial x}\right\} + \frac{\partial}{\partial y}\left\{K_y\frac{\partial c}{\partial y}\right\} \quad . \qquad (2.24)$$

This has the same form as the atmospheric diffusion equation with $\bar{v}$ replaced by $-v_t$ and so the PICK method can be used for the solution. The solution is just a special case of a general analytic solution in two dimensions for particulates in a linear shear wind reported by Neuringer.[15] PICFIC was used with a 75 × 16 grid, in which $\Delta x = \Delta y$ = 1 meter, and 1,000 particles. The calculation was begun after the puff had spread to a $\sigma > 1$ meter, at t = 0.5 seconds. Table IV shows the results of the calculation compared to the analytic solution of Neuringer. The 0.5 sec initial conditions for PICFIC have a 10 percent error in standard deviations due to the random positions of the particles and the coarseness of the cell resolution. By 3.0 seconds the puff had started to approach the edges of the grid and the calculation was stopped. This was after 75 cycles and so an adequate evaluation was

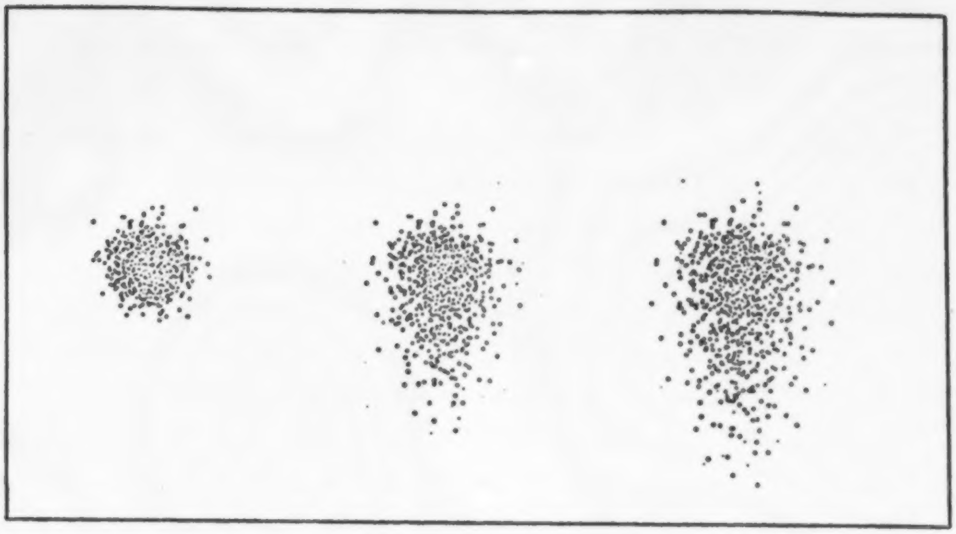

Figure 17a — Pollutant cloud advection in constant wind field with aspherical, position-dependent diffusion. Model of an inversion at the source height.

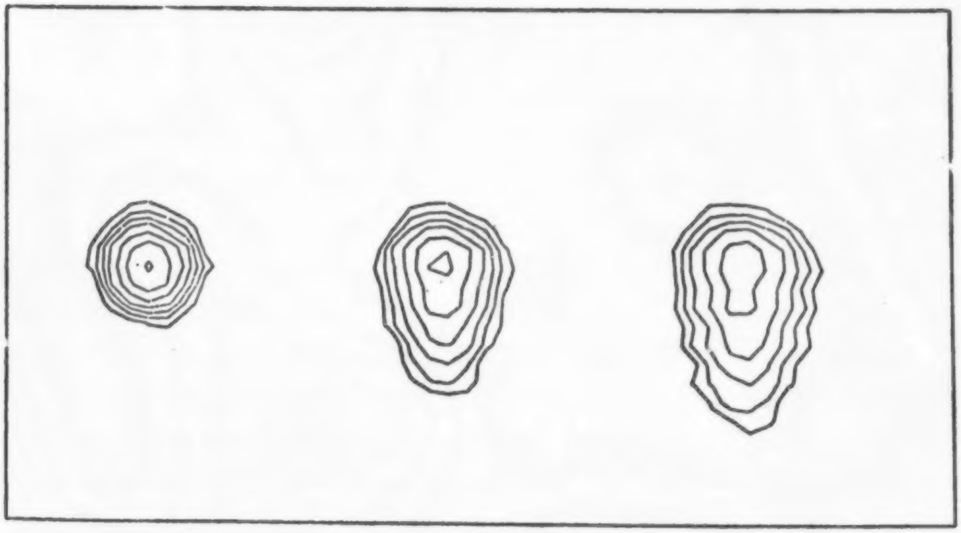

Figure 17b — Same as Figure 17a. Contours at integer powers of two.

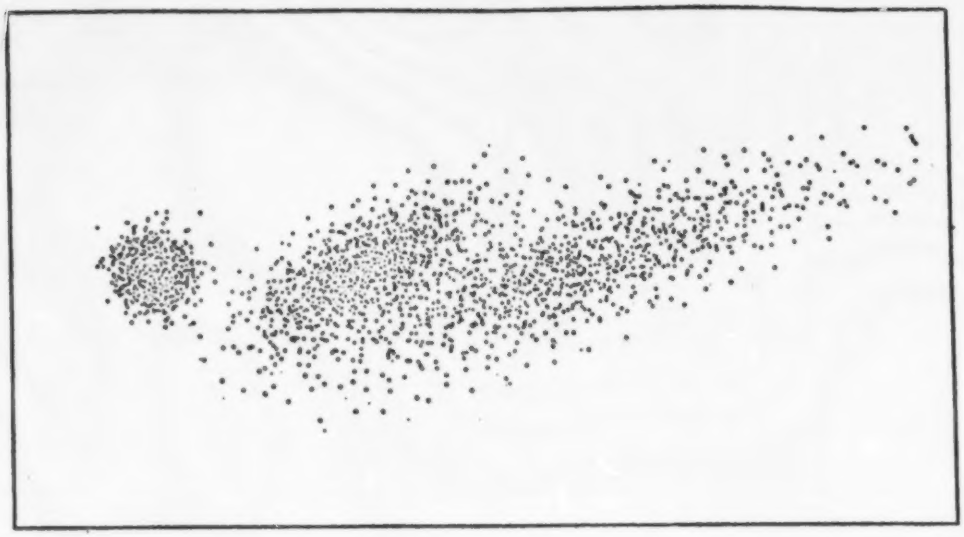

Figure 18a — Pollution cloud advection in shear wind field with spherically symmetric diffusion, three separate times are depicted as the cloud moves to the right.

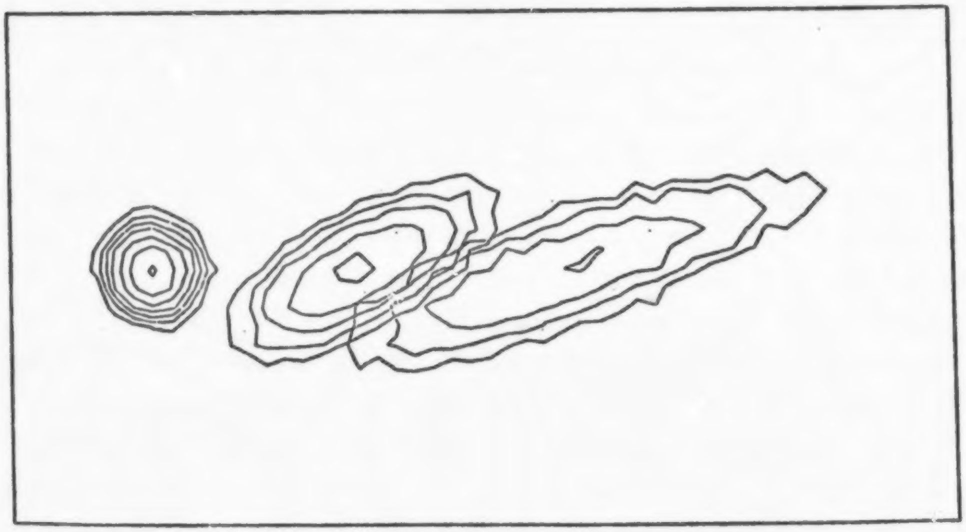

Figure 18b — Same as Figure 18a. Contours at integer powers of two.

TABLE IV

Time (sec)	PICFIC (meters)				ANALYTIC (meters)			
	$\bar{x}$	$\bar{y}$	σ_x	σ_y	$\bar{x}$	$\bar{y}$	σ_x	σ_y
0.5	15.4	10.00	1.14	1.11	15.4	10.00	1.04	1.00
1.0	19.7	9.50	1.67	1.46	20.0	9.50	1.63	1.41
2.0	27.7	8.50	3.06	1.98	28.5	8.50	3.05	2.00
3.0	34.7	7.53	4.87	2.34	36.0	7.53	4.86	2.41

possible. In comparison with the analytic solution at 3.0 seconds, the PICFIC puff had not spread as far in the vertical, and perhaps had not responded to the high velocities at the upper levels and so was retarded in mean x position. Still these errors are less than the initial 10 percent error.

One final test was made in which the accuracy of representing a point source by a distribution with a spread of less than Δx was evaluated. An initial Gaussian distribution with standard deviation of one-eighth of a cell dimension was used in this test. The wind and diffusivity used was the same as in the diffusion tests described in Section 2.3 and the evaluation was the same — a least-square linear fit to the mean positions and standard deviations to calculate effective velocities and effective diffusivities. The effective velocities were correct to three significant places due to the Lagrangian nature of the PICK particles. The effective diffusivities were 92 percent and 60 percent of the correct values in the parallel and cross wind directions, respectively. Thus, while in the

PICK method, strictly speaking, only the cell concentrations are a solution of the atmospheric diffusion equation, the simulation of sub-grid distributions is only slightly degraded. The implication of this empirical result is that small scale distributions, as for example due to point source emissions, can be included in PICK simulations without any special considerations.

2.5 SUMMARY

The two-dimensional PICFIC code has been used to evaluate the accuracy of the PICK method for solution of the equation of turbulent atmospheric diffusion by simulation of advection and diffusion. The accuracy for advection was independent of the number of particles per cell (as long as at least one per cell is used for each cell with non-zero concentration) and was as accurate as the wind field specified at grid cell centers. Diffusion is simulated using a non-solenoidal velocity field so particles must be sufficiently dense to simulate the non-uniform transport. Test problems conducted with the PICFIC code established that the simulated diffusion was less than the correct diffusion when there were too few particles per cell. In a simulation with PICFIC using ten particles per cell, the effective diffusivity in the simulation was over 90 percent of the correct value. With three particles per cell, the effective diffusivity in the simulation had dropped to 60 percent of the correct diffusivity.

PICFIC was used to simulate advection and diffusion of a sub-grid scale distribution ($\sigma = \Delta x/8$). Though PICK was developed to solve the diffusion equation to resolution of a grid cell, the sub-grid scale distribution was advected with an effective wind velocity equal to the correct value to three significant places and was diffused with an effective diffusivities of 92 and 60 percent of the correct values in the parallel and cross wind directions, respectively.

Comparisons of PICK and finite difference methods of solution for pure advection showed the PICK method introduced no artificial dispersion and could obtain an accurate solution for sharply peaked distributions. The results of the first-order finite difference technique were a rapid dispersion of the test distribution, corresponding to a truncation diffusivity, $K = \frac{u\Delta x}{2}\left[1 - \frac{u\Delta t}{\Delta x}\right]$. The fourth-order techniques tested advected a broad distribution ($\sigma = 2.5\ \Delta x$), but could not solve the equation with a sharply peaked distribution (with $\sigma = 1.0\ \Delta x$, negative concentrations were calculated).

The computer storage requirements for the PICFIC code were seven variables for each cell, three variables for each particle, and 3,000 variables used for random positions. This resulted in a 20,000 word computer program for test calculations reported. Analyzing the computational time required for the tests has shown the following time requirements for the S^3 UNIVAC 1108:

- Cell-related calculations: 10-15 basic computer operations or $3\text{-}5 \times 10^{-5}$ seconds per cycle per dimension and
- Particle-related calculations: 40-100 basic computer operations or $1\text{-}3 \times 10^{-4}$ seconds per particle per cycle per dimension.

Using the PICFIC code, the PICK method was used to simulate:

- Pure advection in constant wind field;
- Advection in a shearing wind field;
- Turbulent diffusion (with at least three particles per cell);
- Anisotropic and inhomogeneous diffusion (two component diffusivity and inversion layer); and
- Settling of particulate matter in a gravitational field.

3. NEXUS SIMULATION OF CARBON MONOXIDE IN LOS ANGELES

After testing the PICK method in two dimensions with the PICFIC code, the method was applied to solve the three-dimensional atmospheric diffusion equation, Eq. (1.1). The resulting code was named NEXUS, an acronym for Numerical EXamination of Urban Smog. NEXUS was developed to solve the general atmospheric diffusion equation and thus to simulate air pollution in three dimensions including temporally and spatially variable sources, winds and turbulent diffusivities.

The NEXUS code was applied to the simulation of carbon monoxide (CO) in Los Angeles on September 23, 1966. The particular day and pollutant were chosen to correspond to an air pollution simulation reported by Lamb.[16] The meteorological data compiled by Lamb was used in this NEXUS application. This minimized the effort required to make the calculation and also permitted a comparison of both models. The meteorological data obtained from Lamb consisted of maps of hourly (3:00 A.M. to 8:00 P.M.) isotacks and streamlines for surface winds, and the diffusivities ($K_x = K_y = 1.2\ m^2/sec$, $K_z = 0.6\ m^2/sec$) below the inversion height (1,000 feet) used in his work. NEXUS requires specification of the winds in three dimensions throughout the volume of the simulation. The winds aloft were chosen in a divergence-free manner.

Carbon monoxide was considered inert for the seventeen hour simulation. That is, the simulation contained no CO sinks; the only CO depletion occurred by flow out of the basin.

Since Lamb's CO source inventory was not available, other published data were required to construct the emissions inventory. The main source of CO in Los Angeles is traffic, contributing 97.7 percent of the 11,000 tons per day as reported by the Los Angeles Air Pollution Control District source inventory.[17] Eschenroeder and Martinez[18] published a Los Angeles County traffic distribution for 1951 that they attributed to Teague[19] but has since been traced to Larson, et.al.[20] Both spatial and temporal distributions were reported. This 1951 traffic distribution was used, but was normalized to the 1966 daily CO emissions.

The initial CO concentrations throughout the volume of the basin were required to initialize the simulation (at 3:00 A.M.). The only available data were ground level observations at 12 Los Angeles County Air Pollution Control District (APCD) monitoring stations. These data were interpolated on the surface by Lamb; aloft concentrations were arbitrarily assumed to fall off to a background level of 5 ppm. The methods used to enter the initial concentrations, source and wind data into NEXUS will be discussed in Section 3.2.

The Los Angeles application of NEXUS used a grid of 22 × 16 cells in the horizontal, each 4.47 × 4.47 kilometers; a map of the grid is given in Figure 19. The cells were 100 meters thick and four cells were used in the vertical, resulting in a total height of 400 meters.

The boundary conditions used in NEXUS were an impervious barrier at the ground with transmittive sides and top. The bottom of the lowest layer of cells was assumed to follow the terrain and be at ground level. The vertical velocity used to transport the particles was always assumed to vanish at ground level and vary linearly within the first layer of cells. No particles were permitted to enter the ground. If,

LOS ANGELES BASIN

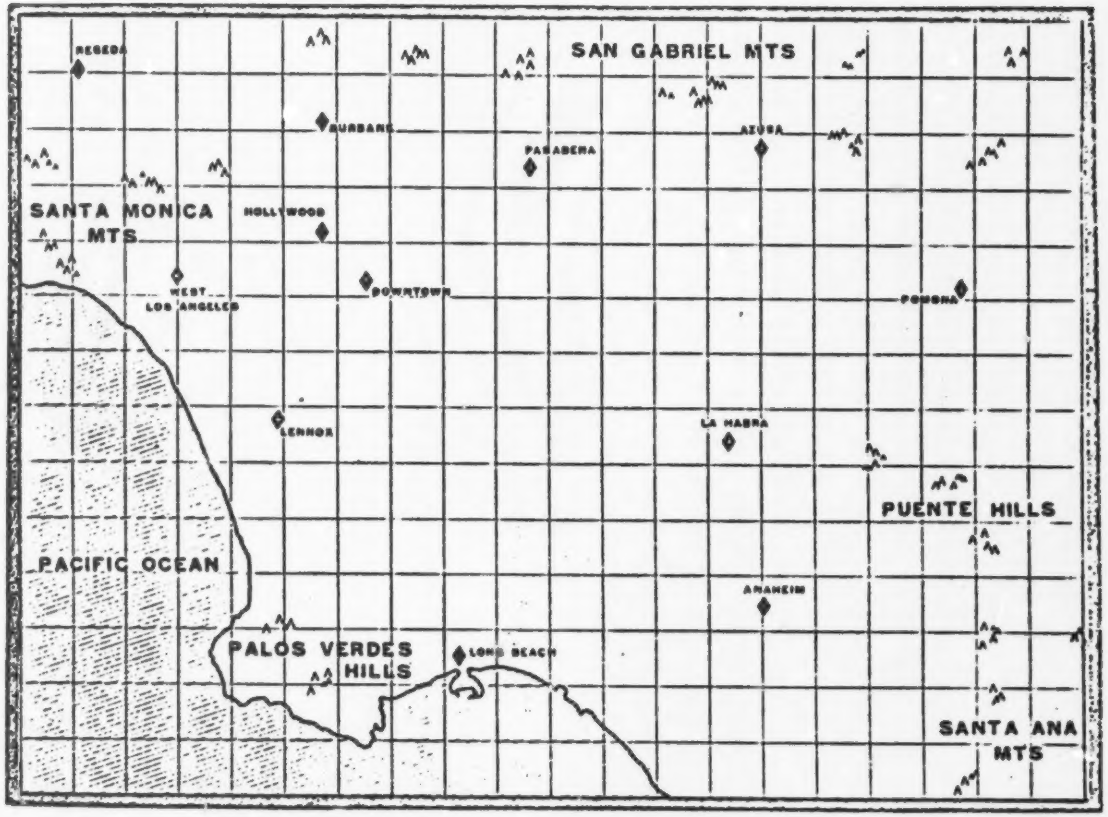
RESEDA
BURBANK
PASADENA
SAN GABRIEL MTS
AZUSA
SANTA MONICA MTS
HOLLYWOOD
WEST LOS ANGELES
DOWNTOWN
POMONA
LENNOX
LA HABRA
PUENTE HILLS
PACIFIC OCEAN
ANAHEIM
PALOS VERDES HILLS
LONG BEACH
SANTA ANA MTS

Figure 19 – Calculational Grid for NEXUS CO Simulation.

by a calculational overshoot a particle were below ground level, it would be re-positioned above. At the transmittive boundaries, when a particle moved into the outer half of the boundary cell it was removed from the calculation, simulating pollutant flow out of the region. Since the boundaries were chosen arbitrarily, there is also the possibility of pollutant flow through the side boundaries into the simulation region. To treat this, NEXUS used large Eulerian cells outside the border. These border cells were outside the volume of the simulation (the central grid) and only a gross treatment was used. The border cells were initially (3:00 A.M.) assumed to have above-background pollutant concentrations, chosen so that pollutant concentrations were continuous across the central grid boundary.

This work has been reported previously in preliminary form.[21,22]

3.1 DESCRIPTION OF THE NEXUS MODEL

In this section, the structure of the NEXUS code will be described. A macro flow chart is shown in Figure 20, with code listings and detailed flow charts included in Volume II, Section 2.

NEXUS and PICFIC both are based on the PICK method. In developing NEXUS from PICFIC, the main changes were the extension to three dimensions, the input of mean winds, diffusivities, and source emissions from tape each cycle, and the treatment of the borders and the upper and lower boundaries.

The main program of NEXUS directs the flow of the calculations and calls the major subroutines. The INPUT subroutine is called first and reads the cards that specify the problem to be run. The NEXUS code has the option of stopping

MAIN PROGRAM

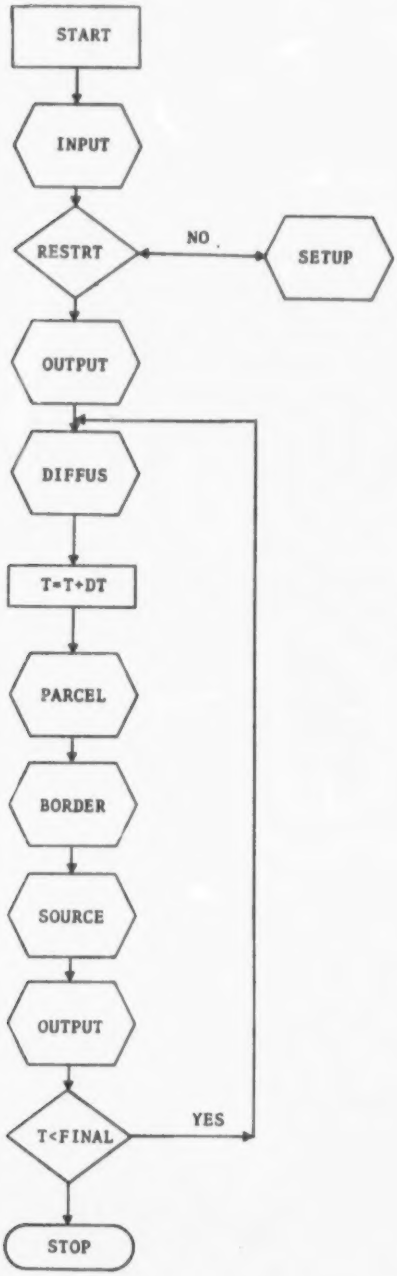
START
INPUT
RESTRT
NO
SETUP
OUTPUT
DIFFUS
T=T+DT
PARCEL
BORDER
SOURCE
OUTPUT
T<FINAL
YES
STOP

Figure 20 – Macro Flow Chart of NEXUS Main Program.

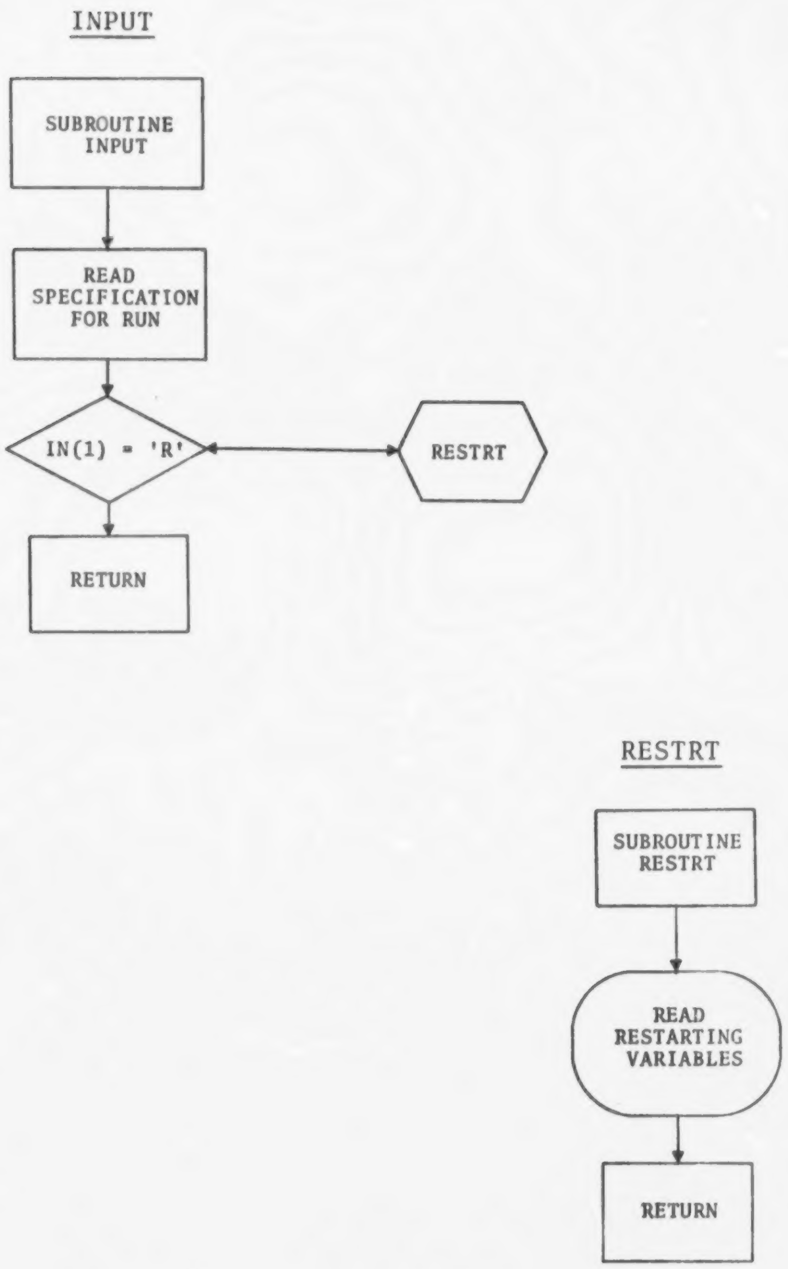

INPUT

SUBROUTINE INPUT
READ SPECIFICATION FOR RUN
IN(1) = 'R'
RESTRT
RETURN

RESTRT

SUBROUTINE RESTRT
READ RESTARTING VARIABLES
RETURN

Figure 20a – Macro Flow Chart of NEXUS Subroutines INPUT and RESTRT.

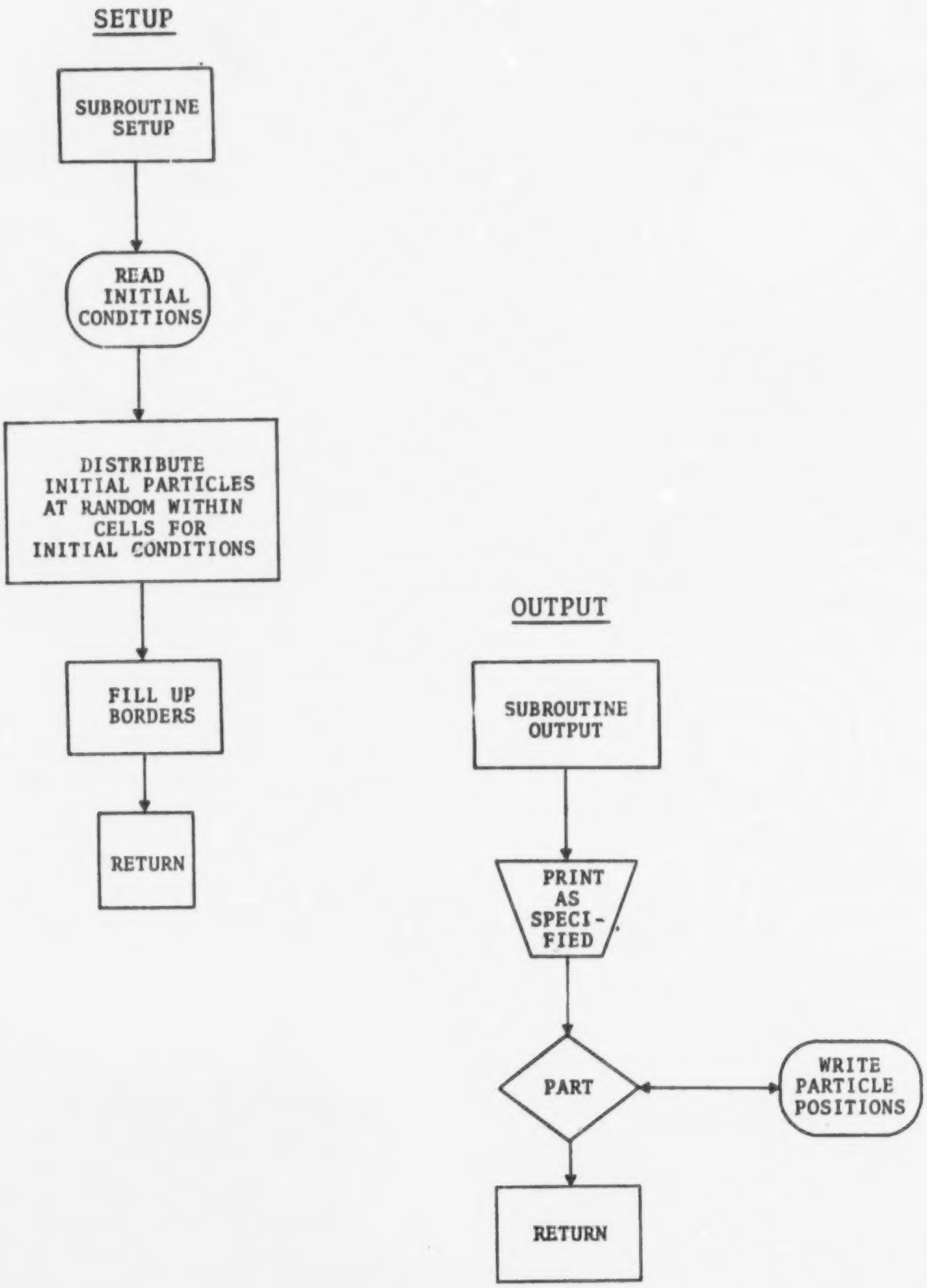
SETUP
SUBROUTINE SETUP
READ INITIAL CONDITIONS
DISTRIBUTE INITIAL PARTICLES AT RANDOM WITHIN CELLS FOR INITIAL CONDITIONS
FILL UP BORDERS
RETURN
OUTPUT
SUBROUTINE OUTPUT
PRINT AS SPECI-FIED
PART
WRITE PARTICLE POSITIONS
RETURN

Figure 20b – Macro Flow Chart of NEXUS Subroutines SETUP and OUTPUT.

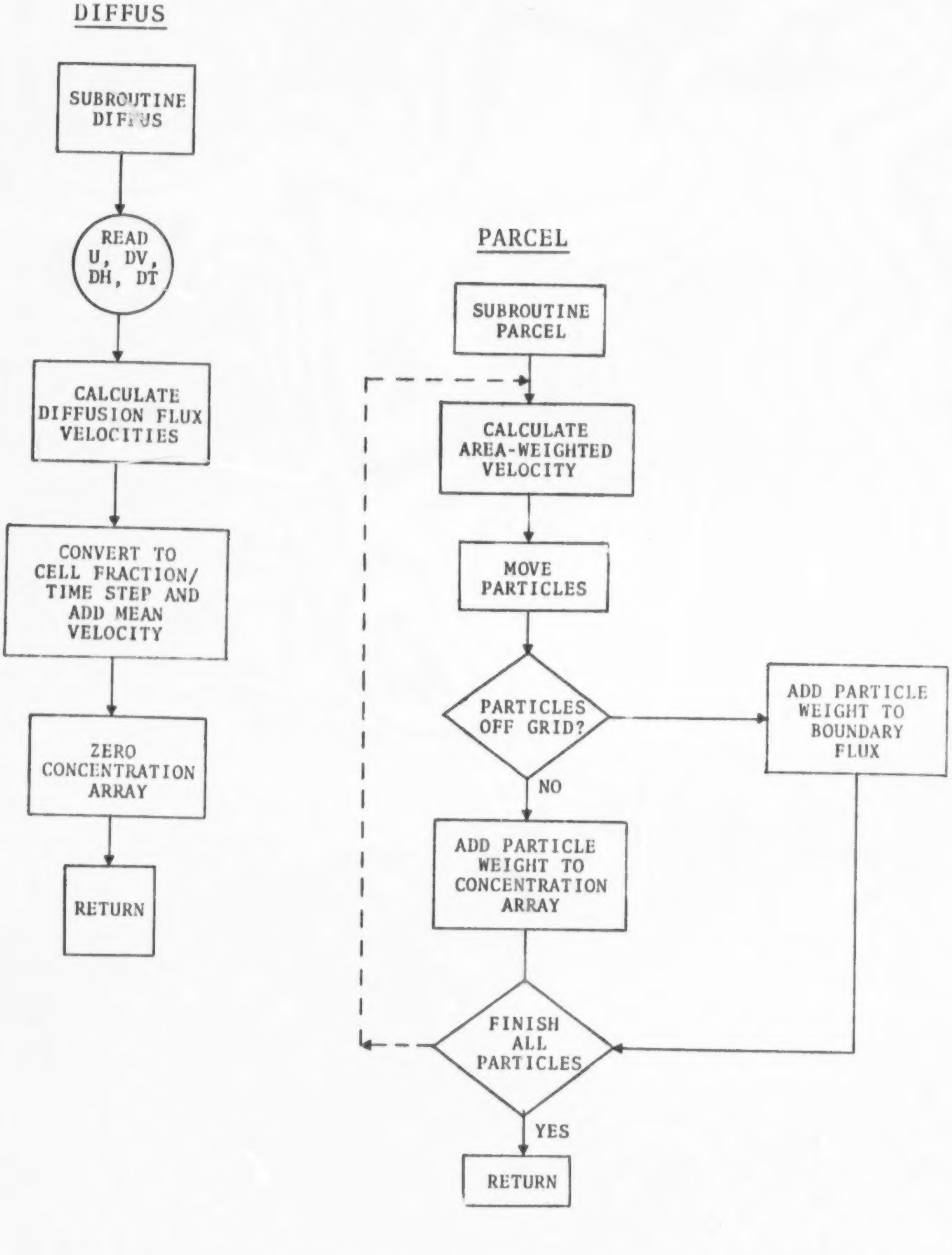
DIFFUS
SUBROUTINE DIFFUS
READ U, DV, DH, DT
CALCULATE DIFFUSION FLUX VELOCITIES
CONVERT TO CELL FRACTION/ TIME STEP AND ADD MEAN VELOCITY
ZERO CONCENTRATION ARRAY
RETURN
PARCEL
SUBROUTINE PARCEL
CALCULATE AREA-WEIGHTED VELOCITY
MOVE PARTICLES
PARTICLES OFF GRID?
ADD PARTICLE WEIGHT TO BOUNDARY FLUX
NO
ADD PARTICLE WEIGHT TO CONCENTRATION ARRAY
FINISH ALL PARTICLES
YES
RETURN

Figure 20c — Macro Flow Chart of NEXUS Subroutines DIFFUS and PARCEL.

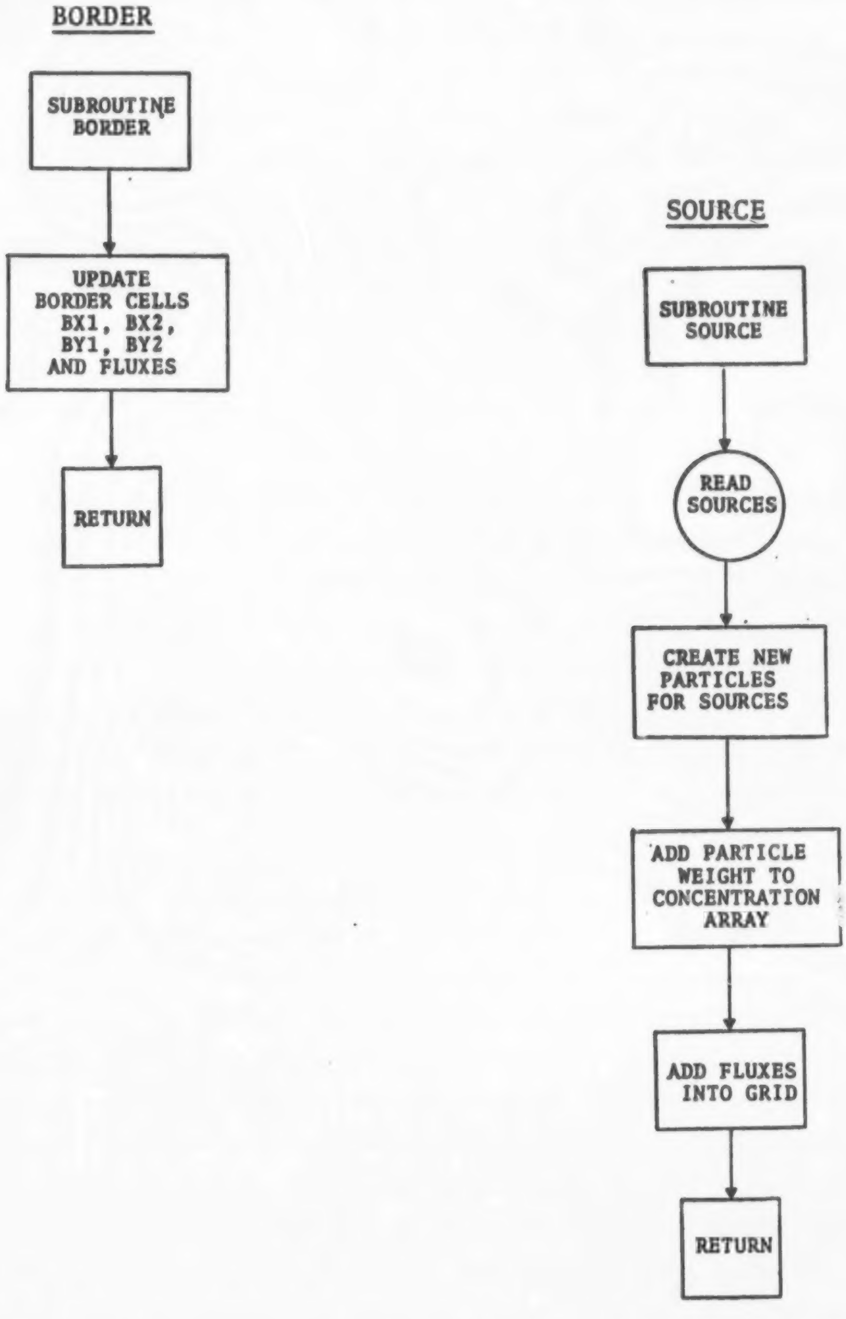
BORDER
SUBROUTINE BORDER
UPDATE BORDER CELLS BX1, BX2, BY1, BY2 AND FLUXES
RETURN
SOURCE
SUBROUTINE SOURCE
READ SOURCES
CREATE NEW PARTICLES FOR SOURCES
ADD PARTICLE WEIGHT TO CONCENTRATION ARRAY
ADD FLUXES INTO GRID
RETURN

Figure 20d — Macro Flow Chart of NEXUS Subroutines BORDER and SOURCE.

and restarting a given problem from magnetic tape. The choice of starting mode is specified to INPUT. Restarting is accomplished with a call to the RESTRT subroutine from INPUT. On the other hand, if a new problem is to be generated, a call to SETUP is made from the main program. SETUP reads the initial concentrations from tapes. The cell concentrations are converted to pollutant mass and assigned to particles. The initial particle placement is random within each grid cell to eliminate any systematic bias. Initial concentrations at ground level within the central grid are known; the upper level within cells and the borders are initialized with an assumed exponential decrease from the known concentrations. That is, the initial vertical profile of pollutant distribution over background concentration is taken to be reduced by one-half every 100 meters, $c(i,j,k)=(c(i,j,1)-b)/2^{(k\Delta z/100)}+6$ for $k > 1$. Away from the central grid the concentration decreases a factor two for each 16 km of distance. These are regions with no observational data and thus assumptions are required for full specification of the initial conditions. The function of the subroutine OUTPUT is to generate computer edits to print concentrations.

The main loop of the main program calls subroutines to calculate in order: the turbulent flux velocity (diffusion), the transport of particles, the border fluxes, the source emissions, and, if desired, edits of the results. The DIFFUS subroutine reads from tape the cell velocities and diffusivities and the time step. The turbulent flux velocity is computed and added to the mean velocity for each cell. This total velocity is then converted to units of cell fraction per time step. Finally, DIFFUS zeroes the cell concentration array which will be recalculated in PARCEL. Historically, the particles in the PICK method have been called "parcels" and the transport subroutine name is PARCEL. Since the total velocity has already been calculated in DIFFUS, PARCEL begins by calculating the area-weighted velocity associated with each particle position and then moving the particles. If the new particle position is outside of the central grid, the particle contributes to a flux across the border that will be treated in BORDER. Particles within the central grid have their mass apportioned by three-dimensional area-weighting among the eight closest cells and added to the cell concentration array; this procedure is applied to all particles.

The function of the BORDER subroutine is the treatment of pollutant mass outside the central grid. In these regions the actual concentrations and sources are unknown and a sophisticated treatment is unwarranted. Treatment of these regions at all is only warranted if there is pollutant flow into the central grid. The border treatment used in BORDER assumes cells twice as high and three times as long as central grid cells. In the border cells, advection is calculated using first-order finite differences and diffusion is ignored. Pollutant flow into the central grid contributes to border fluxes that are treated as additional sources.

The upper boundary is placed such that the inversion height is between the third and fourth layer of cells. The diffusion of particles upward through the fourth layer is very slow and, as will be discussed in the next section, the advection is also minimal. Particles that do penetrate past the middle of the fourth layer are removed from the calculation. At the lower boundary (for particles below the middle of the first level), the three-dimensional area-weighting is reduced to horizontal area-weighting because there are no cells below the particle. The vertical component of the total velocity is set to zero at the bottom of the grid and linearly interpolated to the particle position as described in the next section.

The SOURCE subroutine adds new particles to the calculation in simulation of source emissions and pollutant flow across the borders. The horizontal coordinates of the new particles are chosen at random within the source grid cell. In the Los Angeles basin application, carbon monoxide is emitted by motor vehicles which are assumed to be located at the bottom of the first level of cells. In order to simulate this low level source, the vertical random placement of newly generated particles is restricted to the lowest one-third of the bottom layer of cells – approximately the lowest 100 feet. The new particle mass contributes to cell concentrations through area-weighting.

This concludes the NEXUS calculational cycle. The cycle is repeated until the time period for simulation is completed. The position of each particle as stored in the computer traces out the trajectory of the pollutant mass. Each cycle may be plotted on a Stromberg-Carlson 4020 to form a movie of CO patterns for the day.

3.2 INPUT DATA

The data required for a NEXUS simulation are the source emissions, mean winds and diffusivities specified for each cell throughout the grid during the time period being simulated. The meteorological data were obtained from Lamb.[16] The winds were in the form of hourly averaged horizontal surface streamlines and isotack maps as shown in Figure 21. These were interpolated and extrapolated to the cell centers of the grid, as shown by wind velocity vector plots in Figure 22. Eight directions (north, northeast, east, southeast, etc.) were used for entering the winds into the computer which resulted in discretized patterns in the vector plots. Wind maps for each hour from 3:00 A.M. to 8:00 P.M. were used in the NEXUS simulation. Initial surface pollutant concentrations for the

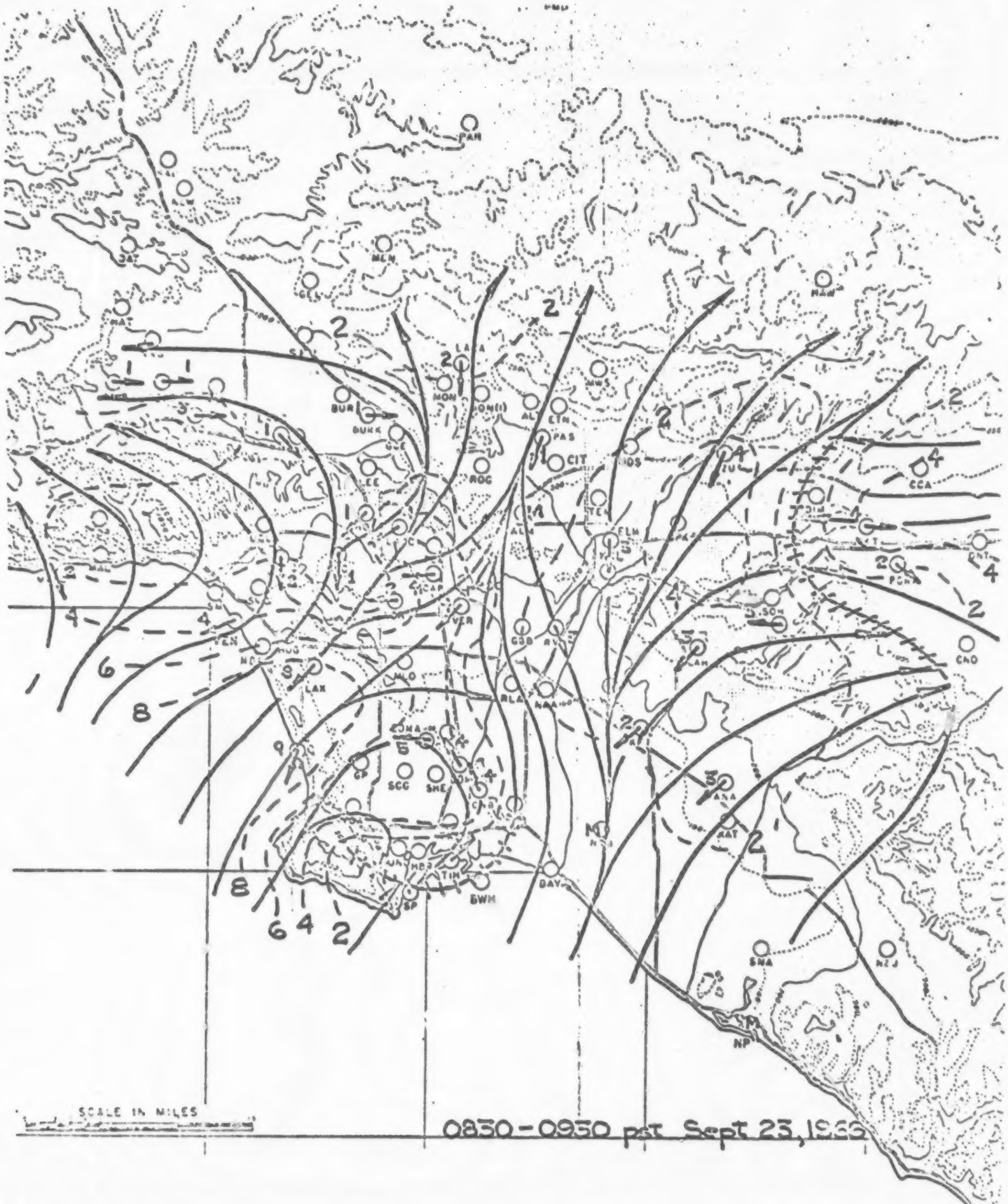
PAM
MEN
BUR
BURK
MON
PAS
CIT
ROC
LAX
SCC
SHE
DAY
SWH
SNA
NZJ
NP
ANA
CCA
CNO
2
1
3
4
5
6
8
SCALE IN MILES
0830-0930 pst Sept 23, 1966

Figure 21 – Supplied Wind Data (Reference 16). The streamlines are shown by solid lines. Isotacks in miles per hour are dashed contours.

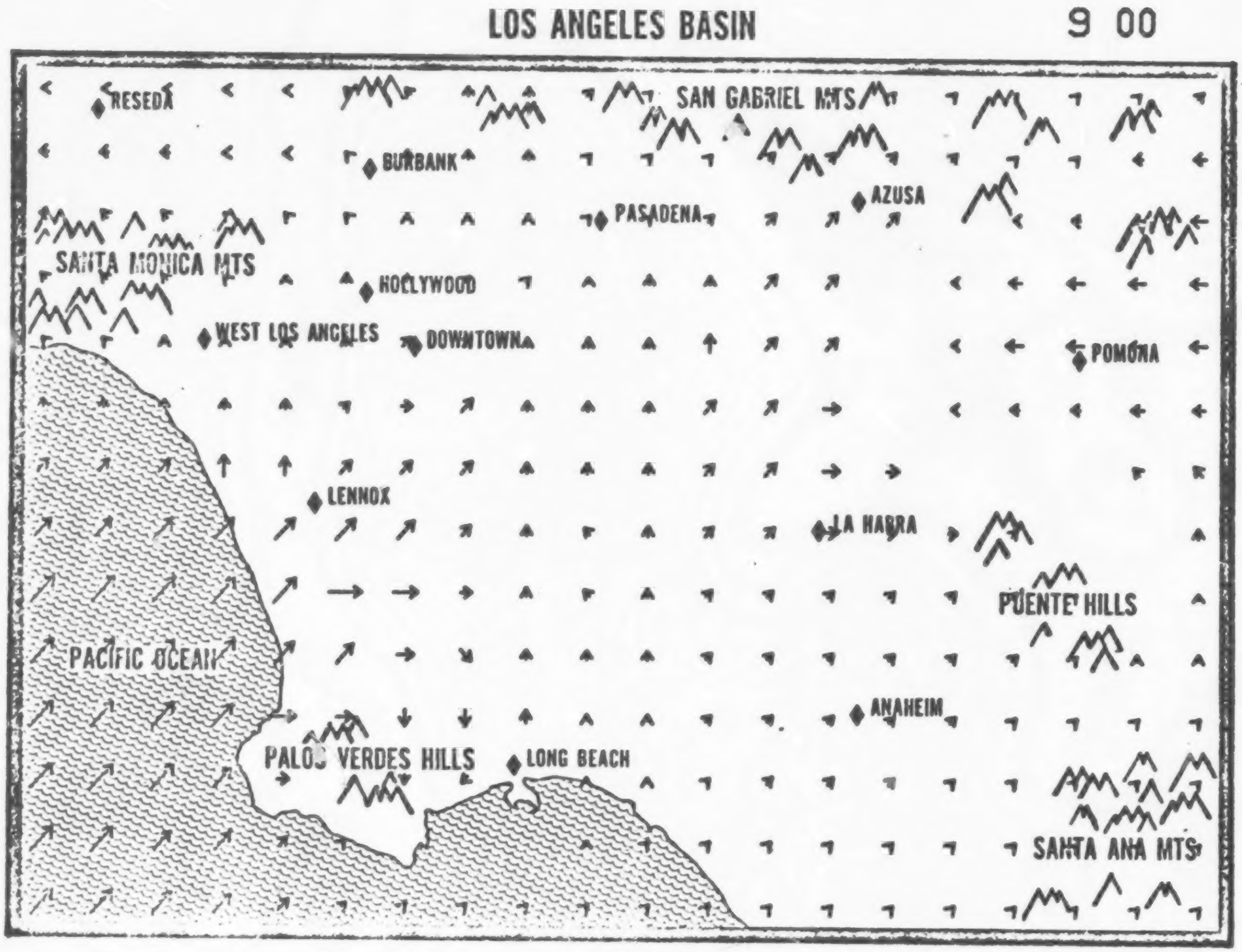
LOS ANGELES BASIN
9 00
RESEDA
SAN GABRIEL MTS
BURBANK
PASADENA
AZUSA
SANTA MONICA MTS
HOLLYWOOD
WEST LOS ANGELES
DOWNTOWN
POMONA
LENNOX
LA HABRA
PUENTE HILLS
PACIFIC OCEAN
ANAHEIM
PALOS VERDES HILLS
LONG BEACH
SANTA ANA MTS

Figure 22 – Winds at 9:00 A.M. in NEXUS Grid. The arrowhead points in the direction of motion and the arrow length is proportional to the wind speed.

simulation were also those of Lamb. The 3:00 A.M. observations of carbon monoxide made by the Los Angeles APCD were interpolated to generate the map of initial surface concentrations shown in Figure 23. The diffusivities used by Lamb were 1.2 m^2/sec and 0.6 m^2/sec in the horizontal and vertical directions, respectively, and were constant in time and space. These diffusivities were used in the S^3 simulation below a 1000 foot inversion height.

The CO source emissions inventory used in the simulation was compiled by Larson, et.al.[20] The spatial traffic distribution is shown in Figure 24 (after interpolation) and the temporal distribution is shown in Figure 25. The total CO emissions within Los Angeles County in 1966 were approximately 10^7 kilograms per day, as reported by the California Air Resources Board.[17] These total daily emissions were used to normalize the distribution so that

$$TDE = \sum_{h=1}^{24} \sum_{j=1}^{22} \sum_{i=1}^{16} S_{ij}(h) \quad , \qquad (3.1)$$

where TDE is the total daily emissions, $S_{ij}(h)$ the hour "h" emissions within cell (i,j) for the 22 × 16 cells in the lowest level of the NEXUS grid.

A computer code, SETUP, was developed to translate the data mentioned above into the computer tape format for the NEXUS code. A general flow chart of SETUP is given in Figure 26 and a detailed listing, flow chart and sample problem input and output is presented in Volume II, Section 2.

The main program of SETUP first calls the INITAL subroutine, which reads cards specifying the average CO mass per

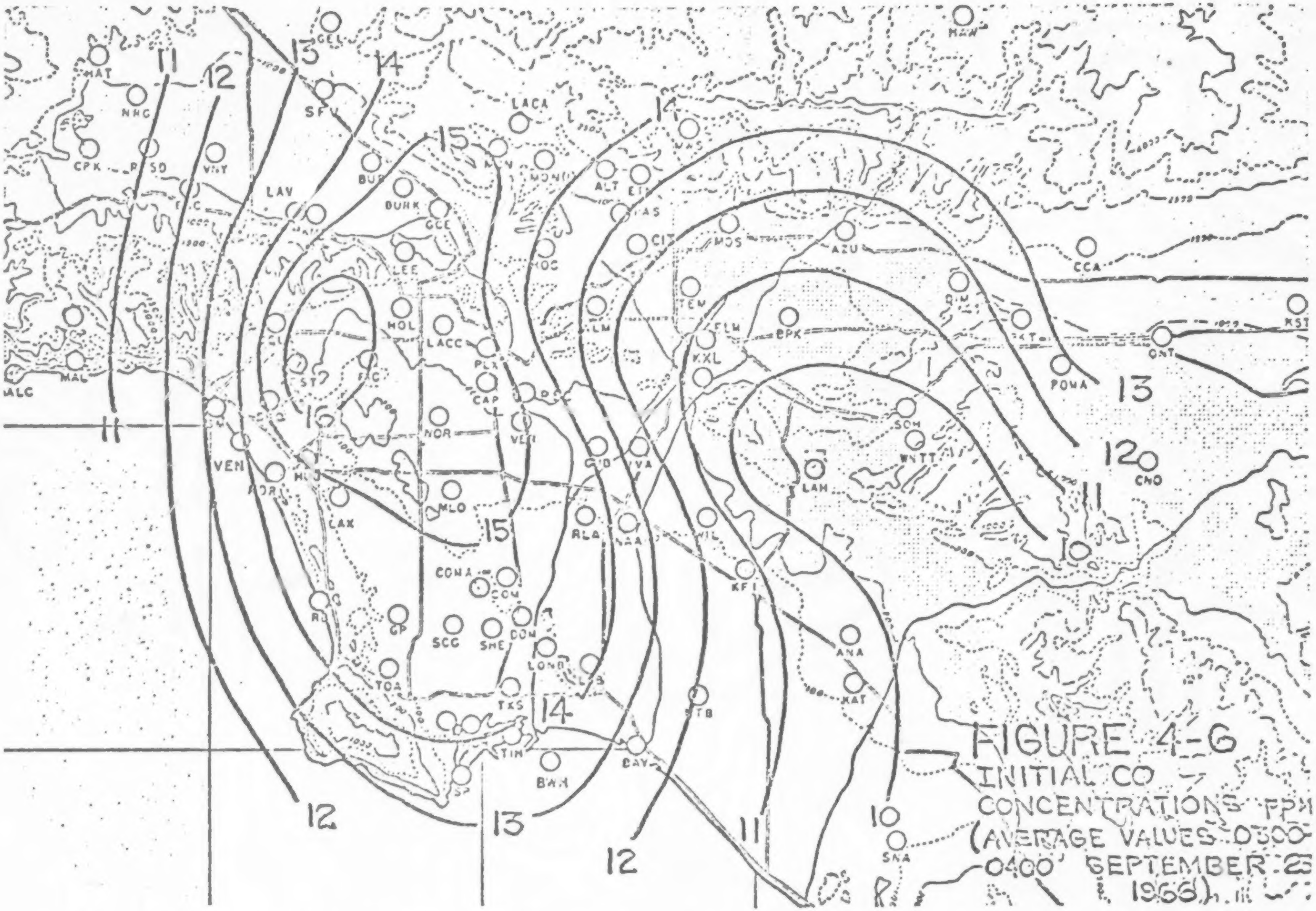
FIGURE 4-6
INITIAL CO
CONCENTRATIONS PPM
(AVERAGE VALUES 0300-0400 SEPTEMBER 23
1966)
11
12
13
14
15
16
15
14
13
12
11
10
12
13
12
11
10
HAT
NHG
CPK
SD
VNY
LAV
SFV
GEL
BUR
BURK
GCE
LACA
MONO
PAS
ALT
CIT
MOS
AZU
POMA
CCA
ONT
KST
CHO
MAW
LEE
MOL
LACC
NOR
VEN
LAX
MLO
COMA
SCC
SHE
LONB
TOA
GP
TKS
TIM
BWH
BAY
RLA
KFI
ANA
KAT
SNA
TB
WIL
LAH
SCH
WNTT
EPK
KXL
TEM
MAL
ALC
ST

Figure 23 – Initial (3:00 A.M.) CO Surface Concentrations (ppm) (Ref. 16).

1	1	1	1	2	1	1															
1	1	1	2	4	3	1	2	2	1												
2	2	4	8	8	10	9	5	4	5	3	1	1									
1	1	3	5	6	13	10	3	6	6	6	7	4	2	1	1	1	1				
1	1	1	3	4	16	10	2	9	17	10	8	4	4	3	2	2	2				
1	1	1	12	15	22	26	40	21	12	7	10	4	4	3	2	3	3				
1	2	3	8	13	22	23	36	19	13	8	5	1	1	1	1	1	2				
0	0	0	5	10	11	20	24	19	14	9	5	1	1	0	1	1					
0	0	0	0	8	11	16	10	15	12	8	2	2									
0	0	0	0	0	11	12	7	13	10	8	3	2									
0	0	0	0	0	4	4	4	5	8	4	3	1									
0	0	0	0	0	3	5	5	9	12	4	3	1									
0	0	0	0	0	2	6	5	12	21	7	3	1									
0	0	0	0	0	0	4	9	0	0	0	4	1									
0	0	0	0	0	0	0	0	0	0	0	0	1									
0	0	0	0	0	0	0	0	0	0	0	0	0									

Figure 24 – Los Angeles County Traffic Distribution.
(Unnormalized relative car miles per cell.)

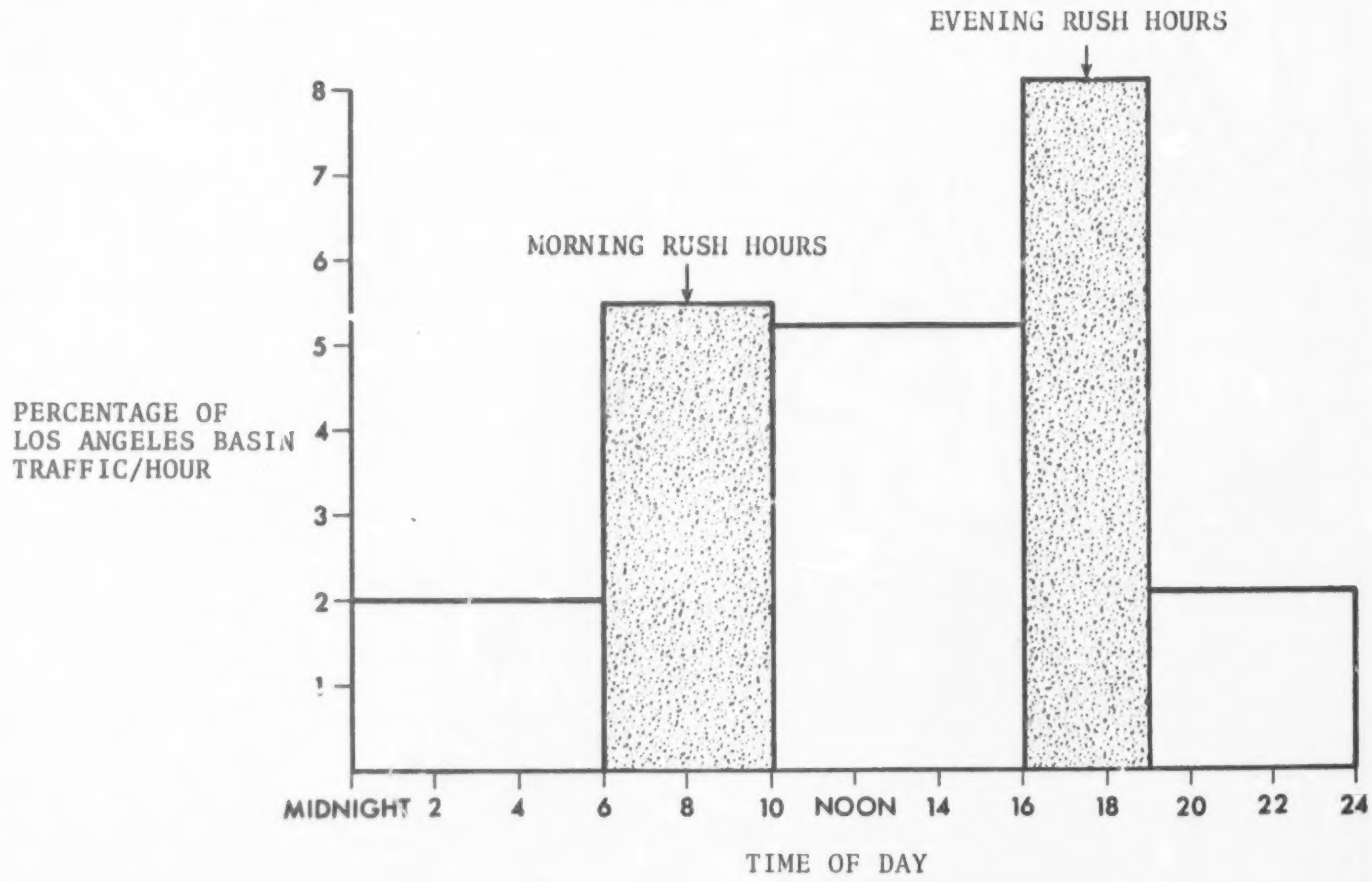

Figure 25 – Temporal Distribution for Los Angeles Basin Traffic.

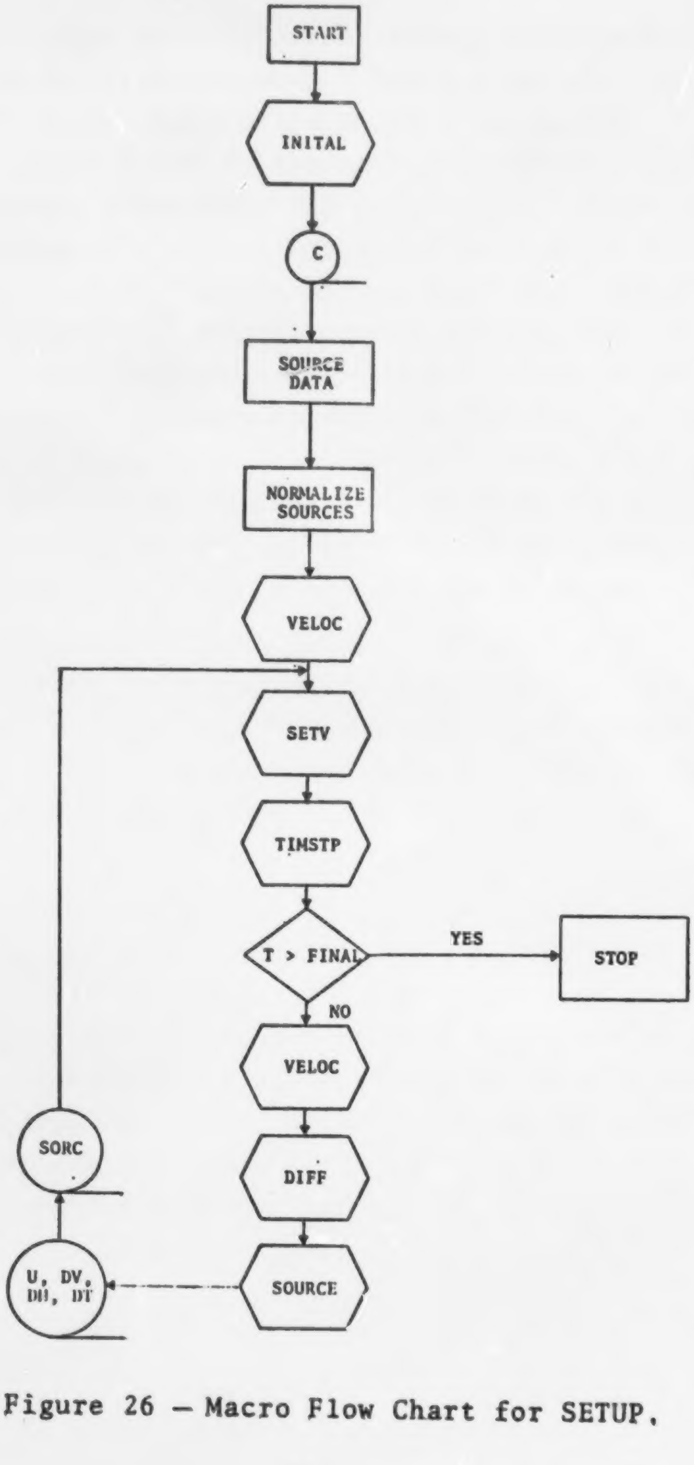
START
INITAL
C
SOURCE DATA
NORMALIZE SOURCES
VELOC
SETV
TIMSTP
T > FINAL
YES
STOP
NO
VELOC
DIFF
SOURCE
SORC
U, DV, DH, DT

Figure 26 — Macro Flow Chart for SETUP.

particle, background concentration and the initial CO concentrations. The background CO concentration must also be specified. The use of a fixed background concentration was suggested by the APCD observations in which measured CO levels never fell below 5 ppm during the simulation period. The advantage of a background concentration is a reduction of the total pollutant mass that is tracked by the particles. Without a background concentration, either more particles or more mass per particle would have been necessary. With a higher background the observed low concentrations could not have been simulated. The average CO mass per particle was chosen so approximately 10 particles per cell would be used in the simulation. Average CO concentrations were 10 ppm so each particle represented one-half ppm (added to the 5 ppm background).

The main program of SETUP next reads cards specifying temporal and spatial source emissions distributions. The VELOC subroutine is called to read cards specifying hourly winds. Two hourly wind card sets are read and linear interpolation is performed to compute the ground level, horizontal winds at the required time.

The main loop of SETUP is a sequence of calls to subroutines SETV, TIMSTP, VELOC, DIFF and SOURCE. SETV uses the ground level, horizontal winds to calculate the wind field by an arbitrary construction that results in a divergence-free field. The horizontal winds on the second level are assumed equal to those in the first level. The continuity equation, Eq. (1.4), is solved on the first level for the vertical component of the wind at the second level as follows:

$$w_{i,j,1} = 0 \quad ,$$

$$w_{i,j,2} = \frac{-3\Delta z}{2}\left[\frac{u_{i+1,j,1} - u_{i-1,j,1}}{2\Delta x} + \frac{v_{i,j+1,1} - v_{i,j-1,1}}{2\Delta y}\right] \quad ,$$

$$u_{i,j,2} = u_{i,j,1} \quad , \quad v_{i,j,2} = v_{i,j,1} \tag{3.2}$$

The vertical component on the third level is assumed equal to that on the second. The horizontal winds on the third and fourth levels are set to be opposite in direction and of the same speed as those of the first and second levels. The fourth level vertical wind is set to zero, as shown below:

$$\begin{aligned} w_{i,j,3} &= w_{i,j,2} \quad , \\ u_{i,j,3} &= -u_{i,j,1} \quad , \\ v_{i,j,3} &= -v_{i,j,1} \quad , \\ w_{i,j,4} &= 0 \quad , \\ u_{i,j,4} &= -u_{i,j,1} \quad , \\ v_{i,j,4} &= -v_{i,j,1} \quad . \end{aligned} \tag{3.3}$$

By this construction, the interpolated wind field is made a divergence-free solution of Eq. (1.4) for level 1 in the form;

$$\frac{u_{i+1,j,1} - u_{i-1,j,1}}{2\Delta x} + \frac{v_{i,j+1,1} - v_{i,j-1,1}}{2\Delta y} + \frac{w_{i,j,3/2} - 0}{\Delta z} = 0 \quad , \qquad (3.4)$$

where $w_{i,j,3/2}$ is interpolated as $w_{i,j,3/2} = \frac{2}{3} w_{i,j,2}$. For other levels the wind field is only approximately divergence-free.

The time step is set in subroutine TIMSTP by requiring $0.4\ \Delta x \geq u\Delta t$, $0.4\ \Delta y \geq v\Delta t$, $0.4\ \Delta z \geq w\Delta t$, for all cells, i.e., during one time step the greatest wind-driven motion is restricted to be less than four-tenths of a cell dimension. Next the time is updated, T = T + DT . At the new time VELOC is called to calculate the new surface velocities.

The subroutine DIFF sets the diffusivities:

$$K_x = K_y = DH = 1.2\ m^2/sec$$

$$K_z = DV = \begin{array}{l} 0.6\ m^2/\text{sec below the inversion height} \\ 0.0\ m^2/\text{sec above the inversion height} \end{array}$$

Finally, SOURCE calculates the source emissions during the time step for each cell from the normalized emissions distribution. The calculated source emissions in each cell for the time step is checked against the average particle mass (particles are required to be within 20 percent of the average mass). Since only integer particles can be used in NEXUS, the cell emissions are added to a storage array until the summed mass is sufficient to create a particle in the cell.

The calculated wind field, diffusivities and source emissions for each cell are written on tape for use in NEXUS. The main loop of SETUP is repeated until the time, T , reaches the final time.

3.3 RESULTS OF NEXUS SIMULATION

The NEXUS calculation, simulating the Los Angeles air basin for 17 hours, used 12 minutes of central processor unit time on the S^3 UNIVAC 1108 and used 60K of computer memory. The numerical results were in two forms: cell concentrations and particle positions for each of the 163 cycles required. The cell concentrations were hour-averaged and contour plots (isopleths) were made for the ground level concentrations. For example, the 10:00 A.M. isopleths are shown in Figure 27. The particle positions can also be plotted to illustrate the NEXUS results; for the ground level at 10:00 A.M. these are shown in Figure 28. The particle positions are not hour-averaged, but are actual positions at 10:00 A.M.

The NEXUS results were compared to observed CO concentrations made by the APCD and compiled by Lamb, and to the results of Lamb's model. Lamb averaged the APCD observations at each of the 12 stations for the 17 hours simulated. These data, the computed results of Lamb's model, and the NEXUS results are shown in Table V. In these comparisons, the observations are taken to be "correct," even though the measurements are known to be in error (in 1966 the APCD did not correct CO observations for water vapor and thus the measurements can be expected to be 3-5 ppm too high). This error also is present in the initial concentrations used to start the NEXUS simulation.

Three statistical tests were used for comparing the NEXUS simulation with observations:

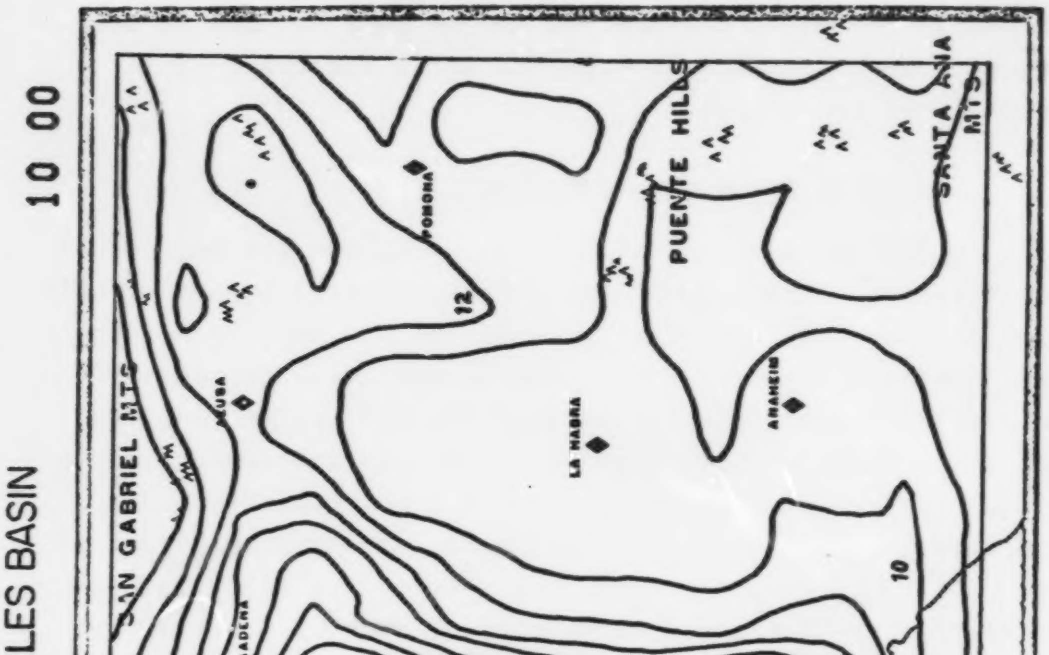
LOS ANGELES BASIN
10 00
SAN GABRIEL MTS
AZUSA
POMONA
12
PUENTE HILLS
SANTA ANA MTS
LA HABRA
ANAHEIM
10
PASADENA
BURBANK
DOWNTOWN
40
30
20
HOLLYWOOD
LENNOX
8
SANTA MONICA MTS
PACIFIC OCEAN
PALOS VERDES HILLS
LONG BEACH
W. LOS ANGELES

Figure 27 — Isopleths for CO at 10:00 A.M.

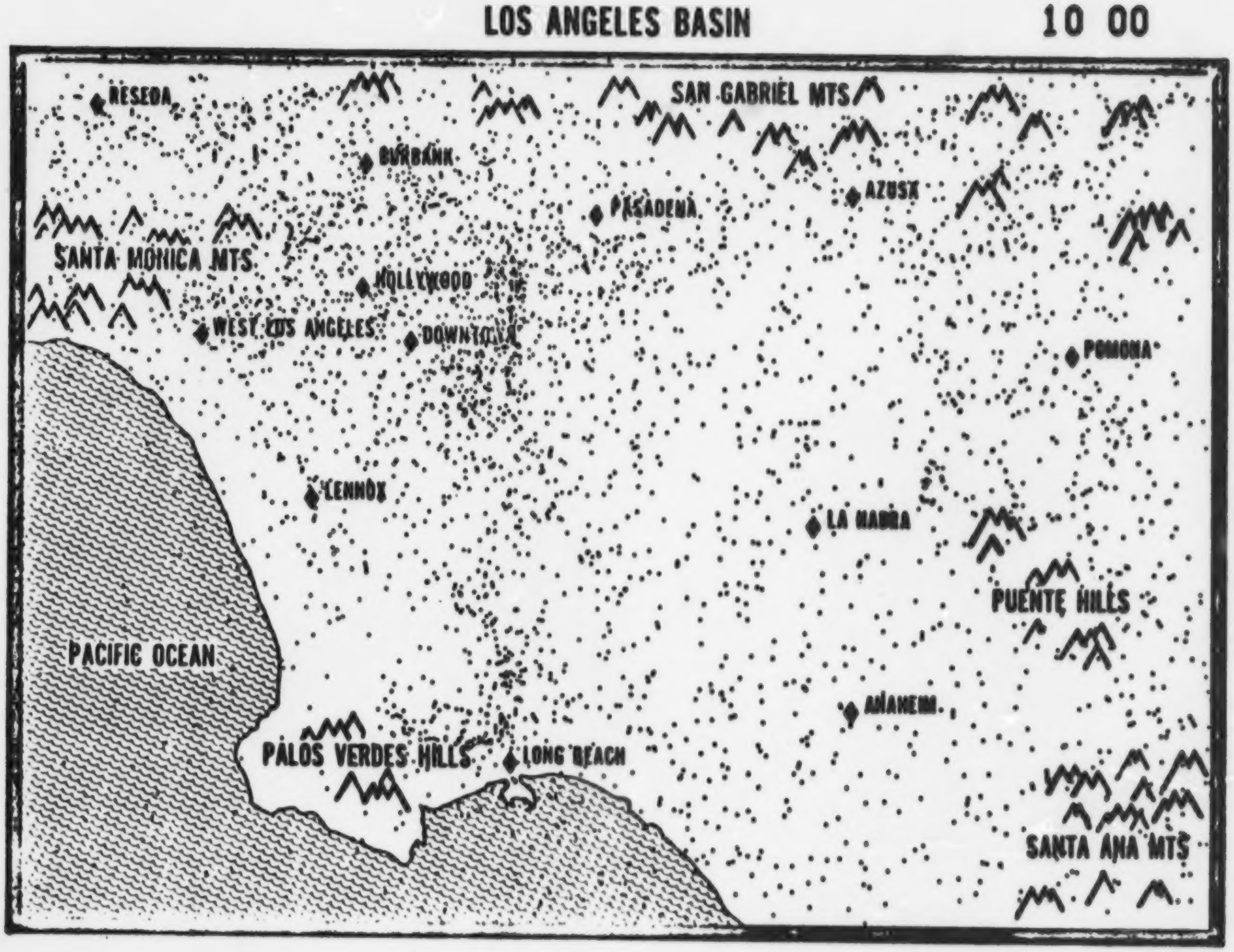
LOS ANGELES BASIN
10 00
RESEDA
BURBANK
PASADENA
SAN GABRIEL MTS
AZUSA
SANTA MONICA MTS
HOLLYWOOD
WEST LOS ANGELES
DOWNTOWN
POMONA
LENNOX
LA HABRA
PUENTE HILLS
PACIFIC OCEAN
ANAHEIM
PALOS VERDES HILLS
LONG BEACH
SANTA ANA MTS

Figure 28 – Plot of Particle Positions at 10:00 A.M.

TABLE V

3:00 A.M. to 8:00 P.M. AVERAGE CARBON MONOXIDE CONCENTRATIONS (CO in ppm)

STATION	OBSERVED	SIMULATED BY THE NEXUS MODEL	LAMB'S MODEL SIMULATION (Ref. 16)
Downtown Los Angeles	16	18	22
Azusa	13	9	3
Pasadena	17	17	15
Burbank	16	17	7
East Los Angeles	12	16	5
West Los Angeles	16	12	13
Long Beach	14	12	8
Hollywood	17	17	7
Pomona	13	9	3
Lennox	13	10	11
Anaheim	9	9	7
La Habra	6	8	3

(1) Mean difference:

$$\overline{\delta} = \sum_{i=1}^{N} (O_i - S_i)/N \quad , \qquad (3.5)$$

(2) Root mean square difference (RMSD):

$$\overline{\delta^2} = \sqrt{\sum_{i=1}^{N} (O_i - S_i)^2/N} \quad , \qquad (3.6)$$

(3) Correlation coefficient:

$$\rho = \frac{\sum_{i=1}^{N} (O_i - \overline{O})(S_i - \overline{S})}{\sqrt{\sum_{i=1}^{N} (O_i - \overline{O})^2/N}\sqrt{\sum_{i=1}^{N} (S_i - \overline{S})^2/N}} \quad , \qquad (3.7)$$

where O_i is the observation at the ith station, S_i the simulated concentration at the ith station, and $\overline{O}$ and $\overline{S}$ the mean of O_i and S_i , respectively.

The mean difference is a measure of the accuracy of the model results averaged over the basin. Such basin- and day-averaged concentrations depend on total emissions, net pollutant flow through the boundaries, and average basin ventilation — both vertical diffusion and mean wind. The mean difference for the NEXUS results was 0.73 ppm, well within the error introduced in the measurements by variations of water vapor. The calculations from Lamb's model had a mean difference of 4.8 ppm.

This could be partially due to his assumption of CO-free air off the ocean and perhaps his source emissions inventory.

The root mean square difference (RMSD) is a measure of the deviations of calculated and observed concentrations at each of the stations. The NEXUS results had a RMSD of 0.67 ppm, Lamb's model 4.8 ppm. Thus, NEXUS simulated the spatial distribution of CO (day-averaged) more accurately. Another statistical test of accuracy of the spatial distribution of CO is the correlation coefficient. The NEXUS results had a correlation coefficient $\rho = 0.73$ and Lamb's model $\rho = 0.35$. Many air pollution models have had to use additive and multiplicative factors to reduce the RMSD of model simulations and observations. These adjustments of the results are a linear transformation of the form:

$$S_i' \approx A + B\, S_i \quad ,$$

where constants A and B are chosen to increase the accuracy of the model to simulate the observations. However, linear transformations do not change the correlation coefficient. In the way it is used here, the correlation coefficient represents the similarity of the spatial distributions of observations and simulated results. Thus, NEXUS was better at the simulation of high and low concentrations in the proper spatial distribution than Lamb's model.

This may be explained on the basis of the 10:00 A.M. isopleth plots. The results of Lamb's model for 10:00 A.M. are shown in Figure 29, and can be contrasted with the NEXUS 10:00 A.M. predictions in Figure 27. Lamb's model predicts highly peaked concentrations — up to 150 ppm. These are not observed, but correspond to convergences in the horizontal winds as shown in Figure 30. Lamb's model used two-dimensional

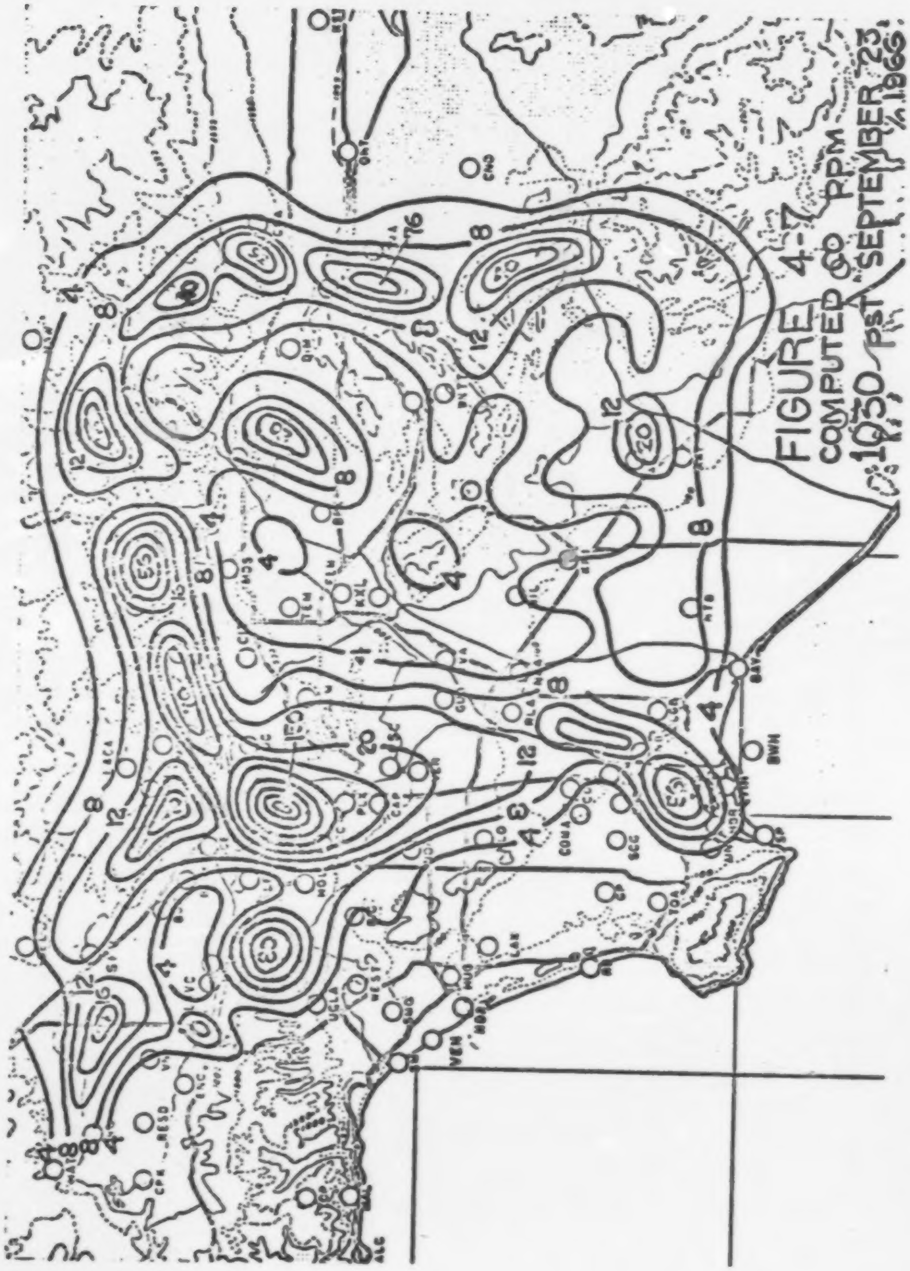
FIGURE 4-7
COMPUTED CO PPM
1030 PST SEPTEMBER 23, 1966

Figure 29 – Isopleths for CO (in ppm) at 10:00 A.M. as Simulated by Lamb's Model. (Reference 16.)

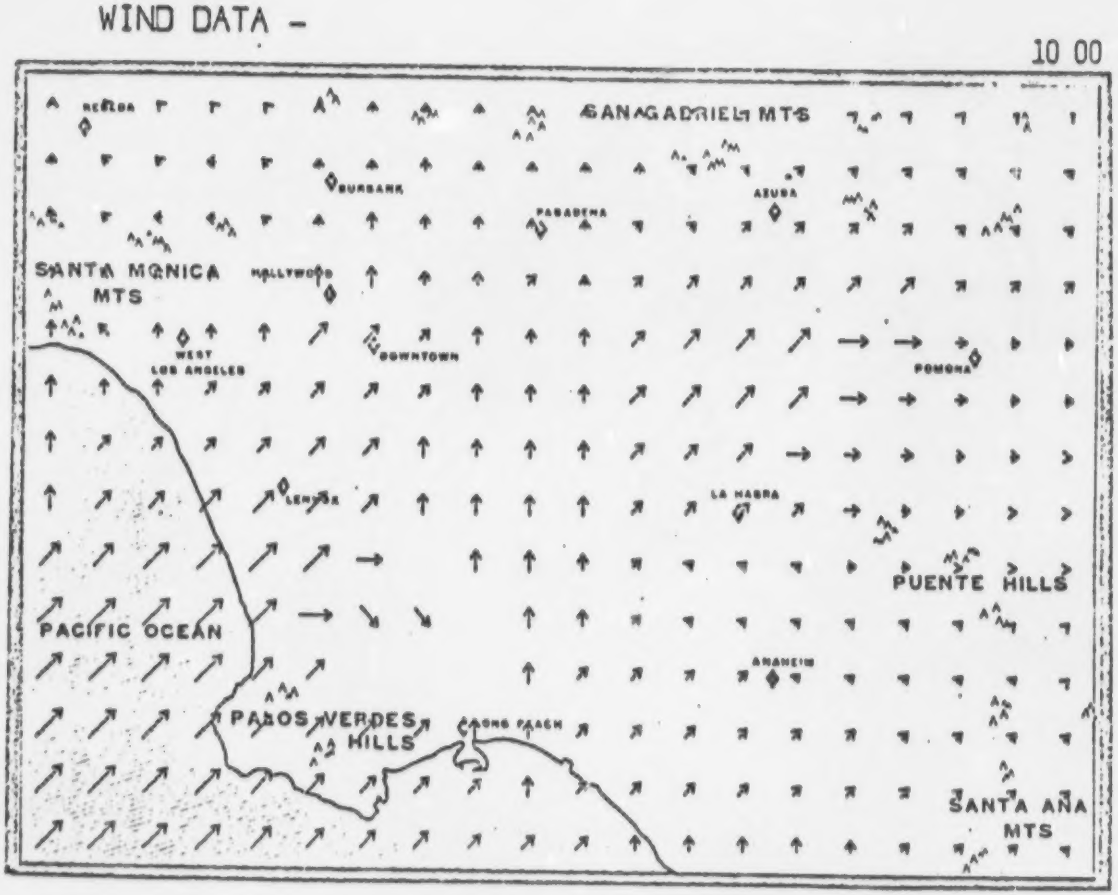
WIND DATA -
10 00
SAN GABRIEL MTS
BURBANK
PASADENA
AZUSA
SANTA MONICA MTS
HOLLYWOOD
WEST LOS ANGELES
DOWNTOWN
POMONA
LENNOX
LA HABRA
PUENTE HILLS
PACIFIC OCEAN
ANAHEIM
PALOS VERDES HILLS
LONG BEACH
SANTA ANA MTS

Figure 30 – Surface Winds at 10:00 A.M. Showing Convergences Near Downtown and Long Beach.

winds that are not divergence-free. NEXUS uses a three-dimensional wind field and so can avoid these unphysical effects.

The day- (or 17 hour) averaged concentrations have smoothed over many of the significant fluctuations of the CO concentrations. Hourly-averaged CO concentrations from both the APCD and NEXUS are plotted in Figure 31. The shapes of these curves are similar but in Downtown Los Angeles and Hollywood, the timing and magnitude of the morning maxima are different. This could be attributed to two assumptions in the input data — the source inventory and inversion height. The source inventory used a basin-wide average time distribution, whereas Downtown Los Angeles and Hollywood could be expected to be strongly influenced by early morning freeway traffic. The constant inversion height was used mainly for comparison with the work of Lamb, this also would have the effect of dispersing the early emissions too rapidly. Each of these possible sources of error is discussed further in Section 3.4.

The NEXUS simulation shows the realistic variation of pollutant concentration with source emissions and meteorological conditions through mean winds and turbulent dispersion. The following sequence of figures (Figures 32 through 36) illustrates the patterns and concentrations that develop during the 17 hour simulation.

At 3:00 A.M. carbon monoxide is distributed throughout the basin with higher concentration in the central basin area, as shown in Figure 32. The 3:00 A.M. winds are represented by arrows in Figure 33. The winds show a slow flow toward the coast line. Carbon monoxide concentrations build up in the slow-moving air throughout the morning rush hours.

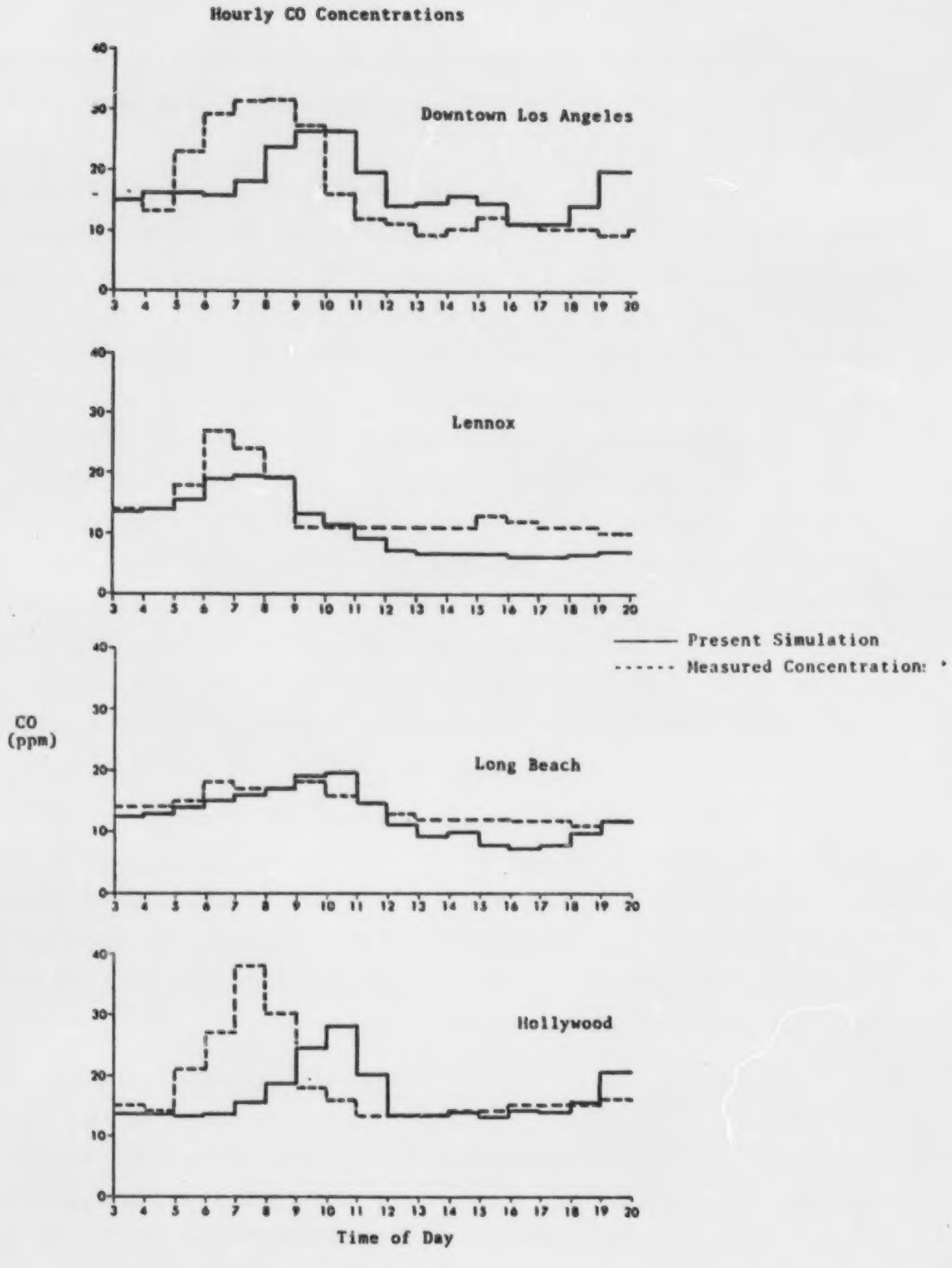

Figure 31 – Simulated Hour-Averaged CO Concentrations Compared to Measured Concentrations at Downtown Los Angeles, Lennox, Long Beach and Hollywood.

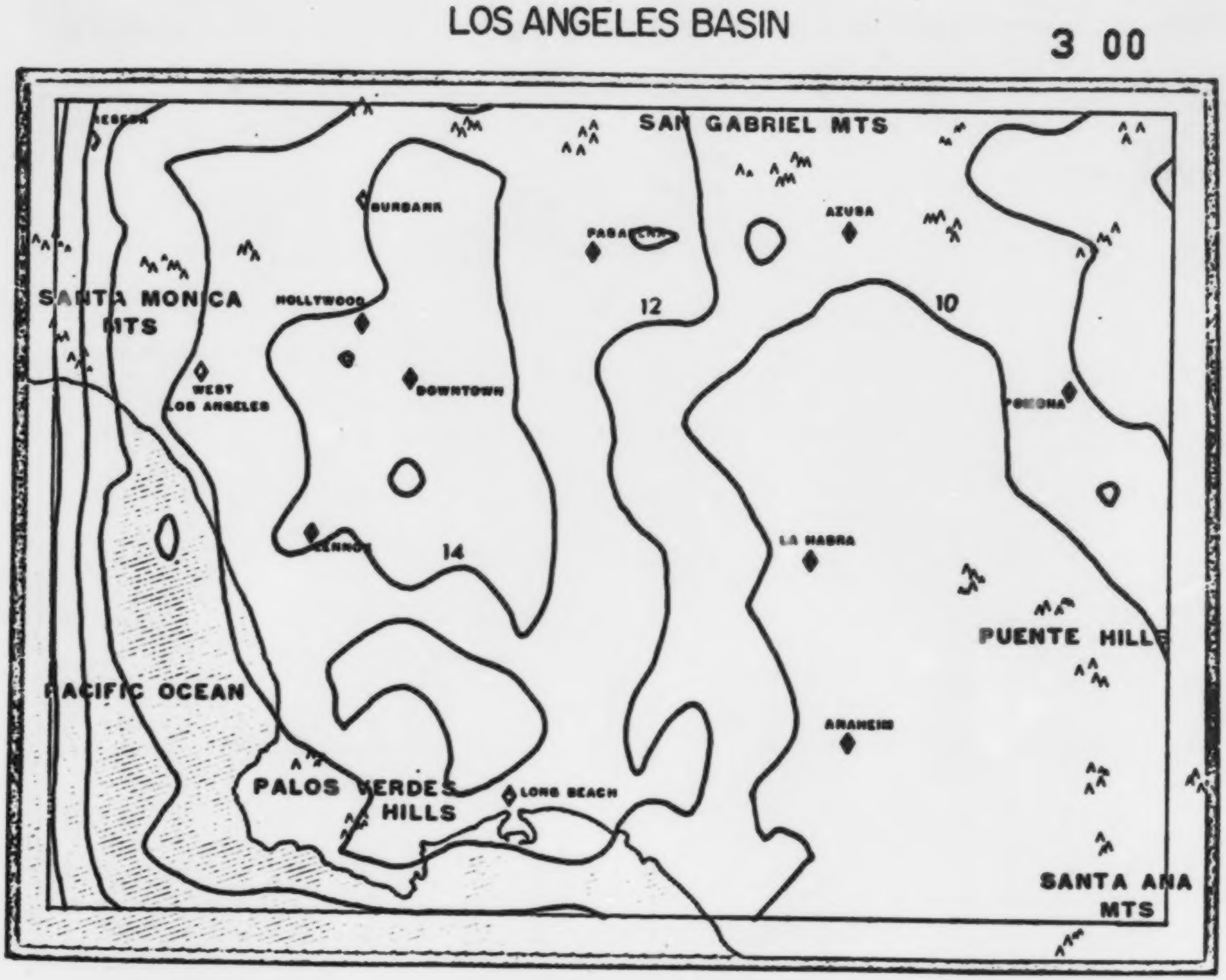
LOS ANGELES BASIN
3 00
SAN GABRIEL MTS
SANTA MONICA MTS
PACIFIC OCEAN
PALOS VERDES HILLS
PUENTE HILLS
SANTA ANA MTS
RESEDA
BURBANK
HOLLYWOOD
WEST LOS ANGELES
DOWNTOWN
LENNOX
PASADENA
AZUSA
POMONA
LA HABRA
ANAHEIM
LONG BEACH
14
12
10

Figure 32 – Surface CO Concentrations Used for 3:00 A.M. Initial Concentrations.

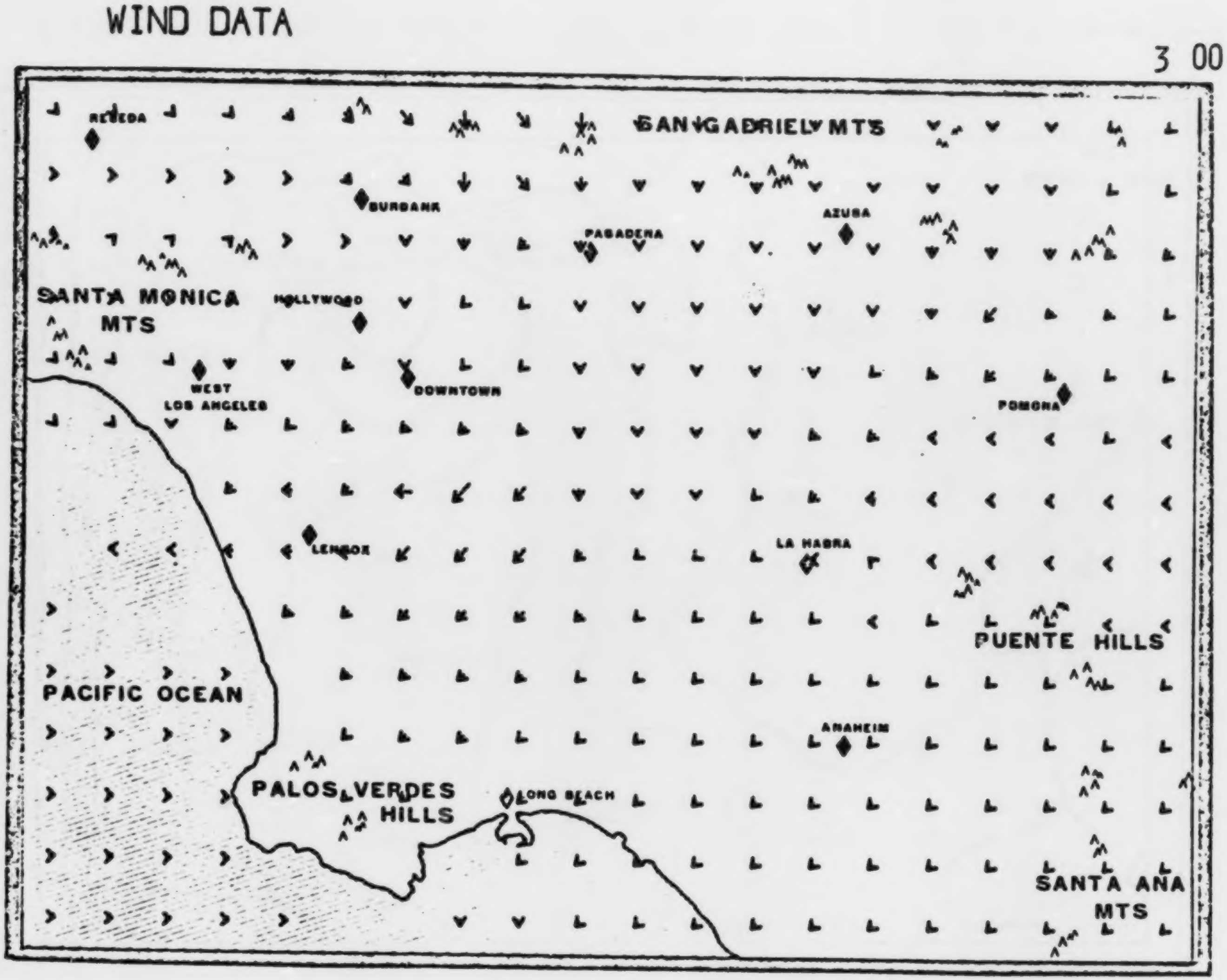
WIND DATA
3 00
RESEDA
SAN GABRIEL MTS
BURBANK
PASADENA
AZUSA
SANTA MONICA MTS
HOLLYWOOD
WEST LOS ANGELES
DOWNTOWN
POMONA
LENNOX
LA HABRA
PUENTE HILLS
PACIFIC OCEAN
ANAHEIM
PALOS VERDES HILLS
LONG BEACH
SANTA ANA MTS

Figure 33 – At 3:00 A.M. the Winds Were Calm and Generally Toward the Coast.

The winds from off the ocean increase during the morning hours; the 10:00 A.M. winds are shown in Figure 30. There is a flow towards Burbank, but the winds are light there. The winds are also blowing pollutants eastward off the map towards Riverside-San Bernardino. The winds form a vortex flow around the Palos Verdes Hills, accompanied by low winds over Long Beach. Heavily polluted air flows into the San Fernando Valley in the Northwest corner of the map either past Burbank through the Cahuenga Pass or over the Santa Monica Mountains. The air then flows slowly across the Valley to the North. Air reaching Long Beach via the vortex around the Palos Verdes Hills has had sufficient time to accumulate high pollutant concentrations. The low winds at Long Beach permit further increase of concentration. Air coming off the ocean still retains an above-background level of carbon monoxide due to pollution from the previous day which was blown out to sea. The air passes over the coastal traffic on its way towards Downtown Los Angeles and additional CO is picked up. Thus, by the time the air reaches Downtown Los Angeles (or even later, Pasadena), pollutant concentrations are very high, Figure 27.

By 3:00 P.M. the sea breeze is fully established and is sweeping across the basin, Figure 34. The low winds in the Northwest corner are the first to be reversed. The Palos Verdes-Long Beach area still has a low-speed vortex in the wind pattern. The strong winds are now carrying air originating further off shore. This air mass is probably less polluted as it reaches the coast. Moving rapidly across the basin, the air has little time to accumulate pollutants. Carbon monoxide concentrations are reduced starting at the southwest corner of the basin, Figure 35. In the San Fernando Valley, the wind reversal and low wind speeds have resulted in high CO concentrations moving towards Burbank.

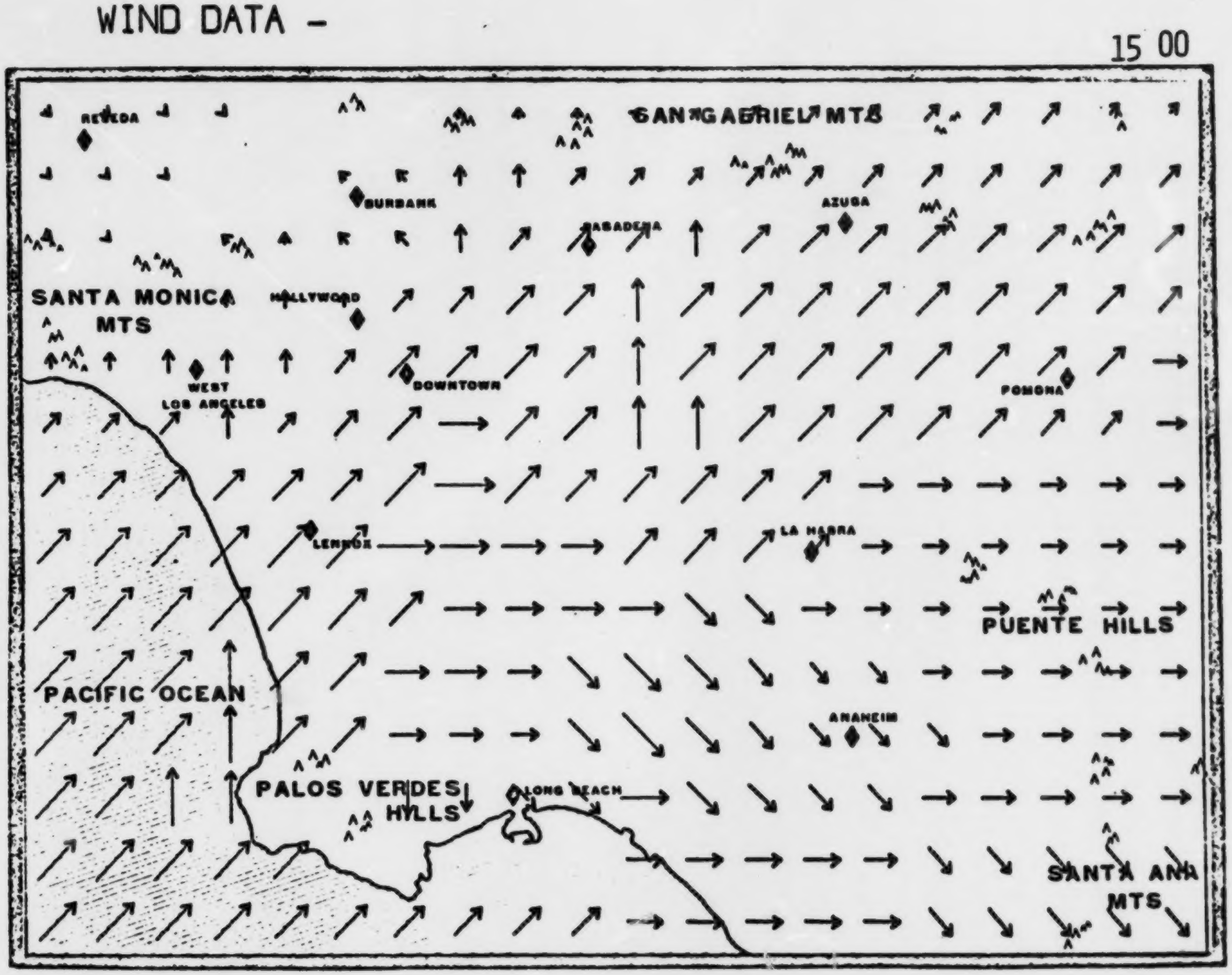
WIND DATA -
15 00
RESEDA
SAN GABRIEL MTS
BURBANK
AZUSA
PASADENA
SANTA MONICA MTS
HOLLYWOOD
WEST LOS ANGELES
DOWNTOWN
POMONA
LENNOX
LA HABRA
PUENTE HILLS
PACIFIC OCEAN
ANAHEIM
PALOS VERDES HILLS
LONG BEACH
SANTA ANA MTS

Figure 34 — High Winds Throughout Most of the Basin with Convergence Near Burbank at 3:00 P.M.

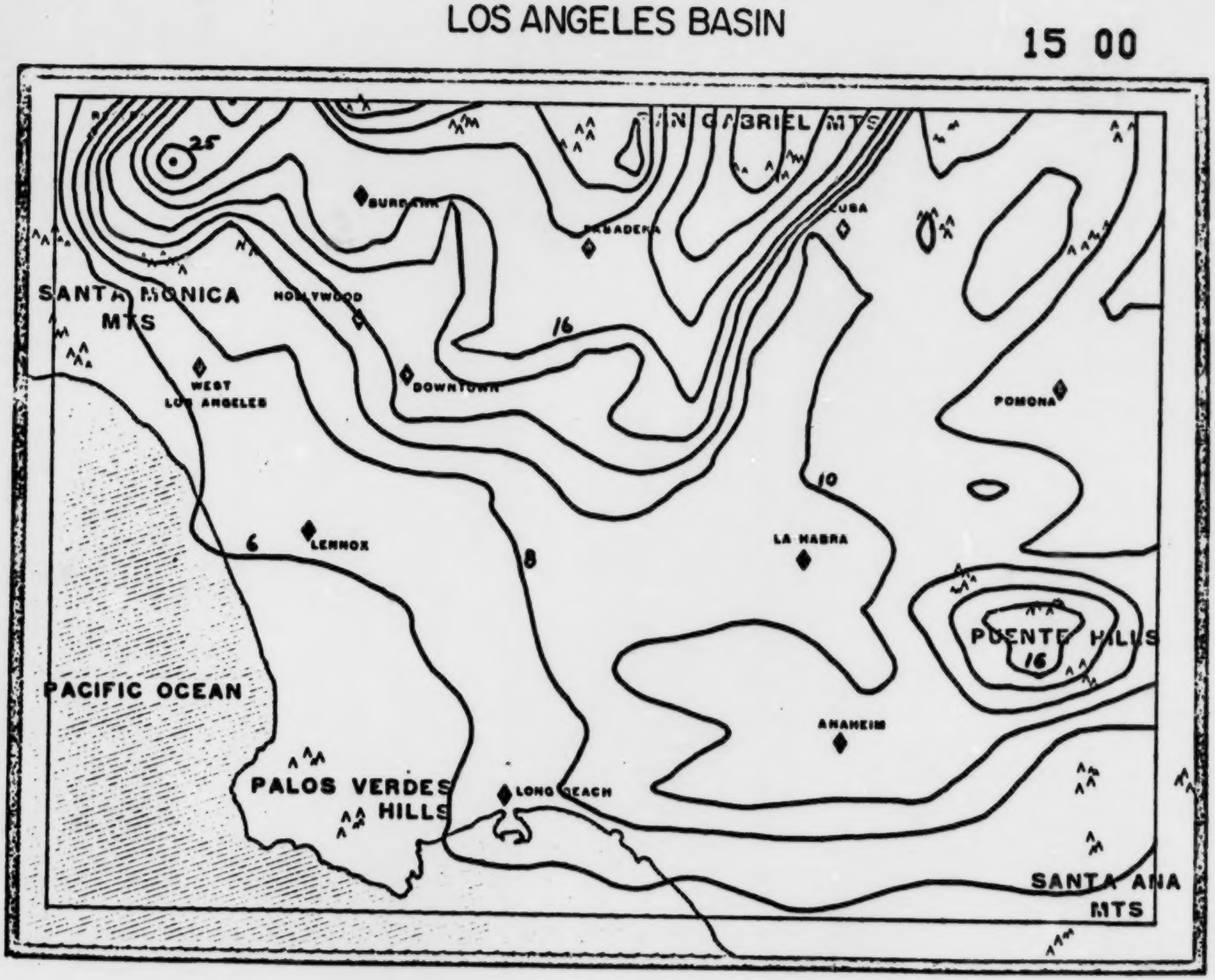
LOS ANGELES BASIN
15 00
SAN GABRIEL MTS
25
BURBANK
PASADENA
USA
SANTA MONICA
MTS
HOLLYWOOD
WEST
LOS ANGELES
DOWNTOWN
16
POMONA
10
6
LENNOX
8
LA HABRA
PUENTE HILLS
16
PACIFIC OCEAN
ANAHEIM
PALOS VERDES
HILLS
LONG BEACH
SANTA ANA
MTS

Figure 35 – The Morning High Concentrations Have Been Blown Into the San Gabriel Mountains and Puente Hills but a New Build-Up is Forming in the Northwest at 3:00 P.M.

The end of the calculational day at 7:50 P.M. is shown in Figure 36. The high CO concentrations in the northern portion of the basin are caused by both polluted air from the Oxnard plane (northwest off the grid) and low wind speeds along the wind front during evening rush hours.

3.4 TESTING OF NEXUS

The NEXUS code was extensively tested to determine (1) sensitivity of the results to wind field and boundary assumptions, to input data and to the initial random locations of particles; (2) possible improvements through a new source inventory and a non-constant inversion height; and (3) the accuracy of variants of the PICK method and comparison of NEXUS computing time with that required by finite difference methods. The NEXUS calculation as described above will be referred to as the standard calculation.

The first series of tests was directed toward evaluating the effects of the wind field construction, Eq. (3.2) and (3.3). The necessity of a divergence-free wind field was seen in the NEXUS comparison to Lamb's model and will be shown again in some of the variants of the PICK method to be described below. The lowest two layers' winds were constructed from horizontal ground level observations and the continuity equation (requiring the winds to be divergence-free). The winds in the upper two levels were chosen arbitrarily but approximately divergence-free. To test the effects of this choice, we conducted two other test calculations. The first test had all velocities on levels 3 and 4 set to zero. This resulted in day averaged concentrations above 20 ppm in Pasadena, Burbank, and East Los Angeles and higher concentrations than the standard results everywhere. This can be explained in terms of the vertical motion of the particles — they could be

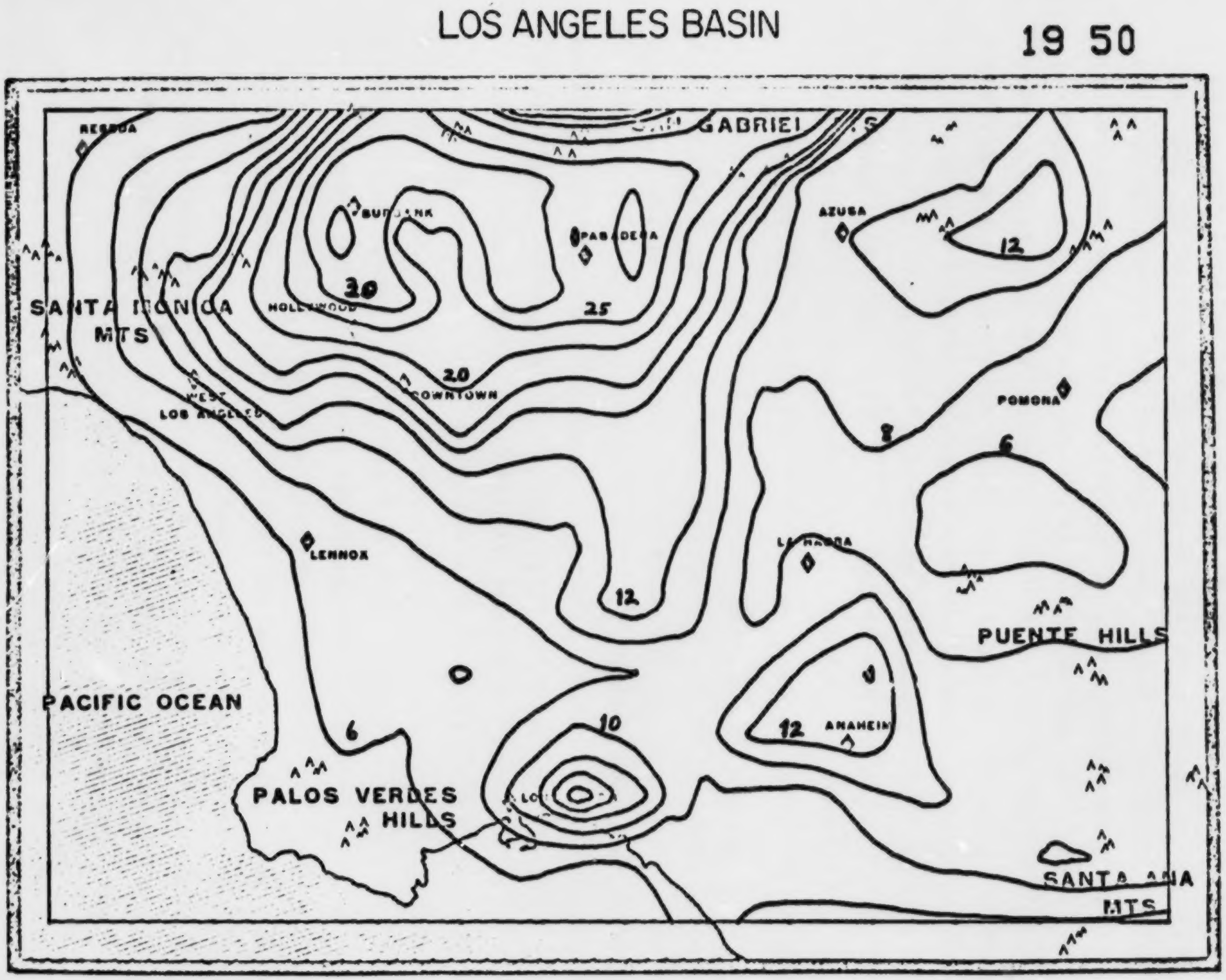
LOS ANGELES BASIN
19 50
RESEDA
SAN GABRIEL MTS
SANTA MONICA MTS
BURBANK
HOLLYWOOD
PASADENA
30
25
20
DOWNTOWN
WEST LOS ANGELES
AZUSA
12
POMONA
8
6
LENNOX
LA HABRA
12
PUENTE HILLS
0
PACIFIC OCEAN
6
10
12
ANAHEIM
PALOS VERDES HILLS
SANTA ANA MTS

Figure 36 – Evening Traffic has Produced a Local Build-Up of CO Over Long Beach and a Large Region of High Concentrations Corresponding to the Surface Wind Convergence in the Burbank-Pasadena-Hollywood Area at 8:00 P.M.

advected by convergent winds and build-up without the possibility of escaping into the vertical as required by the continuity equation. Above the middle of the second layer, the continuity equation would no longer describe the interpolated wind field. The second test retained the vertical component of upper level winds, but used zero for the horizontal components on levels 3 and 4. In this test the results differed by no more than 1 ppm from the standard results for day averaging. This indicates the insensitivity of the results with NEXUS to the form of the wind field above the layers that affect the ground level (lowest two layers due to the area weighting) as long as vertical transport is retained.

The testing of the boundary conditions consisted of a calculation with the concentrations in the border cells set to zero (only air at the background CO concentration, 5 ppm, entered the central grid). The effects of this were minor except during the late afternoon convergence. If the assumed background concentration were lowered the borders could have a greater effect. A series of tests was also conducted to determine the effects of the choice of the background concentration. In successive calculations the background concentration was lowered until, with a 5 ppm background, there was no appreciable change in day averaged results. The number of particles (and, thus, the average mass per particle) were varied in another series of tests. An optimum for computer time and accuracy was determined for 4,000 - 8,000 particles (the number of particles varies as they are created by source emissions and flow off the central grid) corresponding to approximately a metric ton of CO per particle.

Next, the sensitivity of NEXUS results to stochastic variations in the required input data (winds and source inventory) was evaluated. If no systematic errors are assumed in the data, the mean error in the data is zero and the errors in the data could be expected to be normally distributed around zero. That is, if the data used for the standard results were correct, then the data with stochastic errors would be scrambled such that

$$D_{scrambled} = D_{standard} (1 + R) \quad , \qquad (3.8)$$

where R is a normally distributed random variable with mean zero. For these tests the standard deviation for R was taken to be one-fourth. Thus, 90 percent of the time the scrambled data falls within 50 percent of the standard value.

The first test used scrambled source emissions. Equation (3.8) was used with the source emissions spatial distribution for each cell. A second test used a scrambled source emissions temporal distribution. The last test of this type used scrambled winds — each component of the horizontal ground level winds was scrambled separately by use of Eq. (3.8). The results of these tests show that stochastic errors tend to average out. In day-averaged concentrations, the scrambled data resulted in deviations of less than 10 percent from the standard results (the station-by-station comparison is given in Section 3.5); the mean differences, root mean square differences and correlation coefficients are also in close agreement. Hourly-averaged concentrations averaged within 20 percent of the standard results.

The last of the sensitivity analyses was a comparison of three calculations each using different random positions for the placement of particles. Point particle procedure was used in these tests. Eight hour averages were computed — these were within 10 percent of each other. For hourly averages, the maximum variation was under 35 percent and average deviation was approximately 10 percent. The use of the area-weighting procedure would be expected to reduce this deviation because the procedure smoothes out effects of particle position.

Two possible improvements in the standard input data were tested: new source emissions inventory and a time-dependent rising inversion. A source emission inventory was recently completed by Roberts, et.al.[23] and forwarded to us by Roth.[24] In Roberts' inventory, traffic is divided between freeway and non-freeway, each having its own spatial and temporal distribution as shown in Figures 37, 38 and 39. A major difference between this new inventory and the one used previously is the total carbon monoxide emitted per day. In the previous inventory, the emissions were normalized to the 10^7 Kg/day reported by the California Air Resources Board. Roberts' inventory has a total of only 0.6×10^7 Kg/day for approximately the same region. Other differences are in the spatial distributions of the two inventories. These differences may be attributed to traffic changes in the years between their compilation and the greater resolution of Roberts' work. The temporal distributions also differ by their claimed resolution. It was anticipated that the explicit treatment of the freeway traffic in Roberts' inventory would lead to better correlation with the observed early morning rise in CO at the Downtown and Hollywood stations. This was partially borne out by the NEXUS calculation; the morning rise in CO concentration at Downtown between 6:00 and 8:00 A.M. was simulated (approximately an hour later than observed). However, the day averaged results were poor — having a mean difference of almost 2 ppm, a RMSD of 3.2 ppm and a correlation coefficient of only 0.55. Since the correlation coefficient is invariant under a linear transformation of the results, these poor results with Roberts' inventory cannot be attributed entirely to the low value of total CO daily emissions.

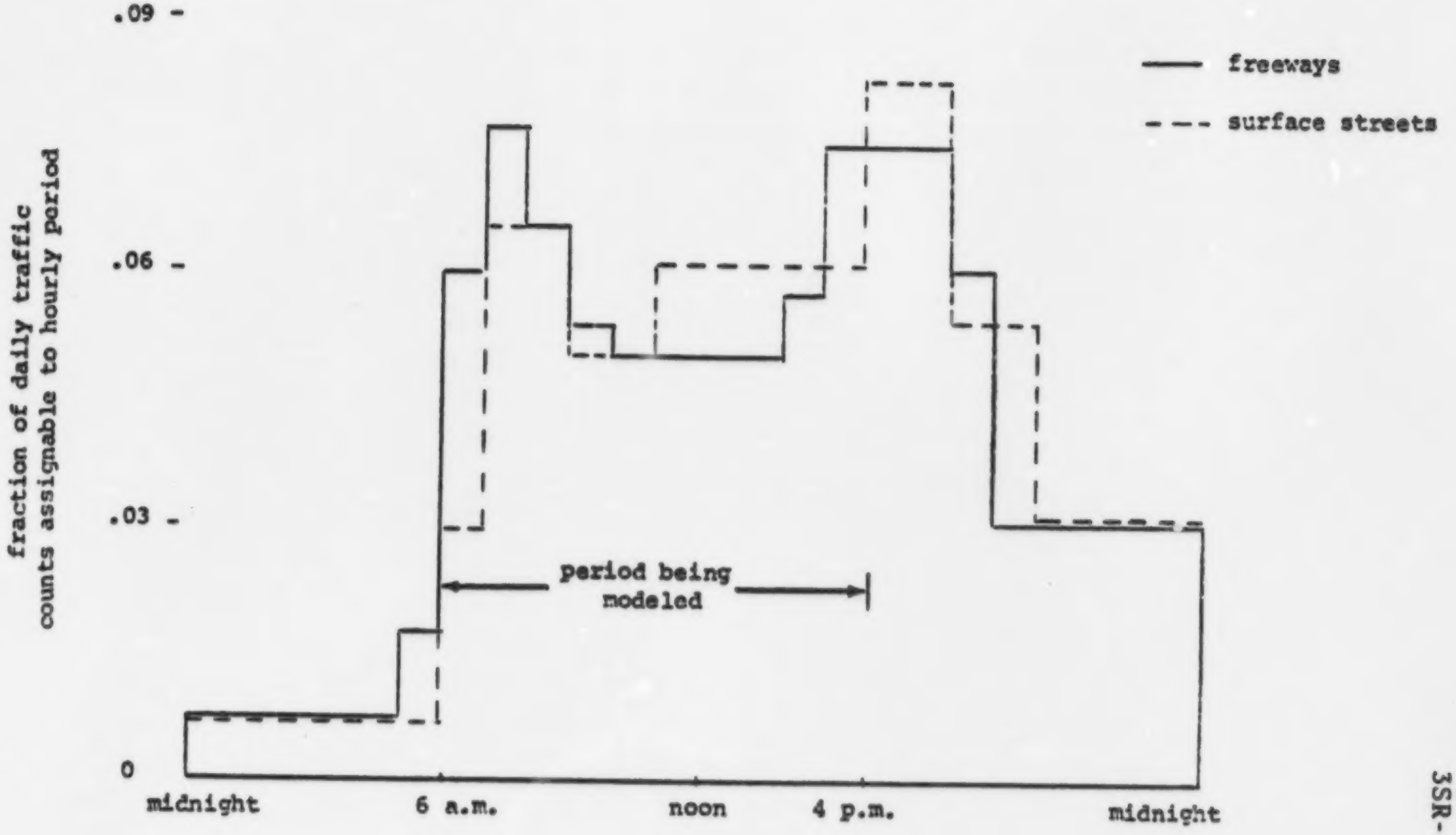

Figure 37 – Temporal Distribution of Traffic for Freeways and Surface Streets. (Reference 23.)

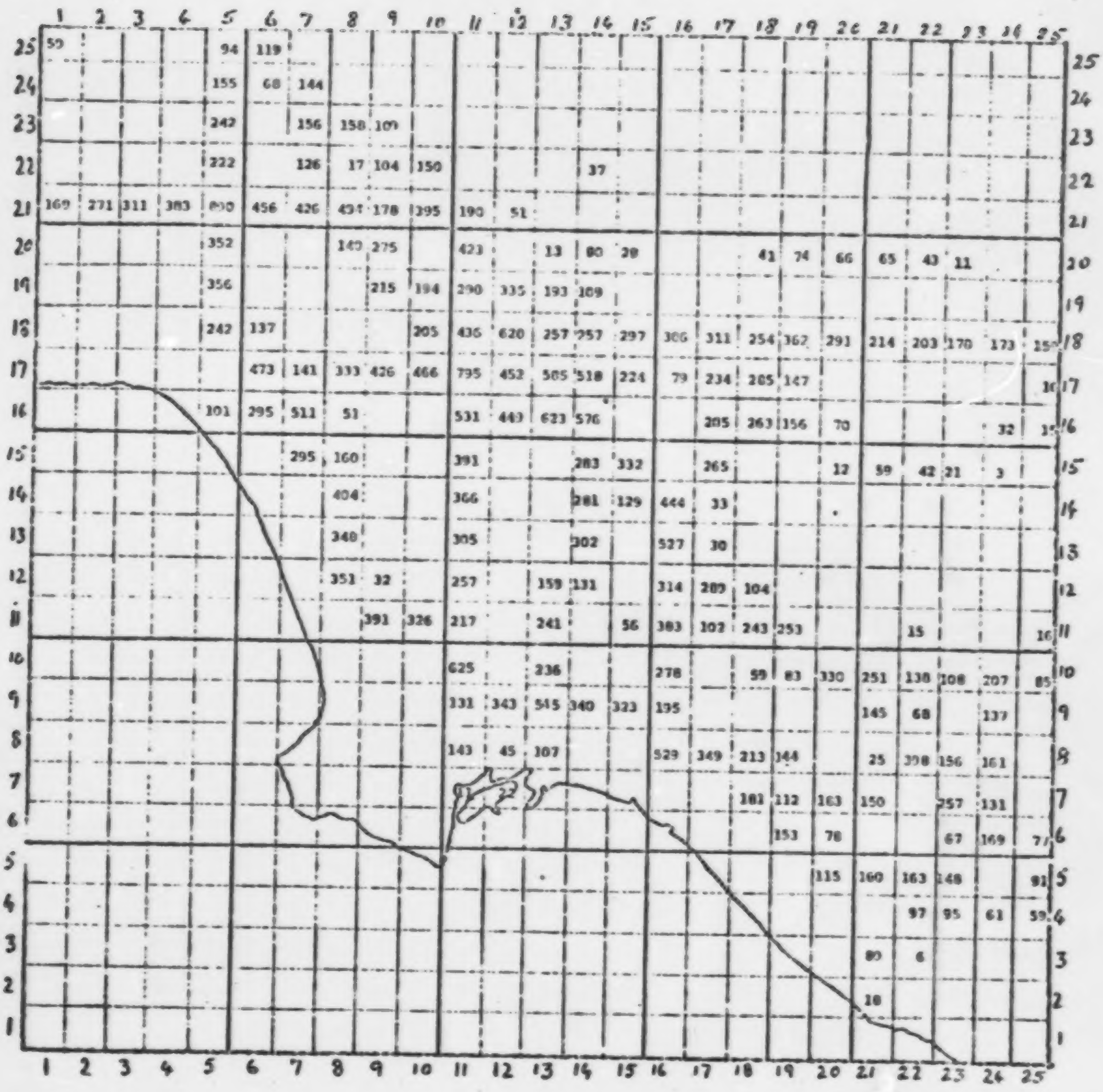
1 2 3 4 5 6 7 8 9 10 11 12 13 14 15 16 17 18 19 20 21 22 23 24 25
25 59 94 119
24 155 68 144
23 242 156 158 109
22 222 126 17 104 150 37
21 169 271 311 383 890 456 426 434 178 395 190 51
20 352 149 275 423 13 80 28 41 74 66 65 43 11
19 356 215 194 290 335 193 109
18 242 137 205 436 620 257 257 297 306 311 254 362 291 214 203 170 173 15
17 473 141 333 426 466 795 452 585 518 224 79 234 205 147 10
16 101 295 511 51 531 443 623 576 205 263 156 70 32 15
15 295 160 391 283 332 265 12 59 42 21 3
14 404 366 281 129 444 33
13 348 305 302 527 30
12 351 32 257 159 131 314 289 104
11 391 326 217 241 56 383 102 243 253 15 16
10 625 236 278 59 83 330 251 138 108 207 85
9 331 343 545 340 323 195 145 68 137
8 143 45 107 529 349 213 144 25 398 156 161
7 181 112 163 150 257 131
6 153 78 67 169 71
5 115 160 163 148 91
4 97 95 61 59
3 89 6
2 18
1
1 2 3 4 5 6 7 8 9 10 11 12 13 14 15 16 17 18 19 20 21 22 23 24 25

Figure 38 – Spatial Distribution of Freeway Traffic (thousand vehicle miles per day). (Ref. 23)

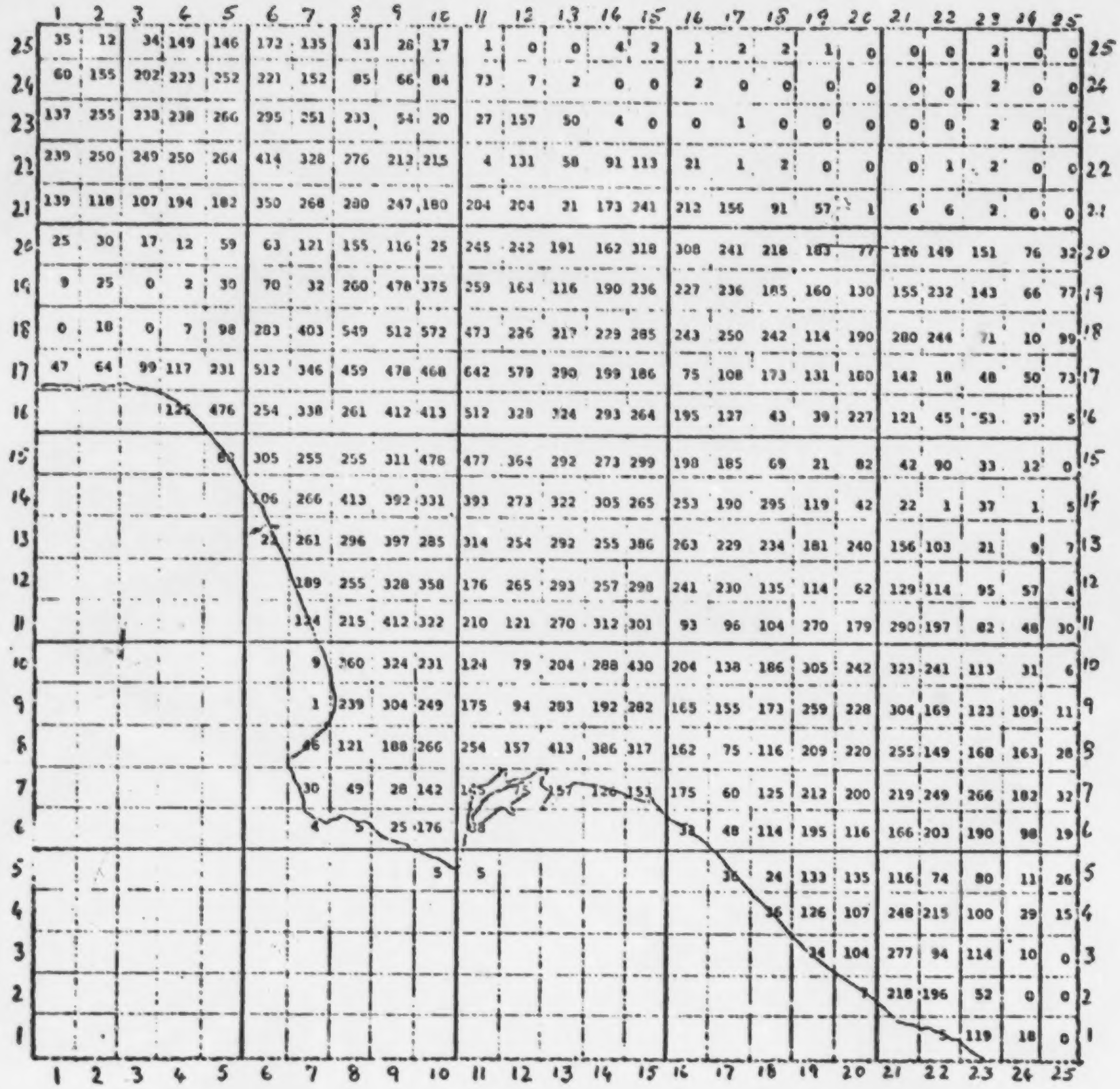

	1	2	3	4	5	6	7	8	9	10	11	12	13	14	15	16	17	18	19	20	21	22	23	24	25
25	35	12	34	149	146	172	135	43	28	17	1	0	0	4	2	1	2	2	1	0	0	0	2	0	0
24	60	155	202	223	252	221	152	85	66	84	73	7	2	0	0	2	0	0	0	0	0	0	2	0	0
23	137	255	233	238	266	295	251	233	54	20	27	157	50	4	0	0	1	0	0	0	0	0	2	0	0
22	239	250	249	250	264	414	328	276	212	215	4	131	58	91	113	21	1	2	0	0	0	1	2	0	0
21	139	118	107	194	182	350	268	280	247	180	204	204	21	173	241	212	156	91	57	1	6	6	2	0	0
20	25	30	17	12	59	63	121	155	116	25	245	242	191	162	318	308	241	218	183	77	186	149	151	76	32
19	9	25	0	2	30	70	32	260	478	375	259	164	116	190	236	227	236	185	160	130	155	232	143	66	77
18	0	18	0	7	98	283	403	549	512	572	473	226	217	229	285	243	250	242	114	190	280	244	71	10	99
17	47	64	99	117	231	512	346	459	478	468	642	579	290	199	186	75	108	173	131	180	142	18	48	50	73
16				125	476	254	338	261	412	413	512	328	324	293	264	195	127	43	39	227	121	45	53	27	5
15					88	305	255	255	311	478	477	364	292	273	299	198	185	69	21	82	42	90	33	12	0
14						106	266	413	392	331	393	273	322	305	265	253	190	295	119	42	22	1	37	1	5
13						22	261	296	397	285	314	254	292	255	386	263	229	234	181	240	156	103	21	9	7
12							189	255	328	358	176	265	293	257	298	241	230	135	114	62	129	114	95	57	4
11							124	215	412	322	210	121	270	312	301	93	96	104	270	179	290	197	82	48	30
10							9	260	324	231	124	79	204	288	430	204	138	186	305	242	323	241	113	31	6
9							1	239	304	249	175	94	283	192	282	165	155	173	259	228	304	169	123	109	11
8							86	121	188	266	254	157	413	386	317	162	75	116	209	220	255	149	168	163	28
7							30	49	28	142	165	75	157	126	153	175	60	125	212	200	219	249	266	182	32
6							4	5	25	176	88					32	48	114	195	116	166	203	190	98	19
5										5	5						36	24	133	135	116	74	80	11	26
4																		36	126	107	248	215	100	29	15
3																			34	104	277	94	114	10	0
2																				7	218	196	52	0	0
1																						5	119	18	0

Figure 39 – Spatial Distribution of Non-Freeway Traffic (thousand vehicle miles per day). (Ref. 23)

The observed early morning rise in CO could also be explained by reduced dispersion during the morning rush hours. The standard results were calculated with a fixed inversion height for comparison with Lamb's work. Next a rising inversion height was included with the standard input for a NEXUS simulation. The same diffusivities as previously used were retained ($K_x = K_y = 1.2$ m²/sec and $K_z = 0.6$ m²/sec or 0.0), but until 6:00 A.M. $K_z = 0.0$ was used for all levels. From 6:00 A.M. to 12 noon, $K_z = 0.6$ m²/sec was used below the inversion height and $K_z = 0.0$ above. The inversion height was obtained by a linear interpolation between ground level at 6:00 A.M. and the standard inversion height (300 meters) at 12 noon. The hourly-averaged carbon monoxide concentrations at two stations are shown in Figure 40.

The rising inversion did have the anticipated effect of limiting early morning dispersion and the calculated results for the early morning hours are in better agreement with the measurements. The day averaged concentrations were higher in this simulation than in the standard results of NEXUS. In comparison with the APCD observations, the rising inversion NEXUS results had a mean difference of -1.17 ppm, RMSD of 3.7 ppm but correlation coefficient of 0.7. Perhaps the below-inversion diffusivities were too low leading to the afternoon concentrations higher than observed. This is suggested by the work of Eschenroeder and Martinez[18] in which a velocity dependent vertical diffusivity is used. Their vertical diffusivity would average about 6 m²/sec in the afternoon, compared to the 0.6 m²/sec used here. These two examples illustrate some of the improvements possible within the framework of NEXUS. Next a few modifications to the framework and to the PICK method used will be described.

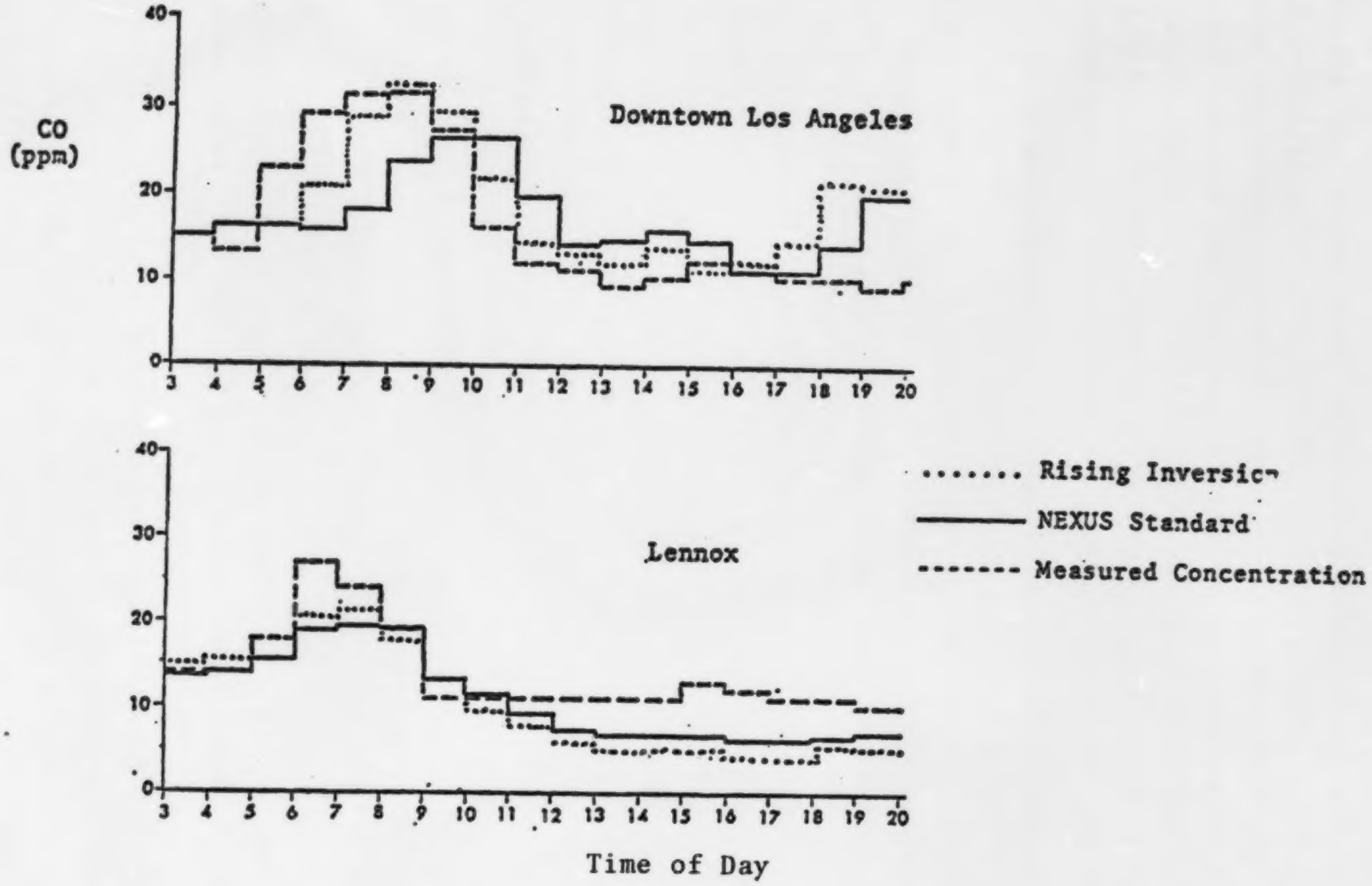

Figure 40 – Hour-Averaged CO (in ppm) calculated with an inversion rising height is compared to the standard results with a fixed inversion height and to the measured concentrations.

The NEXUS model as reported here has a very general formulation, describing three-dimensional advection and diffusion. However, by setting input variables (winds and diffusivities) it can simulate models having only two spatial dimensions. It also has both Eulerian and Lagrangian features. Modifications of NEXUS can be made to emphasize either, and thus evaluate the advantages and disadvantages of Eulerian or Lagrangian methods.

The first modification was the assumption of a single layer below a constant inversion height and use of only the observed, horizontal, ground-level winds. This modification assumes complete mixing below the inversion height. In this respect it is similar to the work of Weisburd, et.al.,[25] with a single cell moving along a Lagrangian trajectory. The statistical comparisons of the day-averaged CO concentrations calculated with the modified NEXUS and the observed concentrations showed a mean difference of -0.33 ppm, a RMSD of 3.39 ppm and a correlation coefficient of 0.49. This indicates time- and space-averaged the concentrations were correctly simulated, but the spatial dependence of the day-averaged concentrations were poorly correlated. The hourly averaged results had sharp peaks of very high concentrations. For example, at Lennox 42 ppm was calculated for 8:00 A.M. when 18 ppm was observed. These unphysical maxima correspond to convergences in the observed horizontal wind field.

Two approaches were suggested to alleviate this problem: (1) "smooth" the observed winds to make a divergence-free, horizontal wind field and (2) modify the calculated concentrations to take into account any non-zero divergence, $\vec{\nabla}\cdot\vec{u} \neq 0$. The first approach was used by Browne.[26] The second approach was adopted for the next test. At each cycle the divergence of the wind field is calculated and the concentrations (and thus the particle masses) are modified by an artificial factor so that:

$$c = c\left[\frac{\Delta x\ \Delta y}{\Delta x\ \Delta y(1 + \Delta t\vec{\nabla}\cdot\vec{u})}\right] \qquad (3.9)$$

where the term in the brackets is a volume change due to the divergence $\vec{\nabla}\cdot\vec{u}$. Since this must be computed for each cell, the divergence was computed by first-order finite differencing:

$$\vec{\nabla}\cdot\vec{u} = \frac{u_{i+1} - u_{i-1}}{2\Delta x} + \frac{v_{i+1} - v_{i-1}}{2\Delta y} \ . \qquad (3.10)$$

With this modification, the correlation coefficient for the resulting day-averaged concentrations was 0.74, but the mean difference was 3.25 ppm and the RMSD 4.13 ppm. That is, the results were lower than the observations but the spatial distribution concentrations were well correlated. This suggests that the vertical mixing was too high in this test, but the modification of the concentration to take into account the non-divergence-free wind field was a step in the right direction.

The last series of tests evaluated the computer time required by finite difference techniques with the 3-D Eulerian grid of NEXUS. The techniques used were similar to the first-order and Fromm's fourth-order methods described in Section 2.2, except that splitting was not used. The first-order method introduced errors that are exhibited as truncation diffusivities which, for the grid used in NEXUS and a typical five minute time step (assuming $u\Delta t/\Delta x \approx 0.4$, $v\Delta t/\Delta y \approx 0.4$ and $w\Delta t/\Delta z \approx 0.4$) were: $K_x = K_y = 800\ m^2/sec$ and $K_z = 4\ m^2/sec$. The fourth-order method computed negative concentrations that had to be ignored. The actual simulation results would be expected to improve if splitting were used, but the time required for computations would be almost identical. The computer time required for 17 hour simulation with the standard input data using the first-order method was four minutes, while the fourth-order method required five minutes. These can be compared with the twelve minutes required by the standard NEXUS.

3.5 SUMMARY AND CONCLUSIONS

The NEXUS code was developed to apply the PICK method to problems of regional air pollution. NEXUS simulates advection and diffusion of a non-reactive pollutant in three-dimensions and was applied to the simulation of CO concentrations in Los Angeles. In the development of NEXUS, the PICFIC code was extended to three dimensions, border cells and boundary conditions at the ground were added. All input data was written on tape by a SETUP routine and read by NEXUS. Using meteorological and source data available in the literature, NEXUS results for 17 hour-averaged CO concentrations at 12 stations averaged within 20 percent of Los Angeles Air Pollution Control District observations. The calculation of CO throughout the region for 17 hours took 12 minutes on a UNIVAC 1108. The NEXUS results were in better agreement with observations than Lamb's model using the same meteorological data.

The results of series of tests with NEXUS are summarized in Table VI. The sensitivity of NEXUS to the input data was tested by introducing random variations (scrambling) in the data. A new vehicle source inventory and a time-dependent (rising) inversion height were tested by NEXUS calculation. NEXUS was used to simulate a two-dimensional well-mixed-layer model and to test a divergence-free modification. Two finite difference methods using the NEXUS Eulerian grid were compared to NEXUS for computing time. The finite difference methods took one-third to one-half as much computer time as NEXUS for the same 17 hour simulation, but encountered difficulties mentioned in Section 2.2.

TABLE VI

	APCD OBSERV.	NEXUS STD.	LAMB'S MODEL	NEXUS NEW SOURCES	NEXUS RISING INVER.	SCRAMBLED TIME DISTRIB.	SOURCES SPATIAL DISTRIB.	SCRAMBLED WINDS	NEXUS 2D WINDS	NEXUS 2D WINDS & $\nabla \cdot u = 0$ MODIFICATION
DOWNTOWN LA	16	18	22	13	19	19	18	18	14	12
AZUSA	13	9	3	10	10	10	10	10	10	10
PASADENA	17	17	15	14	23	19	19	18	22	11
BURBANK	16	17	7	14	20	18	18	18	17	12
EAST LA	12	16	5	14	20	18	18	18	17	12
WEST LA	16	12	13	11	13	12	13	13	12	9
LONG BEACH	14	12	8	11	14	13	13	12	14	9
HOLLYWOOD	17	17	7	13	18	18	17	16	13	12
POMONA	13	9	3	10	10	10	10	10	10	10
ANAHEIM	9	9	7	12	10	10	10	10	14	9
LENNOX	13	10	11	9	11	11	11	11	15	9
LA HABRA	6	8	3	8	8	8	8	8	8	8
Concentration Coefficient		0.73	0.55	0.55	0.70	0.72	0.73	0.71	0.49	0.74
δ		0.67	4.8	1.92	-1.17	-0.33	-0.25	0	-0.33	3.25
δ^2		2.68	6.66	3.20	3.67	2.86	2.66	2.68	3.39	4.13

4. NEXUS/P SIMULATION OF PHOTOCHEMICAL SMOG

In Section 1.3 a technique to introduce the effects of chemical reactions into the PICK method was briefly described. With this technique the NEXUS code was extended to simulate chemically reacting pollutants, forming the NEXUS/P model (Numerical EXamination of Urban Smog with Photochemistry). The major addition was the encoding of the technique by which particles can change mass during the calculation. In NEXUS, each particle has a fixed mass, set when the particle is introduced into the calculation. Chemical reactions occurring in the atmosphere have the effect of removing primary pollutants and forming secondary ones. The net effects are changes in the concentrations of the reacting and product pollutants. The PICK method is based on using particles to represent pollutant mass and so for reacting and product species the mass represented by the particles must be changed and new particles must be created.

The turbulent atmospheric diffusion equation being solved with the NEXUS/P code can be written as

$$\frac{\partial c_s}{\partial t} = -\bar{u}\frac{\partial c_s}{\partial x} - \bar{v}\frac{\partial c_s}{\partial y} - \bar{w}\frac{\partial c_s}{\partial z} + \frac{\partial}{\partial x}\left\{K_x \frac{\partial c_s}{\partial x}\right\} + \frac{\partial}{\partial y}\left\{K_y \frac{\partial c_s}{\partial y}\right\} + \frac{\partial}{\partial z}\left\{K_z \frac{\partial c_s}{\partial z}\right\}$$

$$+ \sum_{r,t} B_{srt}\, c_r\, c_t + \sum_{r,t} P_{sr}\, c_r \ , \tag{4.1}$$

Preceding page blank

where the concentration subscripts have been used to emphasize different chemical species and the two new terms represent bimolecular and photochemical reactions (B and P, respectively). There is a separate differential equation for each species being simulated. The differential equations are no longer linear and are coupled together through the chemical terms.

In the PICK method as used in NEXUS/P, the equations are rewritten as

$$\frac{\partial c_s}{\partial t} = - \frac{\partial u c_s}{\partial x} - \frac{\partial v c_s}{\partial y} - \frac{\partial w c_s}{\partial z} + S_s \quad , \qquad (4.2)$$

where the fictitious total velocity is used for pollutant transport and the chemical terms have been grouped into a source or sink for the "sth" species, S_s. Eq. (4.2) is solved assuming the effects of pollutant transport and of chemical reactions are separable. Pollutant transport is simulated for a time interval, then chemical reactions are simulated for the same interval. That is, the transport and reactions are calculated in sequence. The NEXUS code was used for the pollutant transport and new subroutines were added for reactions. The NEXUS/P code is described in Section 4.1 and photochemical simulation is detailed in Section 4.2. The results of tests made with the NEXUS/P code are given in Section 4.3. A photochemical simulation of Los Angeles smog is described in Sections 4.4 and 4.5.

4.1 DESCRIPTION OF NEXUS/P

The NEXUS/P code was developed from the NEXUS code. Simulating chemical reactions requires re-weighting the particles based on cell concentration changes. A simple reweighting algorithm is possible with the point particle procedure, Eq. (1.15). Thus, NEXUS was re-written for point particles in developing NEXUS/P. In addition, new subroutines were included to simulate the chemical reactions to calculate the changes in cell concentrations and to introduce new particles for product species.

The new subroutines (KEM, CHEM and NPART) are shown in the general NEXUS/P flow chart, Figure 41. The KEM subroutine checks each cell to determine if chemical simulation is necessary. CHEM is used to simulate the effects of chemical reactions as will be discussed in Section 4.2. Subroutine NPART adds new particles. The re-weighting of particle mass is completed in an addition to PARCEL.

The S^3 UNIVAC 1108 has available 64K of central processor computer core. This cannot accommodate the requirements of NEXUS with multiple species. Basically, NEXUS/P requires four variables (x, y, z and mass) for each particle; separate particles for each specie; and winds, diffusivities, species concentrations and the chemical changes in concentration for each cell. For 2,000 cells, 10,000 particles and 5 species, the core required would be approximately 230K. NEXUS/P instead uses bulk storage (magnetic drums) and shifts data into the central processing unit for computations as required. In developing NEXUS/P, NEXUS was re-written to minimize the number of variables needed during each calculation. This has resulted in a requirement for the cell concentrations and chemical changes in concentrations for all species, or, at another time, the winds, diffusivities, concentrations, chemical changes in concentrations, and particle position and mass for a single species (a maximum of 54K for the above example) in the central processing unit at a single time. Two new subroutines, ROLLIN and ROLOUT, were developed to handle the peripheral storage and manipulation for concentration, chemical changes in concentration, and particle position and mass.

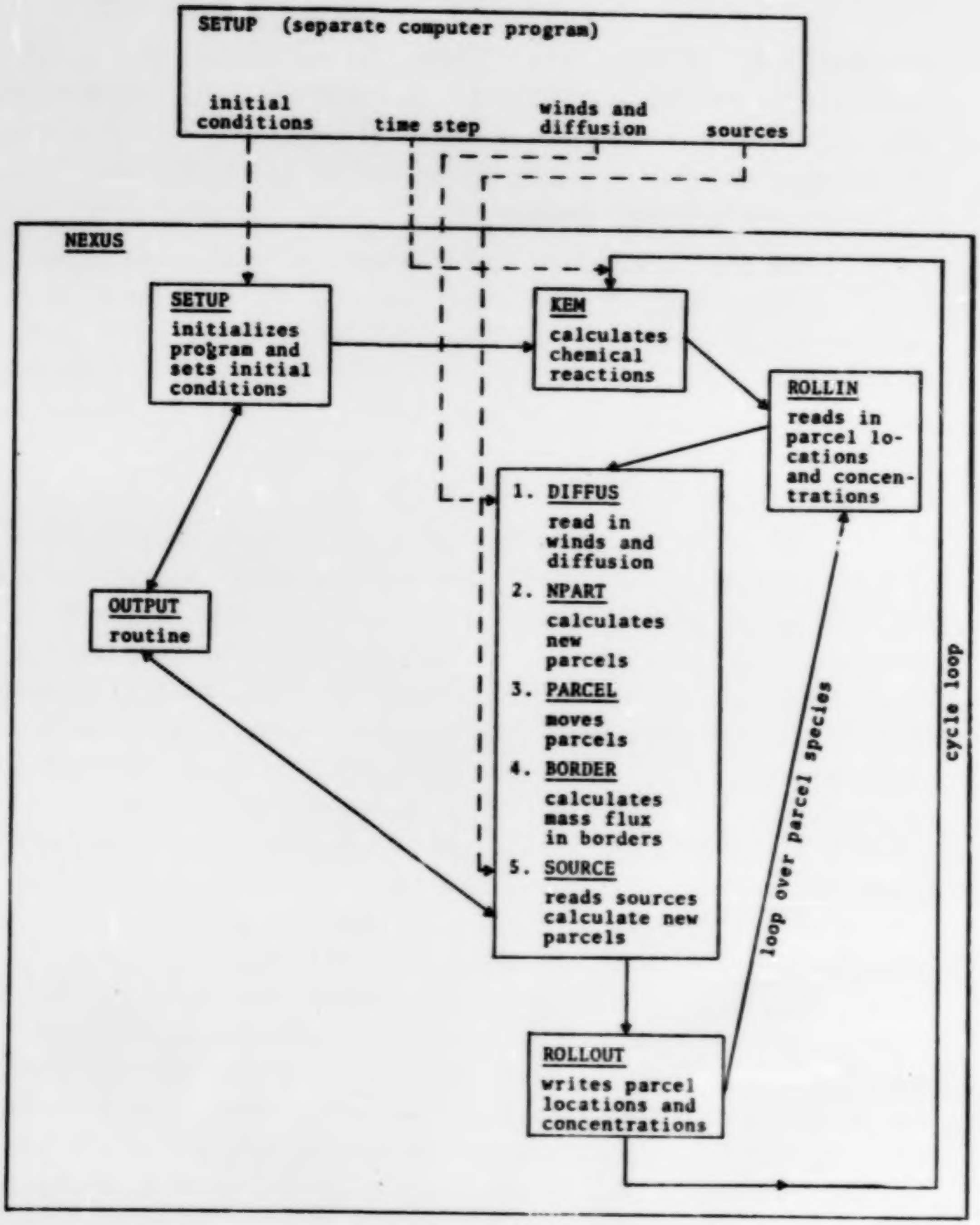
SETUP (separate computer program)
initial conditions
time step
winds and diffusion
sources
NEXUS
SETUP
initializes program and sets initial conditions
KEM
calculates chemical reactions
ROLLIN
reads in parcel locations and concentrations
1. DIFFUS
read in winds and diffusion
2. NPART
calculates new parcels
3. PARCEL
moves parcels
4. BORDER
calculates mass flux in borders
5. SOURCE
reads sources calculate new parcels
OUTPUT
routine
ROLLOUT
writes parcel locations and concentrations
loop over parcel species
cycle loop

Figure 41 – Macro Flow Diagram for Computing Photochemical Pollution.

An operation manual for NEXUS/P was written and is included as Volume III. This manual includes descriptions and listings of the subroutines of NEXUS/P and the input data processing routine SETUP, all translated into IBM 360 FORTRAN IV.

4.2 PHOTOCHEMICAL SIMULATION

The simulation of reactions occurring in photochemical smog begins with the choice of a set of chemical reactions or chemical mechanisms. In the atmosphere the actual number of elemental reactions can be very large, beyond the capacity of present computers. For example, of the many hydrocarbons in an urban atmosphere, at most three types of hydrocarbons are represented in chemical mechanisms reported in the literature.[27,28,29] Present chemical mechanisms are based on lumping many similar species into a single "effective" species and many similar reactions in a single "effective" reaction. The effective hydrocarbon species used in present chemical mechanisms may not be a real hydrocarbon, but instead react as an average of real hydrocarbons. The reactions used may also not be elementary reactions and may even be non-stochiometric. This approach is referred to as the "Lumped Parameter" approximation.

The NEXUS/P model can use any method that predicts the changes in cell concentrations due to chemical reactions. For the Los Angeles photochemical smog simulation reported in Section 4.5, a set of reactions based on the lumped parameter approximation and reported by Eschenroeder and Martinez[29] was used. Eschenroeder's chemical mechanism is given in Table VII.

The set of chemical reactions can be translated into a set of coupled, non-linear, first-order differential equations — the chemical kinetics rate equations. For example,

TABLE VII

RATE COEFFICIENTS FOR ESCHENROEDER'S MODEL OF THE HYDROCARBON/NITRIC OXIDE MECHANISM

(Reference 29)

(Stoichiometry imbalances may occur because of lumped parameter assumptions.)

	REACTION	RATE COEFFICIENTS
1.	$(h\nu) + NO_2 \rightarrow NO + O$	$0.4\ min^{-1}$
2.	$O\ (+ O_2)(+ M) \rightarrow O_3 + M$	$2.64 \times 10^6\ min^{-1}$
3.	$O_3 + NO \rightarrow NO_2\ (+ O_2)$	$40\ ppm^{-1}\ min^{-1}$
4.	$O + HC \rightarrow 2RO_2$	$6100\ ppm^{-1}\ min^{-1}$
5.	$OH + HC \rightarrow 2RO_2$	$80\ ppm^{-1}\ min^{-1}$
6.	$RO_2 + NO \rightarrow NO_2 + 0.5\ OH$	$1500\ ppm^{-1}\ min^{-1}$
7.	$RO_2 + NO_2 \rightarrow PAN$	$6\ ppm^{-1}\ min^{-1}$
8.	$OH + NO \rightarrow HNO_2$*	$10\ ppm^{-1}\ min^{-1}$
9.	$OH + NO_2 \rightarrow HNO_3$*	$30\ ppm^{-1}\ min^{-1}$
10.	$O_3 + HC \rightarrow RO_2$	$0.0125\ ppm^{-1}\ min^{-1}$
11.	$(H_2O +)\ NO + NO_2 \rightarrow 2HNO_2$**	$0.01\ ppm^{-1}\ min^{-1}$
12.	$(h\nu) + HNO_2 \rightarrow NO + OH$	$0.001\ min^{-1}$

*Rate constant incorporates third body concentration.

**Water vapor incorporated into rate coefficient.

RO_2 is used as the chemical symbol for a free radical lumped species.

HC stands for the hydrocarbon lumped species.

Parentheses are used to indicate species concentrations that are not chemically changing and are incorporated into the rate coefficient.

The solar flux is represented by "hν," the maximum solar flux is incorporated into the first rate coefficient.

the inorganic loop of Eschenroeder's mechanism is:

$$1.\quad (h\nu) + NO_2 \xrightarrow{k_1} NO + O$$

$$2.\quad O(+O_2)(+M) \xrightarrow{k_2} O_3 + M$$

$$3.\quad O_3 + NO \xrightarrow{k_3} NO_2(+O_2) \quad ,$$

where $h\nu$ represents ultraviolet photons of the solar flux (which vary from sunrise to sunset), the third body, M, is the total concentration of all species present (necessary for conservation of energy and momentum in the reaction), and the k's are the rate coefficients. Species concentrations that are not varying due to the chemical reaction are usually incorporated into the rate coefficient. In the second reaction, the concentration of molecular oxygen and of M can be assumed constant and incorporated into the rate coefficient $k_2' = k_2[O_2][M]$. The rate for each reaction is given by

$$r_1 = k_1[NO_2]$$

$$r_2 = k_2'[O]$$

$$r_3 = k_3[O_3][NO] \quad , \qquad (4.3)$$

where the square brackets indicate the numerical value of the concentration.

Thus, the chemical kinetics rate equations (differential equations for the total time rate of change of a species) can be written as

$$\frac{d[NO_2]}{dt} = -r_1 + r_3 = -k_1[NO_2] + k_3[O_3][NO]$$

$$\frac{d[O]}{dt} = r_1 - r_2 = k_1[NO_2] - k_2'[O]$$

$$\frac{d[NO]}{dt} = r_1 - r_3 = k_1[NO_2] - k_2[O_3][NO]$$

$$\frac{d[O_3]}{dt} = r_2 - r_3 = k_2'[O] - k_3[O_3][NO] \quad . \qquad (4.4)$$

These differential equations are non-linear and are difficult to solve. The rate equations are all of the form

$$\frac{dc}{dt} = F - Rc \quad , \qquad (4.5)$$

where F is a summation of the rate of all reactions forming species c, and Rc is a summation of all those reactions removing c. F and R are called the formation and removal rates, respectively. For example with the full chemical mechanism, Table VII, the time rate of change of RO_2 can be written in this form as:

$$\frac{d[RO_2]}{dt} = \left\{2k_4[O][HC] + 2k_5[OH][HC] + k_{10}[O_3][HC]\right\}$$
$$- \left\{k_6[NO] + k_7[NO_2]\right\}[RO_2] \quad .$$

The non-linearities have been suppressed in this form, but another difficulty, that of "stiffness," can be discussed. For simplicity in this discussion of stiffness, R and F are assumed constant. Then the solution of

Eq. (4.5) is the sum of a constant term and an exponential term, e^{-Rt} . For solutions decaying to zero (no constant term in the solution, or physically, a small equilibrium value), the solution is reduced by a factor of 1/e in a time 1/R . In typical applications the values of R for different species concentrations may differ by many orders of magnitude. In this case the times associated with significant variations in different species concentrations differ by orders of magnitude and the differential equations are called "stiff." The standard methods for solution of first-order coupled differential equations (Euler's method, Runga-Kutta, Adams predictor-corrector) have a time step limitation of the order of 1/R for the largest removal rate. In essence, the calculation is limited by the fastest reaction even though it may not lead to significant concentration variations. For example, in Eschenroeder's mechanism the atomic oxygen is rapidly removed by reactions with hydrocarbons (reaction 4) and molecular oxygen (reaction 2), but usually is not varying rapidly because it is in equilibrium with photochemical production from NO_2.

An approach designed to treat general stiff equations was reported recently by Gear.[30] S³ has developed a general chemical reaction model, KEM-GEAR, using the Gear method for integrating stiff equations. A test case was computed using KEM-GEAR and compared to results published by Eschenroeder.[29] Eschenroeder used a Padé approximant for the exponential solution of Eq. (4.5) and the two results agreed to the accuracy of the reported concentrations. An advantage of the KEM-GEAR approach was the computer time required. On the S³ UNIVAC 1108 the test case took 7.9 seconds; Eschenroeder reported 50 seconds on a CDC 6400. The CDC 6400 is approximately 20 percent slower than the UNIVAC 1108.

Thus, KEM-GEAR was about a factor of five faster than the Padé approximant method. The disadvantages of KEM-GEAR are the program size and core requirements since it is a multi-step integration method. This motivated the development of a simpler technique.

Some species are formed as rapidly as they are removed so that their concentration does not vary appreciably. These species are in a pseudo-equilibrium. This is not a true equilibrium since the reactants in the forming and removing reactions may still be changing. If a species were in this pseudo-equilibrium, the term dc/dt in Eq. (4.3) would be small compared with F or cr giving

$$c \approx F/R \quad . \tag{4.6}$$

This is much simpler to compute than to integrate Eq. (4.3), and so the results of KEM-GEAR calculations were analyzed to determine if, when and for what species

$$0.999 \leq \left|\frac{c}{(F/R)}\right| \leq 1.001 \quad . \tag{4.7}$$

The analysis showed that species O , RO_2 and OH satisfy Eq. (4.7) and could be accurately solved using Eq. (4.6). These are free radials and could have been expected to be in pseudo-equilibrium due to their fast removal reactions, though HNO_2, another free radical was found not to satisfy Eq. (4.7).

The terminating products (PAN, HNO_3) are only products of the reaction and so would not control the time step for the standard methods. Of the other species, the three radicals mentioned above can be solved from Eq. (4.6) and only the remaining five species (NO, NO_2, O_3 HC and HNO_2) must be calculated by solving the differential equations. A small code, CHEM, was developed in which these five remaining differential equations are solved. The solution is based on the analytic solution of Eq. (4.2) for a time step, Δt , assuming constant F and R :

$$c(t+\Delta t) = F/R + [c(t) - F/R]e^{-R\Delta t} \quad . \qquad (4.8)$$

For a sufficiently small Δt , R and F are almost constant and the solution is a good approximation. This method has been used by Keneshea.[31] In CHEM the species concentrations are predicted as indicated by Eq. (4.8). Then F and R are recalculated using the predicted concentrations, c_p , and new "corrected" concentrations, c_c , are calculated again using Eq. (4.8). A desired fractional error limit, ER , is used to compute the appropriate time step, Δt , from a trial time step $\Delta t'$:

$$\Delta t = ER \left| \frac{c_p + c_c}{c_p - c_c} \right| \Delta t' \quad . \qquad (4.9)$$

An initial time step of 10^{-9} seconds is used to insure starting accuracy. With an ER = 0.005, the CHEM results agreed with those of KEM-GEAR to better than 10 percent at the NO_2 maximum concentration and, at worst, less than a 20 percent difference at the end of the calculation (150 minutes). CHEM required only 1.8 seconds computer time for the same calculation KEM-GEAR used 7.9 seconds . . . better than a factor of four savings in computer time or about twenty times faster than Eschenroeder's solution.

The CHEM code was incorporated as a subroutine into the NEXUS/P code for chemical simulation to form the quantity

S_s in Eq. (4.2). An intermediate subroutine KEM was developed to call CHEM for each cell in which chemical reactions are significant. The CHEM subroutine calculates new cell concentrations due to chemical reactions for a time interval equal to the NEXUS/P time step. The CHEM subroutine returns the fractional change in concentration for each species:

$$CF = \frac{c(t+\Delta t)}{c(t)} \quad . \tag{4.10}$$

If the initial cell concentration of a species produced by chemical reactions were zero, CHEM would return the negative of the concentration produced:

$$CF = -c(t+\Delta t) \quad .$$

The negative sign is used as a flag to indicate that CF is the new concentration instead of the fractional change.

4.3 NEXUS/P TESTING

The accuracy of the NEXUS/P code was tested for (1) a stationary pollutant puff with chemical reactions, (2) an advecting puff with chemical reactions, and (3) an advecting and diffusing puff with chemical reactions.

The first test evaluated chemical reaction simulations in the NEXUS/P formalism. The pollutants (NO, NO_2, and HC) were initially set in a cube of five cells on a side. The winds and diffusivities were set to zero. In NEXUS/P, initial concentrations were converted to particle masses. The CHEM subroutine was used to calculate the fractional changes in concentrations for each species and cell. Then the particle masses were re-weighted to account for changes in mass due to chemical reactions. Finally, the new concentrations were calculated from particle positions (which had not changed because the winds and diffusivities were zero) and masses. Since no advection or diffusion was permitted, the changes in the concentrations depended only on the reactions and so could be compared directly to the results of the CHEM code above.

In the second test, the simulation of advection was added to that of chemical reactions. In this test, the non-linearities of the chemical kinetics rate equations are important. As the initial 125-cell pollutant puff is advected downwind, the cell concentrations along the leading and trailing edges do not remain constant, and the non-linear chemical equations introduce errors.

To illustrate this important point, consider a one-dimensional problem as illustrated in Figure 42a.

Cell	1	2	3	4	5	6
	0.0	1.0	1.0	1.0	0.0	0.0

Figure 42a — Initial Distribution of Primary Pollutant A.

Initially, cells 2-4 each have only primary pollutant, A, with cell concentration equal to 1.0. The effects of advection for a wind blowing four-tenths of a cell in time step Δt are simulated first, resulting in the distribution shown in Figure 42b.

Cell	1	2	3	4	5	6
	0.0	0.6	1.0	1.0	0.4	0.0

Figure 42b — Distribution of Primary Pollutant A After Advection.

If a quadratic chemical mechanism $(A + A \rightarrow B)$ is hypothesized to illustrate the non-linearities in chemical kinetics rate equations, the rate equations can be written as

$$\frac{d[A]}{dt} = -k[A]^2$$

$$\frac{d[B]}{dt} = +k[A]^2 \quad .$$

Furthermore, if k is small, then $k[A]^2 \; \Delta t \ll [A]$ and the effects of the chemical reaction on the concentration of A can be ignored in order to focus on the secondary pollutant production. With $[A]$ approximately constant during the reactions the equation for production of $[B]$ can be integrated

$$[B] = k[A]^2 \; \Delta t \quad .$$

That is, the production of the secondary pollutant is proportional to the square of the concentration of the primary pollutant. If, as an Eulerian technique would require, the cell concentrations of A are used in this equation, the distribution of B would be:

Cell 1	2	3	4	5	6
0.0	0.36 $k\Delta t$	1.0 $k\Delta t$	1.0 $k\Delta t$	0.16 $k\Delta t$	0.0

Figure 42c – Distribution of Secondary Pollutant, B, Calculated from Cell Concentrations given in Figure 42b.

On the other hand, the concentration of A inside the puff is 1.0 and outside 0.0. That is, in a Lagrangian frame the production of B would be:

$$[B] = k[1.0]^2 \Delta t = k\Delta t \quad ,$$

and would be distributed:

Cell 1	2	3	4	5	6
0.0	0.6 $k\Delta t$	1.0 $k\Delta t$	1.0 $k\Delta t$	0.4 $k\Delta t$	0.0

Figure 42d – Distribution of Secondary Pollutant, B, Calculated from Lagrangian Concentration.

This is the physically correct picture. The methodology used in chemical simulation with Eulerian cell concentrations introduced errors of 40 percent in cell 2 and 60 percent in cell 5. The random initial positions of the particles introduces even further irregularities in the concentrations. The NEXUS/P advection test resulted in average concentrations for the center 27 cells of the 125-cell cube that were within 10 percent of the correct values for the primary pollutants (NO, NO_2, and HC) and within 20 percent for ozone after 40 cycles.

A third test of NEXUS/P was conducted which also included the effects of diffusion. In this test, the concentrations do change, even in Lagrangian coordinates, and so no comparison to the CHEM results were made. Qualitatively, the results were correct, but no adequate method for evaluation was known.

These tests evaluated the changes made in NEXUS in the development of NEXUS/P and demonstrated the difficulties inherent in chemistry with Eulerian concentrations when sharp gradients are present. A series of tests was also made with an initial Gaussian distribution of pollutants with $\sigma_x = 2\Delta x$, $\sigma_y = 2\Delta y$ and $\sigma_z = 2\Delta z$. These results are shown in Table VIII for the central cell concentrations and should agree with the CHEM results. In these calculations, very few particles per cell were used (5 particles per cell for primary pollutants and an average of 1.5 particles per cell for O_3) and thus, the comparisons represent the upper range of the error introduced by Eulerian chemistry for this smooth distribution. Even so the errors in the central cell were within an acceptable range ($\sim$15 percent) and NEXUS/P was next applied to a real photochemical smog problem.

4.4 INPUT DATA

The NEXUS/P code was used to simulate photochemical smog in Los Angeles on September 30, 1969. This day was chosen to correspond to data supplied by others. The grid used is shown in Figure 43, a total of 22 cells in the x-direction (cells 3 to 24) × 21 cells in the y-direction (cells 4 to 24) × 4 in the z-direction with each cell 2 miles × 2 miles × 100 meters. Dickson and Start[32] supplied surface winds. The inversion height was obtained from Roth[24] and the source emissions inventory from Roberts, et.al.[23]

TABLE VIII

GAUSSIAN PUFF ($\sigma_x = 2\Delta x$, $\sigma_y = 2\Delta y$, $\sigma_z = 2\Delta z$) CENTRAL CELL CONCENTRATIONS

CYCLE	POLLUTANT	CHEM (Alone)	NEXUS/P (No Winds or Diffusion)	NEXUS/P (Winds, No Diffusion)
0	NO	5.3	5.3	5.3
	NO_2	1.0	1.0	1.0
	HC	10.0	10.0	10.0
	O_3	0.0	0.0	0.0
5	NO	4.4	4.4	4.4
	NO_2	1.9	1.9	1.9
	HC	9.3	9.3	9.3
	O_3	8.8×10^{-3}	8.8×10^{-3}	9.3×10^{-3}
10	NO	2.4	2.4	2.6
	NO_2	3.6	3.6	3.2
	HC	7.7	7.7	7.7
	O_3	2.8×10^{-2}	2.8×10^{-2}	2.6×10^{-2}

- The wind data from Dickson and Start consists of Los Angeles APCD wind network observations interpolated, extrapolated and smoothed to form hourly surface wind fields. The inversion height data obtained from Roth are shown in Figure 43. The inversion heights shown were used for the maximum heights with inversion height rising linearly from ground level at 6:00 A.M. to the maximum height at noon. This is the same procedure used in a NEXUS simulation of CO in Los Angeles. In addition to the mobile source inventory shown in Figures 37-39, Roberts compiled emissions from power plants, refineries and aircraft as well as the low level distributed sources.[23] Hydrocarbon emissions were separated into high and low reactivity. However, Eschenroeder's chemistry mechanism only uses a single hydrocarbon, so all hydrocarbons were lumped together. The oxides of nitrogen data were not separated into NO and NO_2 so an arbitrary 19 to 1 ratio was used for NO to NO_2 in emissions.

The initial concentrations of NO, NO_2, and HC were interpolated from LA APCD observations at 6:00 A.M. The APCD data were very sparse (only three stations reporting total hydrocarbons), so a "$1/r^2$" interpolation was used throughout the grid. That is, the value at surface point x,y is given by:

$$c(x,y) = \frac{\displaystyle\sum_{i=1}^{m} \frac{c_i}{(x - x_i)^2 + (y - y_i)^2}}{\displaystyle\sum_{i=1}^{m} \frac{1}{(x - x_i)^2 + (y - y_i)^2}}$$

where the ith of m stations has concentration c_i.

The SETUP code for NEXUS/P is described in the NEXUS/P operations manual, Volume III.

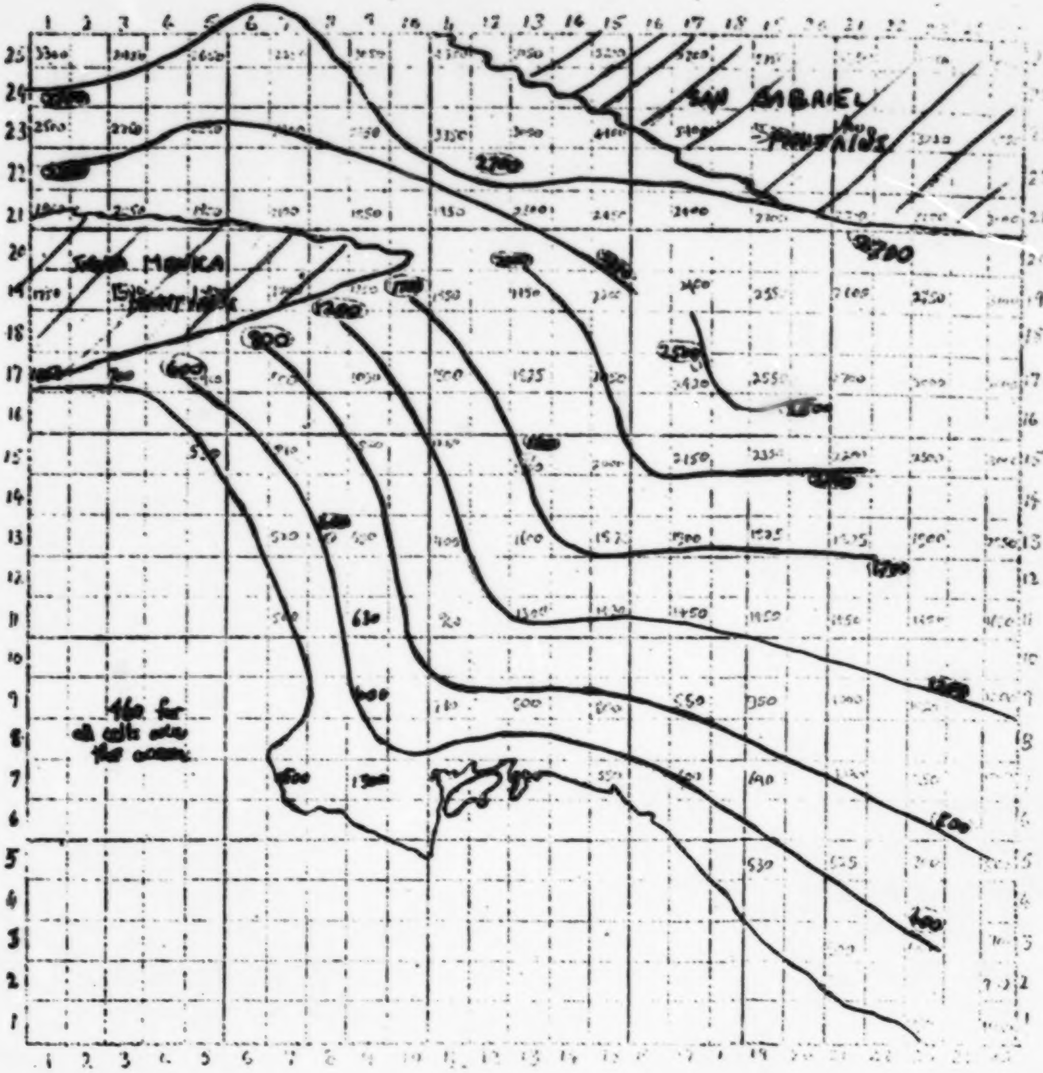
SAN GABRIEL MOUNTAINS
SANTA MONICA MOUNTAINS
2700
2700
1200
900
600
520
460 for all cells over the ocean

Figure 43 – Inversion Height (feet above sea level) at 12 noon on September 30, 1969. (Reference 24)

4.5 RESULTS OF THE NEXUS/P SIMULATION

The Los Angeles photochemical smog from 6:00 A.M. to 10:00 P.M. was simulated by NEXUS/P. The total computation time on the S^3 UNIVAC 1108 was less than one and one-half hours for the 185 cycles. This was a five species (NO, NO_2, HC, O_3 and HNO_2) simulation on the 22 × 21 × 4 grid covering 44 miles × 42 miles × 400 meters.

The prime concern of this study was to demonstrate the feasibility of the PICK method for the solution of the atmospheric diffusion equation and, in this section, for the simulation of photochemical smog. The results of photochemical smog simulation are very sensitive to the chemical mechanism and source emissions inventory. Eschenroeder's photochemical mechanism is still being developed and an expanded reaction set was reported recently.[33] The mobile source emissions inventory was not satisfactory even for the CO simulation. For these reasons, the results were given only cursory analysis and comparison with LA APCD observations. In Table IX, the calculated pollutant hour averages are averaged for the locations of all APCD stations reporting observations. This is the closest possible comparison to a regional hour-averaged concentration. The NEXUS/P results show a faster oxidation of NO to NO_2 than is observed. The NO_x (the sum of NO and NO_2) is removed too rapidly in the simulation by the product forming reactions (PAN,HNO_2). Oxidant (O_3) concentrations usually remain low due to reaction 3, converting NO to NO_2. With NO_x too low, O_3 is too high. Both NEXUS/P results and APCD observations show a double maximum in NO_2; in the calculated results at 7:00 A.M. and 2:00 P.M., and in the APCD observations at 9:00 A.M. and 1:00 P.M. The morning peak may be due to the morning emissions being oxidized as the sun rises (the UV radiation is required for reactions 1 and 12). The afternoon

TABLE IX

REGIONAL AVERAGE OF STATIONS REPORTING
(observations are in parentheses)

	POLLUTANT			
TIME	NO (pphm)	NO_2 (pphm)	HC (ppm)	O_3 (pphm)
6:00 A.M.	32 (33)	7 (6)	8 (7)	0 (1)
7:00	14 (30)	22 (10)	8 (7)	6 (2)
8:00	5 (22)	17 (17)	7 (4)	22 (4)
9:00	1 (11)	10 (18)	6 (4)	26 (6)
10:00	1 (4)	5 (14)	6 (4)	27 (9)
11:00	1 (3)	6 (11)	5 (4)	32 (12)
12:00 Noon	1 (4)	9 (15)	5 (5)	33 (14)
1:00 P.M.	1 (5)	11 (18)	5 (4)	40 (13)
2:00	1 (1)	12 (16)	3 (3)	38 (10)
3:00	1 (2)	10 (10)	2 (3)	31 (8)
4:00	2 (3)	8 (11)	2 (3)	26 (6)
5:00	3 (3)	8 (10)	2 (3)	24 (4)
6:00	3 (3)	7 (10)	1 (4)	18 (2)
13-Hr. Average	5 (10)	10 (13)	5 (4)	24 (7)

maximum occurs because the only stations reporting are located in high NO_2 regions. As expected, the NO results have the proper time dependence — almost a monotonicly decreasing function from morning rush hours to evening rush hours, when new emissions are large. The hydrocarbons (HC) also decrease until evening rush hours. The poor comparison of average HC concentration simulated by NEXUS/P at 6:00 P.M. may be due to the use of only a three-station average as well as reactions with the higher-than-observed O_3 concentrations.

Only three LA APCD stations reported hourly averages for HC. In Table X, the observations at these three stations are compared to the NEXUS/P results. Even on this station-by-station comparison the same conclusions can be reached: the NO conversion to NO_2, removal of NO_x and oxidant formation are too rapid. For example, the peak in O_3 simulated for the Downtown LA station at 8:00 A.M. is related to the over-calculation of NO_2 at 7:00 A.M.

TABLE X

LOS ANGELES APCD STATIONS REPORTING MOST COMPLETE DATA
(observations are in parentheses)

Station: 1 Location: Downtown Los Angeles

		POLLUTANT		
TIME	NO (pphm)	NO_2 (pphm)	HC (ppm)	O_3 (pphm)
6:00 A.M.	48 (45)	5 (2)	10 (10)	0.1 (1)
7:00	21 (51)	41 (1)	8 (9)	8 (3)
8:00	2 (30)	24 (7)	8	50 (7)
9:00	2 (10)	3 (11)	6	23 (8)

Table X, contd.

TIME	NO (pphm)	NO_2 (pphm)	HC (ppm)	O_3 (pphm)
	POLLUTANT			
10:00 A.M.	2 (10)	5 (12)	5	29 (15)
11:00	1 (7)	12 (8)	4 (4)	45 (22)
12:00 Noon	1	17	4 (3)	48 (15)
1:00 P.M.	1	7	4 (2)	67 (17)
2:00	1	7	3 (2)	51 (13)
3:00	2 (3)	9 (8)	1 (2)	28 (6)
4:00	2 (4)	10 (10)	2 (2)	36 (5)
5:00	2 (2)	14 (8)	2 (2)	37 (4)
6:00	2 (2)	15 (6)	1 (2)	23 (2)
Average of Hour Reported:	8 (16)	14 (7)	4 (4)	33 (9)

Station: 60 Location: Azusa

TIME	NO (pphm)	NO_2 (pphm)	HC (ppm)	O_3 (pphm)
	POLLUTANT			
6:00 A.M.	6 (4)	8 (6)	8 (8)	1 (1)
7:00	1 (8)	12 (8)	7 (7)	7 (3)
8:00	1 (2)	7 (13)	6 (5)	14
9:00	0 (1)	5 (16)	6 (5)	21 (7)
10:00	0 (1)	4 (11)	5 (5)	20 (13)
11:00	0 (1)	4 (9)	5 (5)	23 (17)
12:00 Noon	0	4	5 (6)	21 (18)

Table X, contd.

TIME	NO (pphm)	NO_2 (pphm)	HC (ppm)	O_3 (pphm)
1:00 P.M.	0	4	5 (6)	31 (27)
2:00	0 (1)	5 (4)	3 (4)	24 (19)
3:00	0 (1)	14 (4)	2 (5)	45 (15)
4:00	1 (1)	13 (4)	2 (4)	37 (12)
5:00	0	10 (5)	1 (5)	30 (7)
6:00	2 (1)	11 (7)	1 (6)	9 (3)
Average of Hours Reported:	1 (2)	8 (7)	4 (5)	22 (11)

Station: 79 Location: Pasadena

TIME	NO (pphm)	NO_2 (pphm)	HC (ppm)	O_3 (pphm)
6:00 A.M.	26 (23)	8 (6)	8 (5)	0 (1)
7:00	5 (19)	20 (9)	8 (5)	9 (1)
8:00	1 (3)	10 (11)	8 (3)	4 (1)
9:00	1 (1)	3 (9)	6 (3)	25 (1)
10:00	1 (1)	3 (14)	6 (3)	45 (1)
11:00	1 (1)	3 (17)	6 (4)	44 (2)
12:00 Noon	0	3	5 (5)	53 (7)
1:00 P.M.	0	3	5 (3)	67 (7)
2:00	0	5	4 (2)	46 (9)
3:00	0 (1)	3 (5)	3 (2)	26 (4)

Table X, contd.

TIME	NO (pphm)	NO_2 (pphm)	HC (ppm)	O_3 (pphm)
4:00 P.M.	1 (1)	8 (6)	2 (2)	24 (3)
5:00	1 (1)	12 (11)	2 (2)	21 (2)
6:00	1 (2)	9 (14)	2 (3)	2 (1)
Average of Hours Reported:	4 (5)	8 (11)	5 (3)	33 (3)

The meteorological effects are similar to those discussed in Section 3.4 for the CO simulation. The photochemistry, a non-linear process, complicates the analysis, but nevertheless the same conclusions about the effects of the winds, inversion and horizontal wind convergences were evident in this simulation also.

The computer drawn isopleths calculated with NO and NO_2 averaged over the initial hour simulated (6:00 A.M.) are shown in Figures 44 and 45. At 6:00 A.M., the hydrocarbon (HC) concentrations averaged above 5 ppm and oxidant (O_3) concentrations below 1 pphm and were both not plotted. By 10:00 A.M. (illustrated in Figure 46 - 48) the combination of morning emissions and slowly increasing on shore winds would have led to build-up of NO in the central basin, but the chemical reactions have proceeded too rapidly converting NO to NO_2. NO is below 5 pphm and not plotted. NO_2 has also been removed by the reactions and oxidants have been formed. In Figures 46 and 47, NO_2 is below measured levels, but oxidants are over predicted. In the afternoon the observations

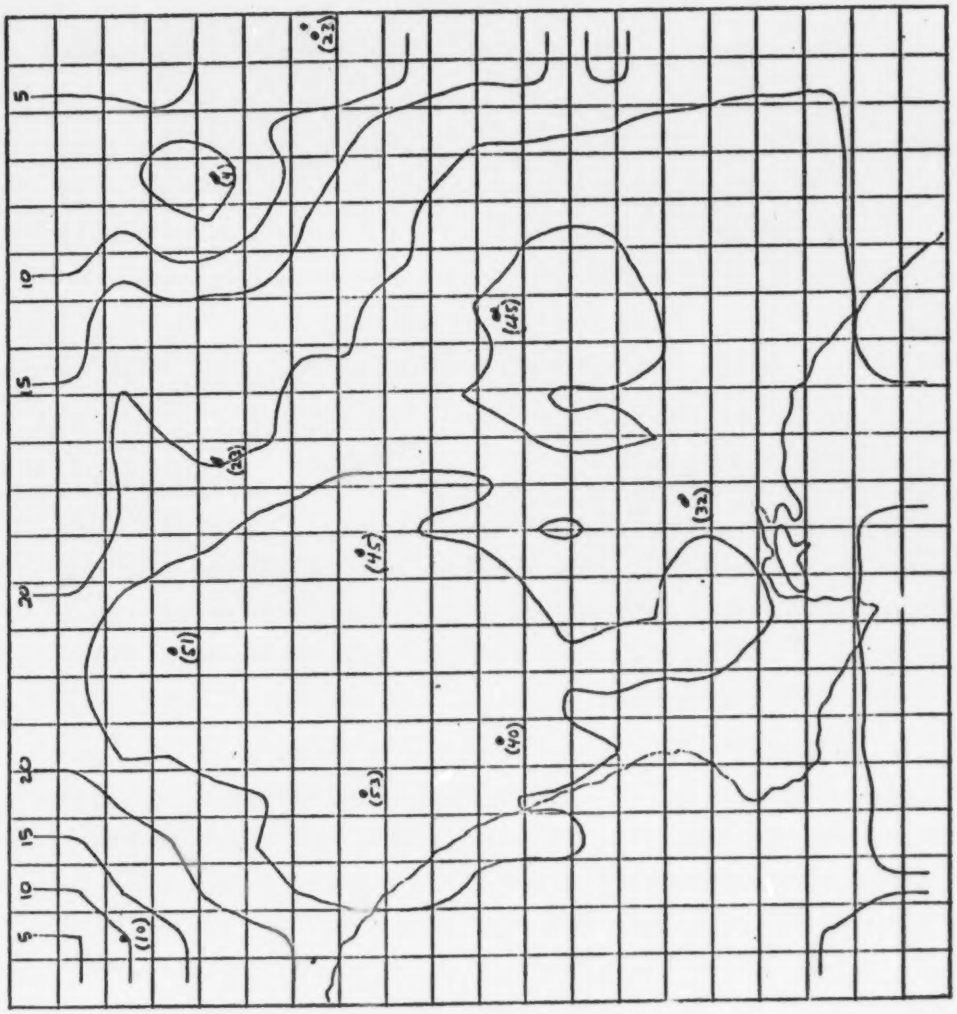
5
10
15
20
20
15
10
5
(22)
(41)
(45)
(20)
(45)
(32)
(51)
(40)
(53)
(10)

Figure 44 – NO concentration in pphm at 6:00 A.M.

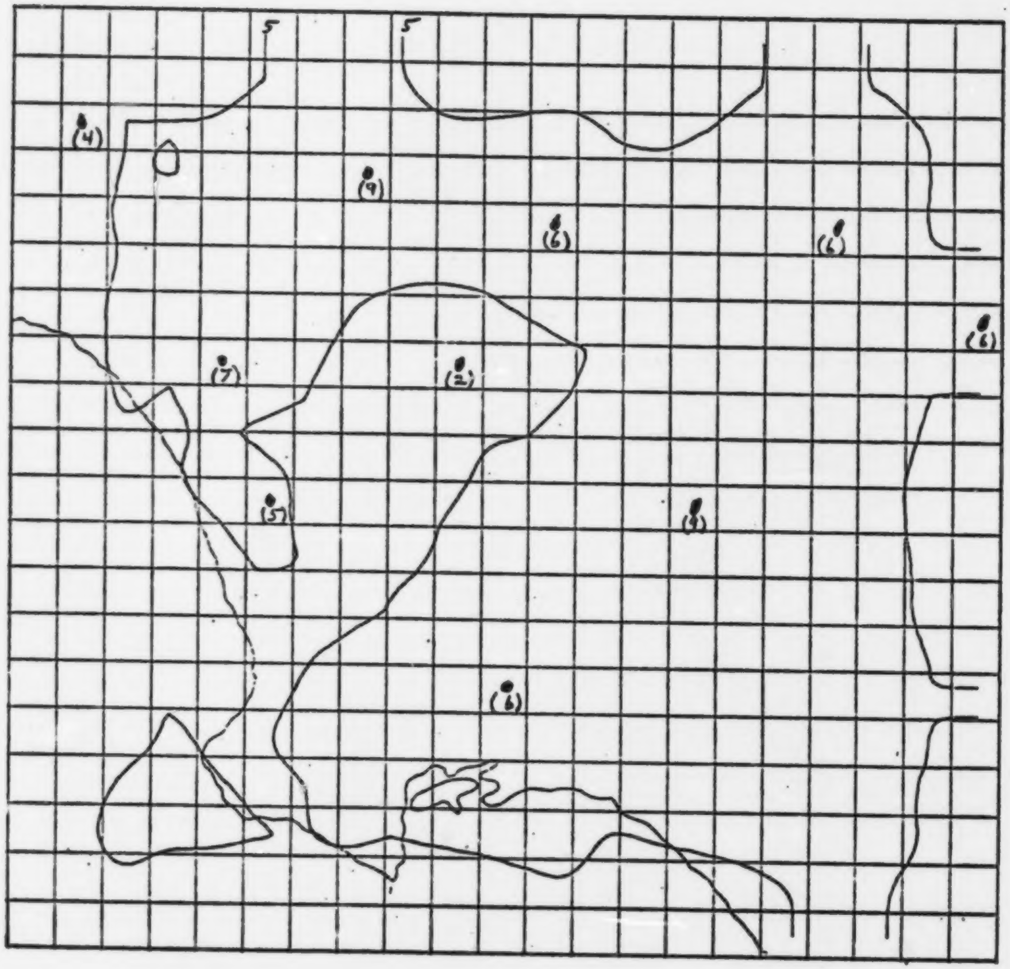
5
5
(4)
(9)
(6)
(6)
(6)
(7)
(2)
(5)
(6)

Figure 45 — NO_2 concentration in pphm at 6:00 A.M.

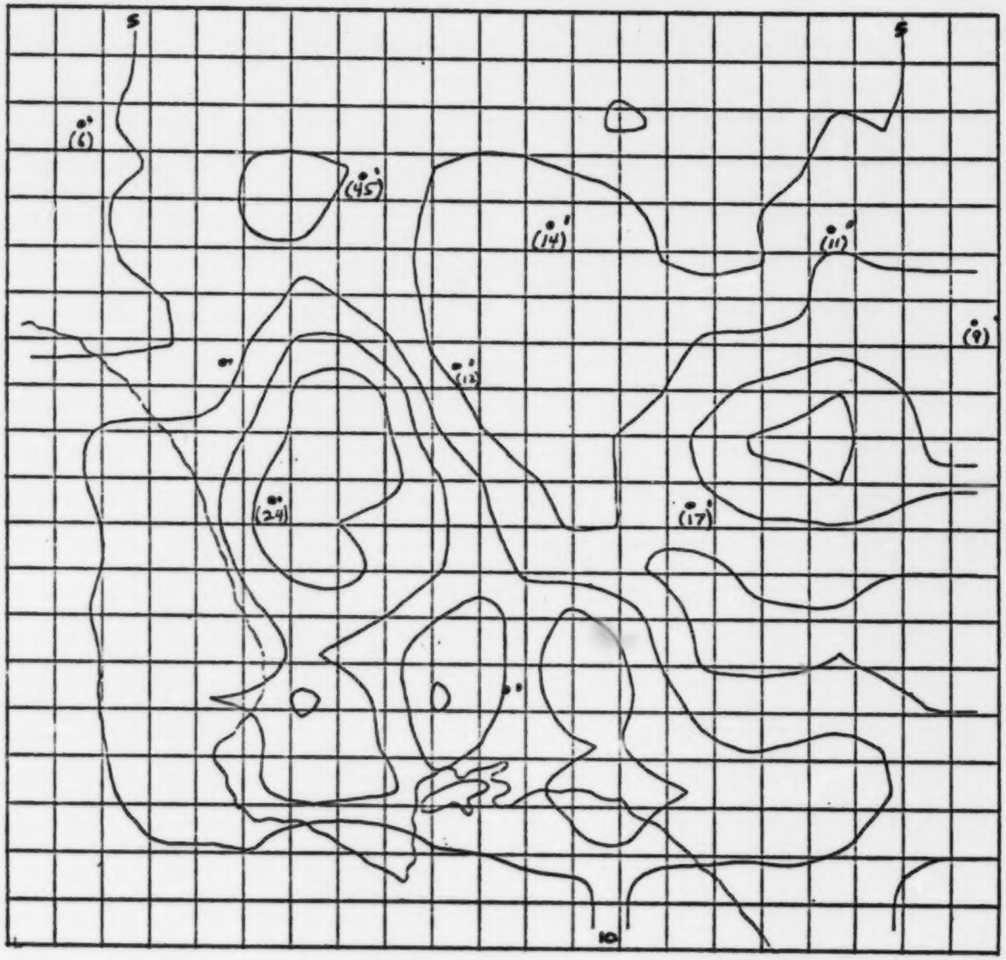
5
5
(6)
(45)
(14)
(11)
(9)
(12)
(24)
(17)
10

Figure 46 – NO_2 concentration in pphm at 10:00 A.M.

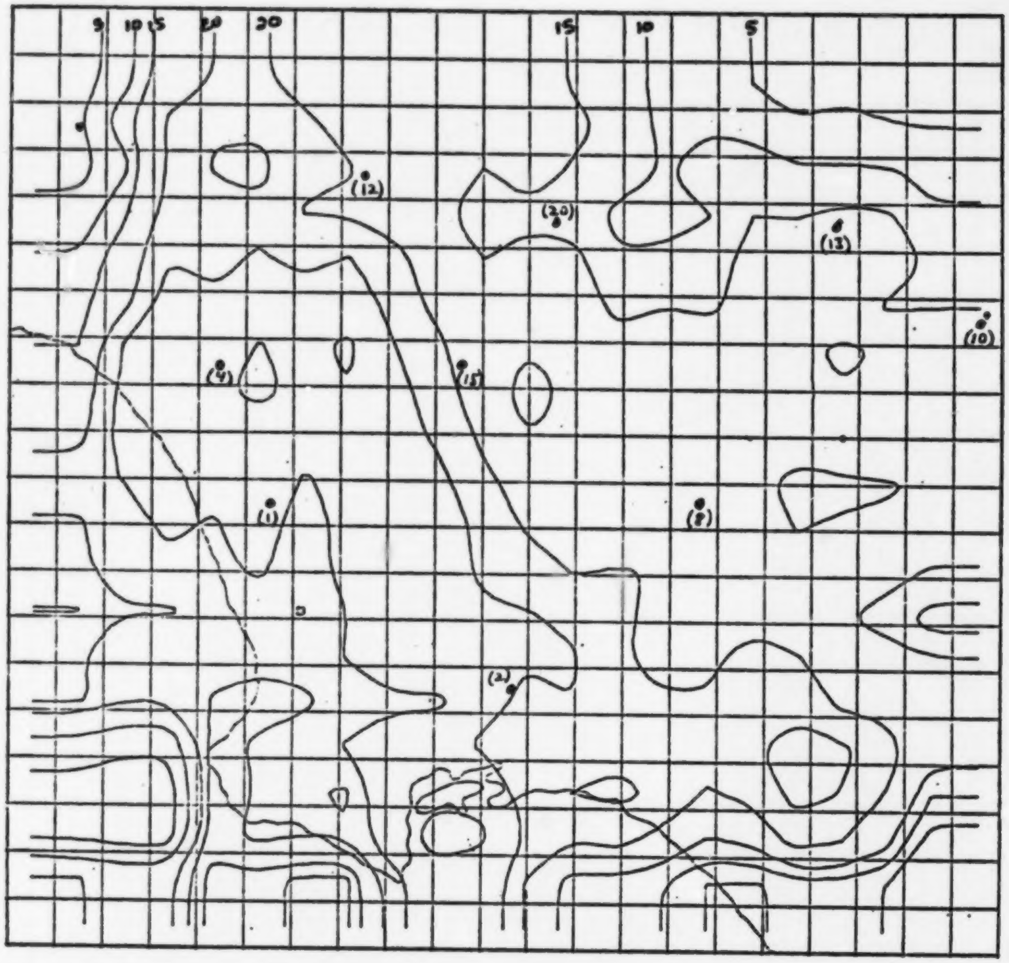
5
10
15
20
20
15
10
5
(12)
(20)
(13)
(10)
(4)
(15)
(1)
(8)
(2)

Figure 47 – O_3 concentration in pphm at 10:00 A.M.

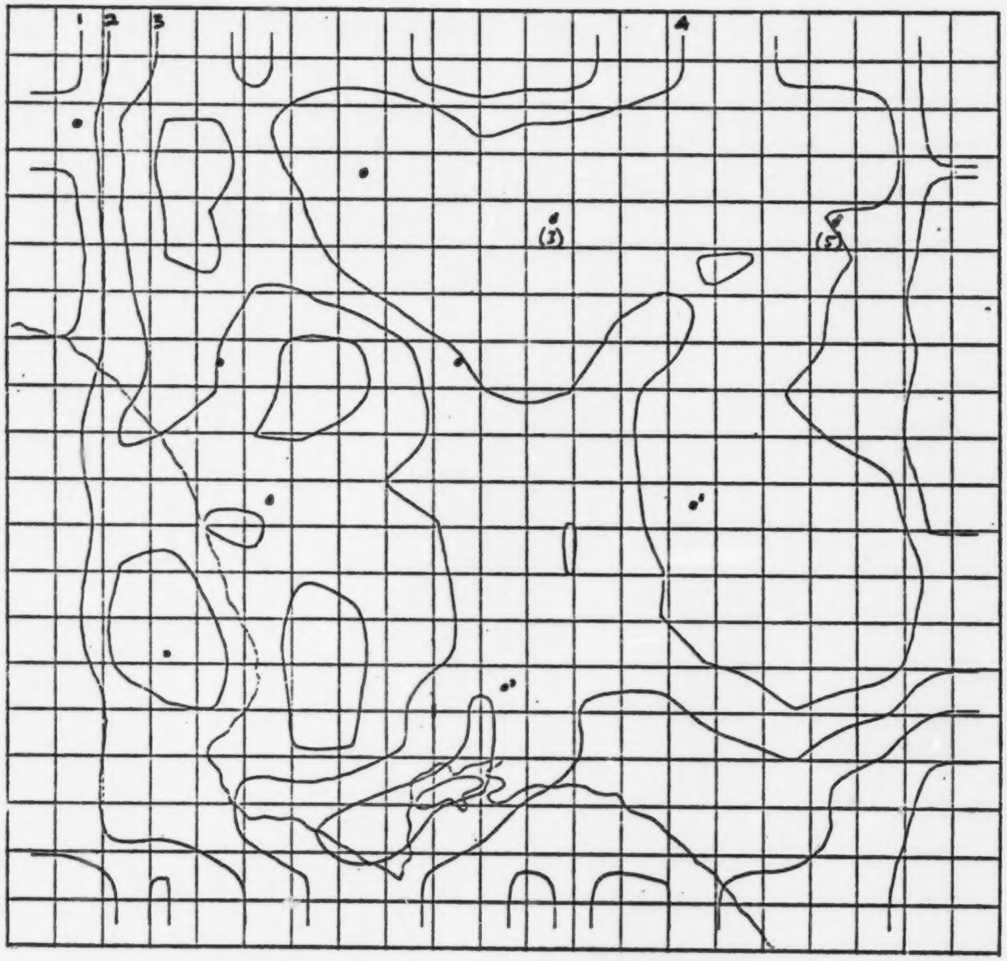

Figure 48 – HC concentration in ppm at 10:00 A.M.

show NO_2 being depleted and so the NEXUS/P results are in better agreement with observations (Figure 49). The oxidant isopleths (Figure 50) are still too high, but show a spatial distribution similar to the observations. The winds in the afternoon have transported the major high levels of oxidants toward the northeast. At 6:00 P.M. after the evening rush hours, the NO_2 and HC show considerable similarities, but the oxidants remain too high. The NO_2 distribution (Figure 52) shows areas of higher concentrations near convergences in the surface winds even though this is a secondary pollutant produced after conversion of emitted NO.

4.6 SUMMARY AND CONCLUSIONS

The NEXUS/P code was developed from NEXUS with the addition of subroutines for chemical simulation and for particle mass re-weighting to treat changes in concentration calculated in the chemical simulation. The CHEM code was developed to solve the chemical mechanism reported by Eschenroeder[29] and was 40 times faster than Eschenroeder's reported technique.

The NEXUS/P was first applied to simulating a puff of reactive pollutants. This simple application was used to evaluate the compatibility of the PICK formalism as used in NEXUS and the simulation of chemical reactions by the CHEM code. In the first test, the simulated reactive puff was stationary and the NEXUS/P results agreed with the CHEM simulation alone. For the next test, the reactive puff was moved with a constant velocity. At the boundaries of the puff, errors were observed due to the use of Eulerian concentrations for non-linear chemical simulation, as described in Section 4.3. When concentration gradients were reduced by the use of a Gaussian distribution for the advecting puff, the errors were

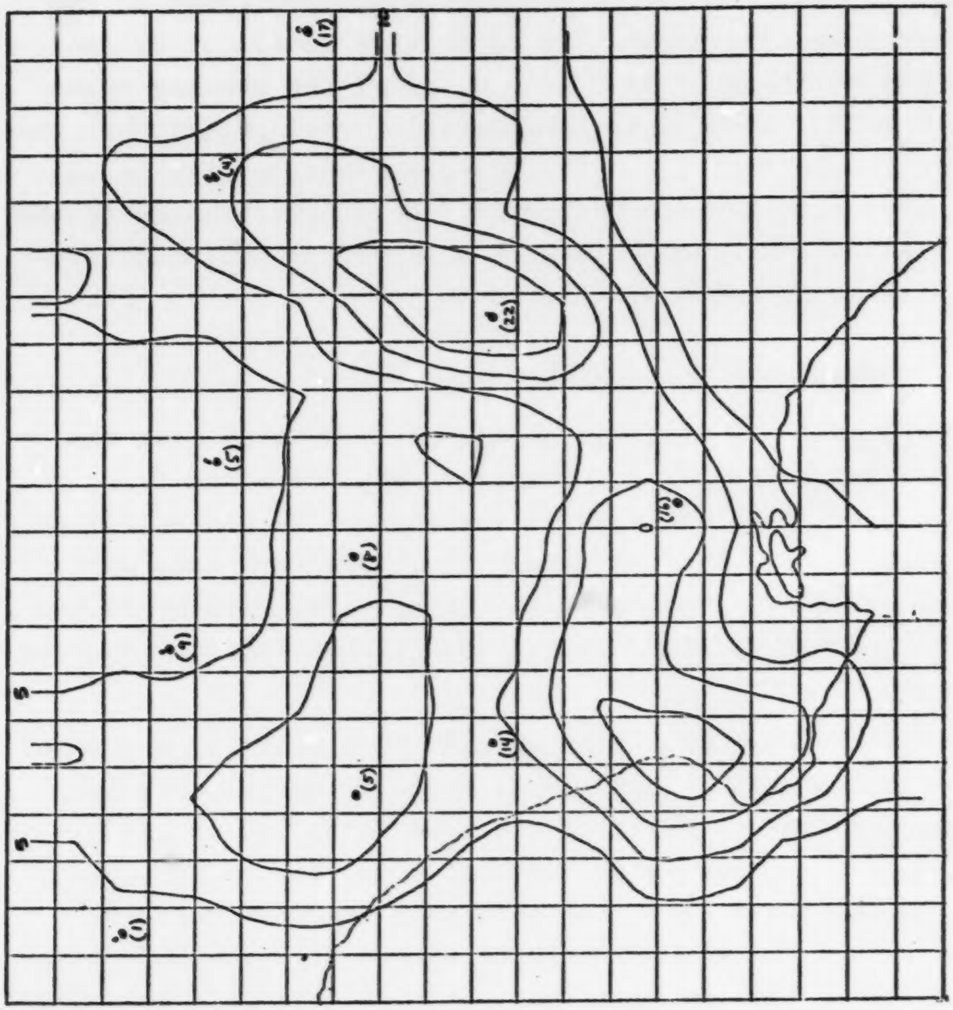
10
5
5
(17)
(11)
(22)
(5)
(8)
(9)
(16)
(14)
(5)
(1)

Figure 49 — NO_2 concentration in pphm at 3:00 P.M.

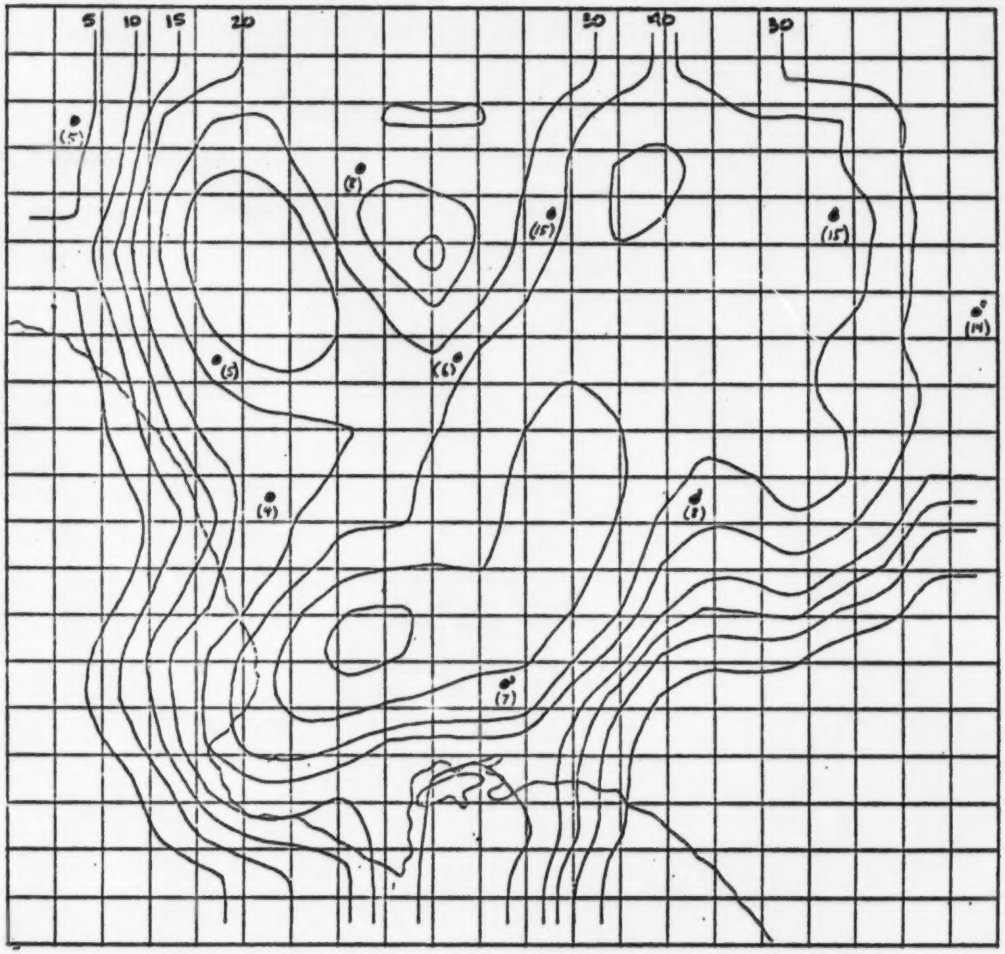
5
10
15
20
50
40
30
(5)
(8)
(15)
(15)
(14)
(5)
(6)
(4)
(8)
(7)

Figure 50 – O_3 concentration in pphm at 3:00 P.M.

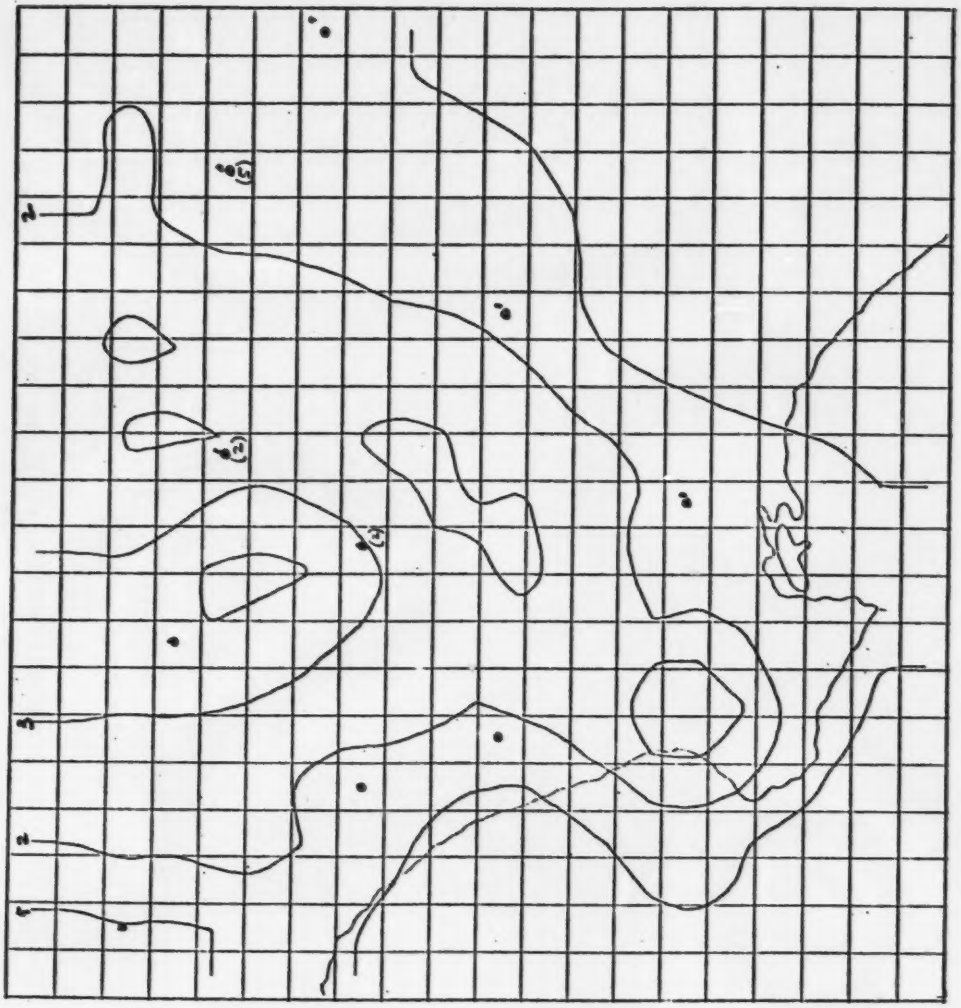

Figure 51 – HC concentration in ppm at 3:00 P.M.

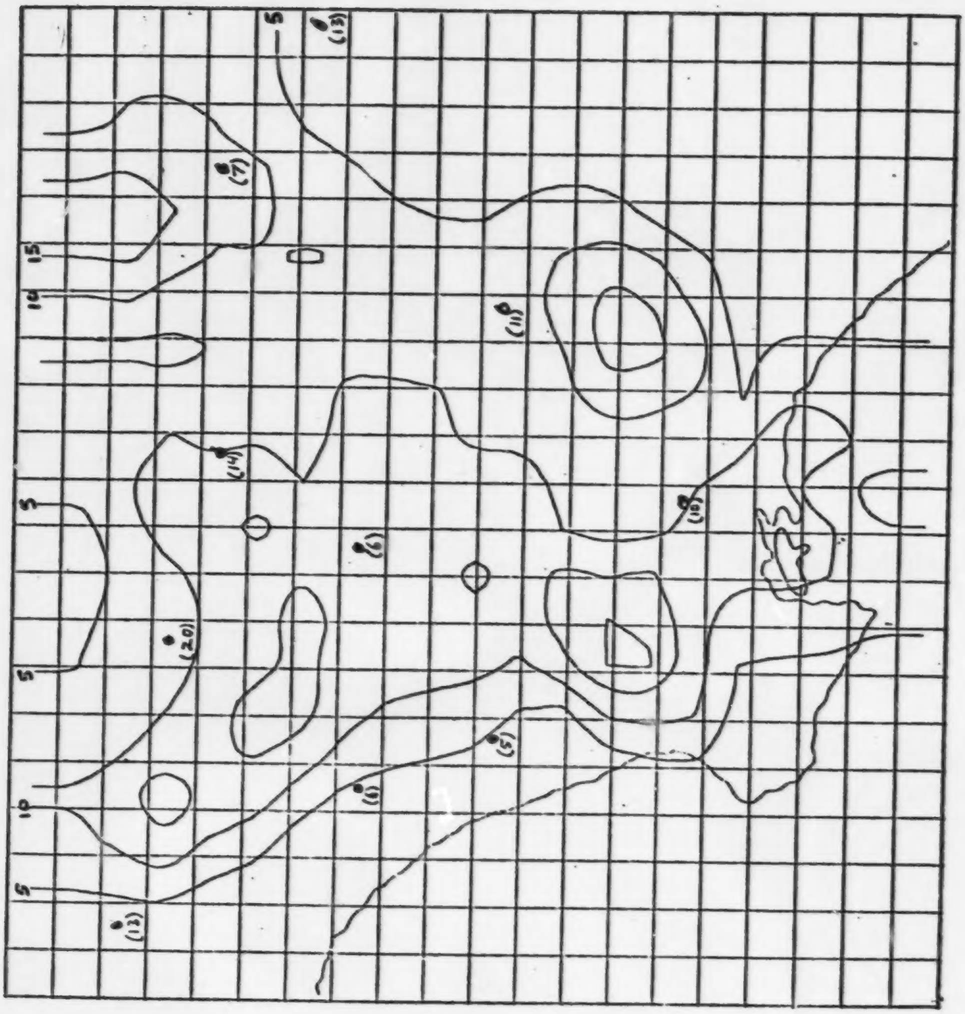
5
(13)
(7)
15
10
(11)
(14)
5
(18)
(6)
(20)
5
(5)
(6)
10
5
(12)

Figure 52 - NO_2 concentration in pphm at 6:00 P.M.

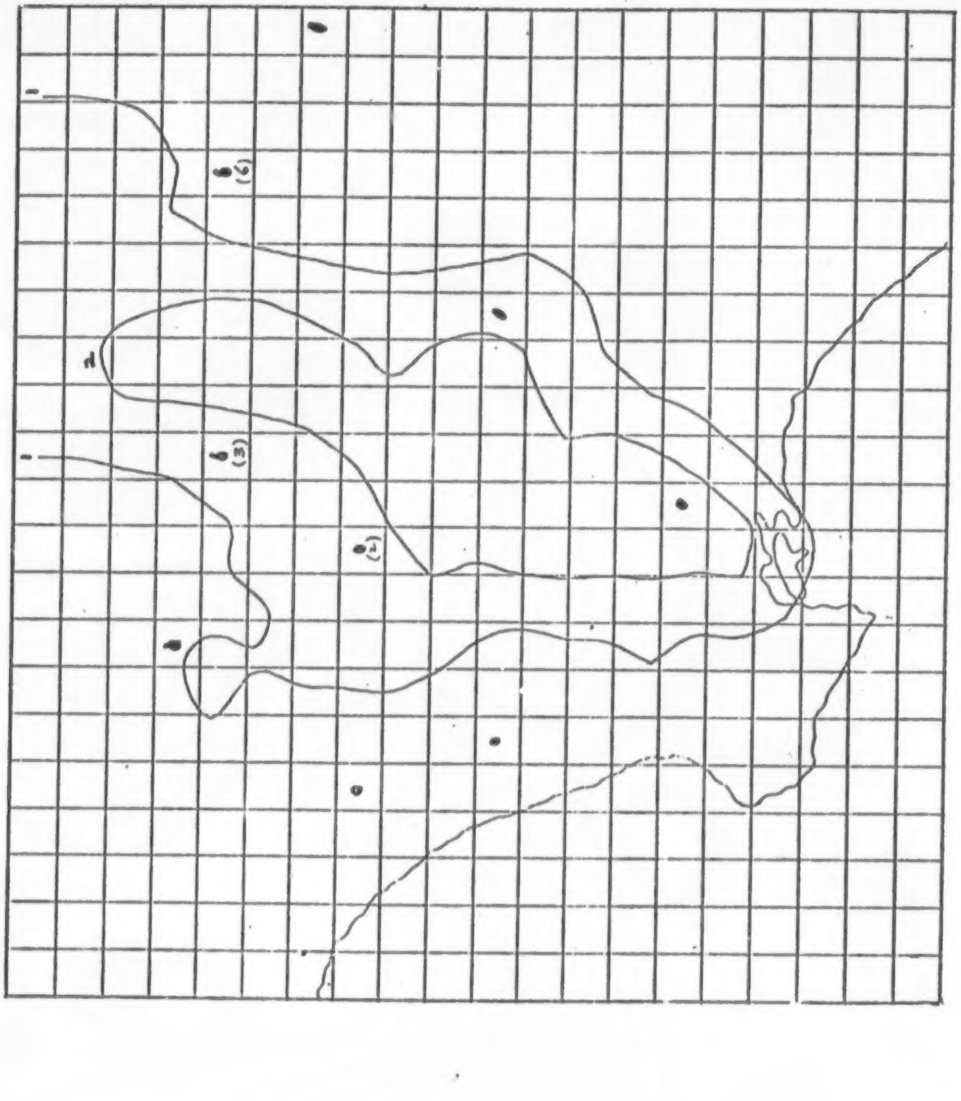

Figure 53 — HC concentration in ppm at 6:00 P.M.

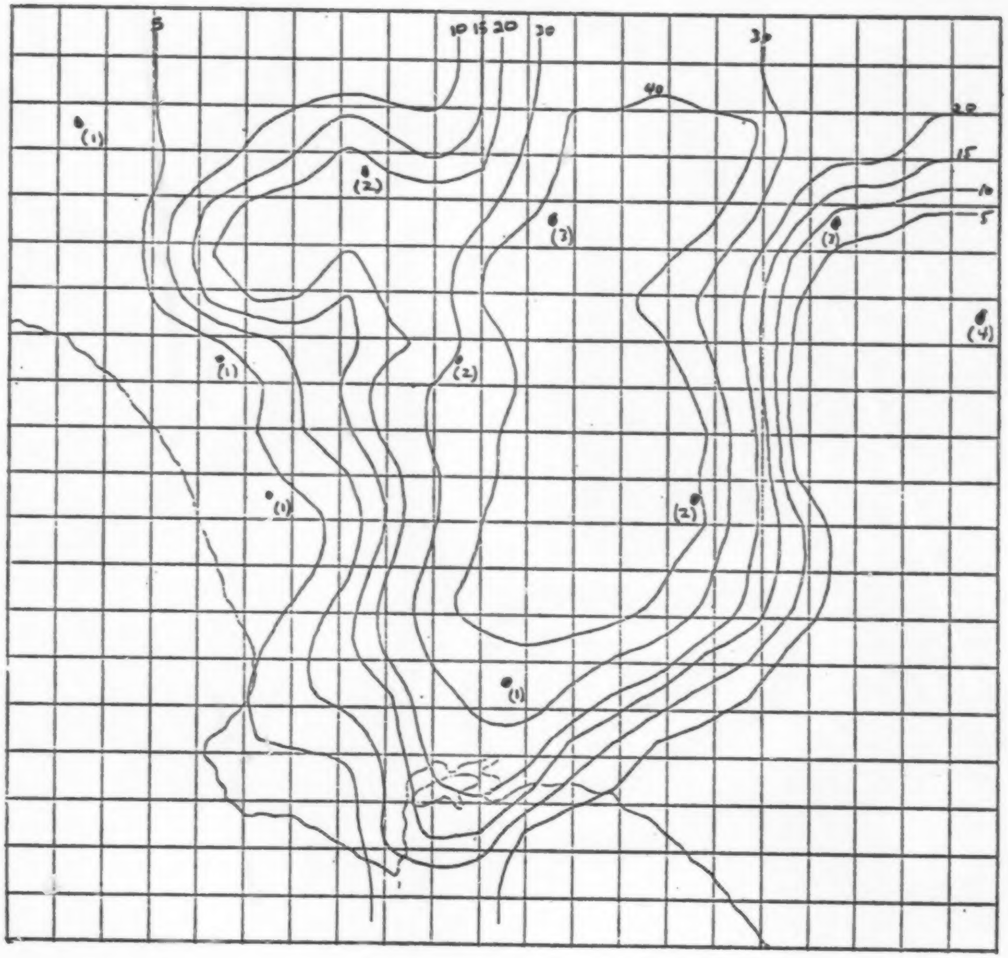
5
10 15 20
30
30
40
20
15
10
5
(1)
(2)
(3)
(3)
(4)
(1)
(2)
(1)
(2)
(1)

Figure 54 — O_3 concentration in pphm at 6:00 P.M.

reduced. The magnitude of these errors for a realistic application is not known at this time and should be investigated. An advecting and diffusing reactive puff was also simulated but a correct solution for comparison was not known.

Photochemical smog in Los Angeles was simulated using NEXUS/P. The 16-hour real time simulation required 1.5 hours on a UNIVAC 1108. Approximately one-half hour was spent in chemical simulation and one-half hour in data manipulation. The photochemical smog was simulated using a mechanism developed by Eschenroeder[29] with five calculated species (NO, NO_2, HC, O_3 and HNO_2) and three species in pseudo-equilibrium (O, RO_2 and OH). The source inventory used was reported by Roberts, et.al.[23] The required meteorological data was obtained from Dickson and Start[31] (winds) and Roth[24] (inversion height).

The results of the NEXUS/P simulation were compared to Los Angeles APCD observations. In the simulation, NO was converted to NO_2 too rapidly, total NO + NO_2 was depleted too fast and too much O_3 was produced. These deviations from the observations occur basin-wide and are attributable to inaccuracies in the chemical mechanism used in the simulation. Some generally observed trends were reproduced — double maximum in NO_2, NO + NO_2 and HC depletion during the day and O_3 build-up and depletion. The calculated spatial distributions of primary and secondary pollutants have the same general features as observed but inaccuracies in the chemical mechanism complicate any analysis.

5. SUMMARY AND CONCLUSIONS

The PICK particle-in-cell method for solution of the atmospheric dispersion equation has been developed, tested and applied to air pollution problems. The PICK method was used in a two-dimensional computer code, PICFIC, for evaluation of the method and comparison to finite difference methods as applied to advection test problems.

In the simulation of advection, PICFIC is faster and more accurate than the finite difference methods tested, and PICFIC produced a solution for cases which the finite difference techniques failed to solve due to truncation errors. PICFIC was also evaluated for accuracy of diffusion simulations and for speed with different grid sizes and different numbers of particles per grid cell. The accuracy of the PICFIC diffusion simulation decreased with decreasing numbers of particles per cell. Using ten particles per cell, the effective diffusivity calculated with PICFIC was 0.90 of the actual value and with three particles per cell was 0.60 of the actual value. The computing time required was 30-50 micro-seconds per cell per dimension and 100-300 micro-seconds per particle per dimension for each cycle on the S^3 UNIVAC 1108. Thus, greater resolution and accuracy may be gained at the least expense by increasing the number of cells for a constant number of particles (as long as more than three particles per cell are used). PICFIC was also used to simulate particulate matter falling in a gravitational field from a line source in a shear wind; less than 10 percent deviation from the analytic solution resulted.

PICFIC was extended to three dimensions forming NEXUS. NEXUS was developed with boundary conditions and input/output routines appropriate for regional air pollution problems. NEXUS was used to simulate carbon monoxide in Los Angeles. The meteorological and source emissions data were obtained from the literature. This first application had very good correlation with Los Angeles Air Pollution Control District observations. A correlation coefficient of 0.73 was obtained by comparing NEXUS results with observations at 12 stations. The 17-hour simulation took 12 minutes on the S^3 UNIVAC 1108. Tests were conducted with NEXUS to determine the effects of different assumptions made for the boundary conditions, upper levels winds and source emissions. The sensitivity of the results to random errors in the meteorological and source emissions data was also evaluated. A movie was made that depicts the flow of pollutants as simulated by NEXUS.[34] In the movie, dots are used to represent particle positions.

A second major application of the PICK method to an air pollution problem was the simulation of photochemical smog in Los Angeles. A technique for incorporating the effects of chemical reactions was added to NEXUS to form NEXUS/P. A subroutine, CHEM, was developed to solve the chemical mechanism reported by Eschenroeder and Martinez[29] with five calculated species (NO, NO_2, O_3, HC and HNO_2). When NEXUS/P was tested on an advecting puff of reacting pollutants, errors were introduced by the use of Eulerian cell concentrations in the non-linear chemical simulation. The errors are small for small spatial gradients in concentration as may be the case in some regional air pollution problems of interest. For Los Angeles, the 16-hour photochemical smog simulation took 1.5 hours on the S^3 UNIVAC 1108. The NEXUS/P calculation showed that NO is converted to NO_2 too fast and too much O_3 is produced. These features in the results are attributed to the chemical reaction mechanism. The development of a better chemical mechanism is central to an accurate photochemical smog model. The errors introduced by the use of Eulerian cell concentrations in chemical simulation should be investigated to determine the significance of these errors for photochemical modeling of actual air pollution problems and to eliminate or minimize the errors.

This study has developed and demonstrated a new method for simulating atmospheric advection and diffusion. The PICK method has been shown to be more accurate and reliable than the finite difference techniques for advection. PICK is the preferred method for many air pollution problems where its greater accuracy will result in a less expensive simulation than finite difference methods using a smaller grid cell size. The PICK method, being a hybrid Lagrangian-Eulerian method, offers a unique capability to assess the importance of the errors introduced by the use of Eulerian cell concentrations in chemical simulation. Due to the accuracy of advection with the PICK method, it may also make a significant contribution to hydrodynamic modeling for meteorological applications.

REFERENCES

1. A.A. Amsden, "The Particle-In-Cell Method for the Calculation of the Dynamics of Compressible Fluids," Report No. LA-3466 (1966), Los Alamos Scientific Laboratory, New Mexico.

2. J.E. Welch, F.H. Harlow, J.P. Shannon, and B.J. Daly, "The MAC Method," Report No. LA-3425 (1965), Los Alamos Scientific Laboratory, New Mexico.

3. F.H. Harlow and A.A. Amsden, "Fluid Dynamics: An Introductory Text," Report No. LA-4100 (1970), Los Alamos Scientific Laboratory, New Mexico.

4. K.L. Calder, "On the Equation of Atmospheric Diffusion," Qtrly. J. Royal Meteorological Society (1965), 91, 390, pp. 514.

5. O.G. Sutton, Micrometeorology, McGraw-Hill, New York (1953).

6. F. Pasquill, Atmospheric Diffusion, D. Van Nostrand, New York (1962).

7. J.E. Fromm, "A Method for Reducing Dispersion in Convective Difference Schemes," J. Computational Physics (1968), 3, 176.

8. W.P. Crowley, "Numerical Advection Experiments," Monthly Weather Review (1968), 96, 1, pp. 1.

9. W.P. Crowley, "Second-Order Numerical Advection," J. Computational Physics (1967), 1, 471.

10. R.D. Richtmyer and K.W. Martinez, Difference Methods for Initial-Value Problems, second ed., Interscience Publishers, New York (1967). The first-order advection differencing scheme described on pp. 292 is attributed to R. Lelevier.

11. B.A. Egan and J.R. Mahoney, "A Numerical Model of Urban Air Pollution Transport," Conference on Air Pollution Meteorology, AMS, Raleigh, North Carolina, April 5-9, 1971.

12. J.P. Pandolfo, M.A. Atwater and G.E. Anderson, "Prediction by Numerical Models of Transport and Diffusion in An Urban Boundary Layer," (1971), Center for The Environment and Man, Hartford, Connecticut.

Preceding page blank

13. R.C. Sklarew, "The Grid Model of Urban Air Pollution," APCA Paper No. 70-79 (June 1970), Systems, Science and Software, La Jolla, California.

14. A.D. Taylor, letter to K.L. Calder, dated 26 May 1970.

15. J.L. Neuringer, SIAM J. Appl. Math. (1968), 16, 4, pp. 834.

16. R. Lamb, "An Air Pollution Model of Los Angeles," Masters Thesis (1969), University of California, Los Angeles.

17. State of California, Air Resources Board, "Air Pollution Control in California," Annual Report (1969), pp. 13.

18. A.Q. Eschenroeder and J.R. Martinez, "Mathematical Modeling of Photochemical Smog," AIAA Eighth Aerospace Sciences Meeting, New York (January 1970), Paper No. 70-116.

19. D.M. Teague, "Los Angeles Traffic Pattern Survey," Vehicle Emissions I, SAE Progress in Technology (1964), 6, 102.

20. G.P. Larson, J.C. Chipman and E.K. Kauper, "Distribution and Effects of Automotive Exhaust Gases in Los Angeles," Vehicle Emissions I, SAE Progress in Technology (1964), 6, 7.

21. R.C. Sklarew, "Preliminary Report of the S^3 Urban Air Pollution Simulation of Carbon Monoxide in Los Angeles," (1970), Systems, Science and Software, La Jolla, California.

22. R.C. Sklarew, Systems, Science and Software, "Simulation Models for Air Quality Control," IEEE Conference on Decision and Control, Miami Beach, Florida, December 1971.

23. P.J. Roberts, P.M. Roth and C.L. Nelson, "Contaminant Emissions in the Los Angeles Basin – Their Sources Rates and Distribution," Report No. 71 SAI-6 (1971) Systems Applications, Inc.

24. P.J. Roth, private communication (1971).

25. M. Weisburd, L.G. Wayne, R. Danchick and A. Kokin, "Development of A Simulation Model for Estimating Ground Level Concentration of Photochemical Pollutants," Report No. TM-(L)-4673/000/00 (1971), System Development Corp., Los Angeles, California.

26. N.E. Browne, "Simulation Model for Air Pollution Over Connecticut," J. Air Pollution Control Association (1969), 19, pp. 570.

27. L.G. Wayne and T.E. Ernest, "Photochemical Smog, Simulated by Computer," APCA Paper No. 69-15 (1969), New York.

28. J.V. Behar, "Simulation Model of Air Pollution Photochemistry," Project Clean Air Research Reports 4, (1970), University of California.

29. A.Q. Eschenroeder and J.R. Martinez, "Concepts and Applications of Photochemical Smog Models,"

30. C.W. Gear, "A407 – DIFSUB for Solution of Ordinary Differential Equations," (1971), Communications of the ACM 14, 3, pp. 185.

31. T.J. Keneshea, "A Technique for Solving the General Reaction-Rate Equations in the Atmosphere," Report No. AFCRL-67-0221 (1967), Air Force Cambridge Research Laboratories, Cambridge, Massachusetts.

32. C.R. Dickson and G. Start, private communication (1971).

33. J.R. Martinez, R.A. Nordsieck and A.Q. Eschenroeder, "Morning Vehicle-Start Effects on Photochemical Smog," Report No. CR-2-191 (1971), General Research Corporation, Santa Barbara, California.

34. R.C. Sklarew, "Computer Simulation of Carbon Monoxide in Los Angeles," (1970), Systems, Science and Software, La Jolla, California.